Nuclear Science ISBN 92-64-01082-3

Physics and Safety of Transmutation Systems

A Status Report

NEA No. 6090

NUCLEAR ENERGY AGENCY
ORGANISATION FOR ECONOMIC CO-OPERATION AND DEVELOPMENT

ORGANISATION FOR ECONOMIC CO-OPERATION AND DEVELOPMENT

The OECD is a unique forum where the governments of 30 democracies work together to address the economic, social and environmental challenges of globalisation. The OECD is also at the forefront of efforts to understand and to help governments respond to new developments and concerns, such as corporate governance, the information economy and the challenges of an ageing population. The Organisation provides a setting where governments can compare policy experiences, seek answers to common problems, identify good practice and work to co-ordinate domestic and international policies.

The OECD member countries are: Australia, Austria, Belgium, Canada, the Czech Republic, Denmark, Finland, France, Germany, Greece, Hungary, Iceland, Ireland, Italy, Japan, Korea, Luxembourg, Mexico, the Netherlands, New Zealand, Norway, Poland, Portugal, the Slovak Republic, Spain, Sweden, Switzerland, Turkey, the United Kingdom and the United States. The Commission of the European Communities takes part in the work of the OECD.

OECD Publishing disseminates widely the results of the Organisation's statistics gathering and research on economic, social and environmental issues, as well as the conventions, guidelines and standards agreed by its members.

* * *

This work is published on the responsibility of the Secretary-General of the OECD. The opinions expressed and arguments employed herein do not necessarily reflect the official views of the Organisation or of the governments of its member countries.

NUCLEAR ENERGY AGENCY

The OECD Nuclear Energy Agency (NEA) was established on 1st February 1958 under the name of the OEEC European Nuclear Energy Agency. It received its present designation on 20th April 1972, when Japan became its first non-European full member. NEA membership today consists of 28 OECD member countries: Australia, Austria, Belgium, Canada, the Czech Republic, Denmark, Finland, France, Germany, Greece, Hungary, Iceland, Ireland, Italy, Japan, Luxembourg, Mexico, the Netherlands, Norway, Portugal, Republic of Korea, the Slovak Republic, Spain, Sweden, Switzerland, Turkey, the United Kingdom and the United States. The Commission of the European Communities also takes part in the work of the Agency.

The mission of the NEA is:

- to assist its member countries in maintaining and further developing, through international co-operation, the scientific, technological and legal bases required for a safe, environmentally friendly and economical use of nuclear energy for peaceful purposes, as well as
- to provide authoritative assessments and to forge common understandings on key issues, as input to government decisions on nuclear energy policy and to broader OECD policy analyses in areas such as energy and sustainable development.

Specific areas of competence of the NEA include safety and regulation of nuclear activities, radioactive waste management, radiological protection, nuclear science, economic and technical analyses of the nuclear fuel cycle, nuclear law and liability, and public information. The NEA Data Bank provides nuclear data and computer program services for participating countries.

In these and related tasks, the NEA works in close collaboration with the International Atomic Energy Agency in Vienna, with which it has a Co-operation Agreement, as well as with other international organisations in the nuclear field.

FOREWORD

Under the auspices of the NEA Nuclear Science Committee (NSC), the Working Party on Scientific Issues in Partitioning and Transmutation (WPPT) was created in June 2000 to examine and provide information on the status and trends of scientific issues in partitioning and transmutation (P&T). In line with the scope of the WPPT and in order to cover a wide range of different disciplines in the P&T field, four subgroups were formed, each delegated with the task of producing a state-of-the-art report in its specialised field. The four subgroups address:

- accelerator utilisation and reliability;
- chemical partitioning;
- fuels and materials;
- physics and safety of transmutation systems.

The mission of the Subgroup on Physics and Safety of Transmutation Systems is to: 1) organise theoretical and experiment-based benchmarks on minor actinide burner systems, 2) evaluate beam-trip consequences on accelerator-driven systems, 3) perform sensitivity studies on the main parameters and 4) propose a safety approach for new P&T systems. In carrying out its mission, the Subgroup carried out several benchmark studies and produced the corresponding reports.

This status report begins by providing a clear definition of P&T, and then describes the state of the art concerning the challenges facing the implementation of P&T, scenario studies and specific issues related to accelerator-driven system (ADS) dynamics and safety, long-lived fission product transmutation and the impact of nuclear data uncertainty on transmutation system design.

Acknowledgements

The Secretariat expresses its sincere gratitude to all members of the Subgroup for their valuable contributions and to the authors of this report. Special thanks are conveyed to Ms. Andrea Griffin-Chahid for having prepared the report for publication.

TABLE OF CONTENTS

Chapter 1

P&T AND THE ROLE OF ADS

This chapter will be devoted to a survey of partitioning and transmutation (P&T) and the role of ADS. Many previous publications have discussed these issues; however, it is worthwhile to revisit the subject in light of recent progress in the field. Section 1.1 of this chapter deals with defining P&T and its associated challenges. The physics basis and methods of transmutation will be recalled. In Section 1.2 the intercomparison of different transmutation concepts and modes of recycle will be summarised. Section 1.3 is devoted to systems dedicated to transmutation and to the role of ADS. Finally, Section 1.4 will provide an overview of the issues related to the practical implementation of P&T: scenarios, potential benefits and challenges.

1.1 P&T definition and challenges

1.1.1 Spent fuel from current reactors and the role of partitioning and transmutation (P&T)

The spent fuel (or some of its constituents) discharged from nuclear power plants constitutes the main contribution to nuclear waste.

Figure 1.1 gives the composition of the spent nuclear fuel of a standard PWR with UO_2 fuel and irradiated up to a burn-up of 33 GWd/t. Extended burn-ups or the use of MOX fuel increases the amount of minor actinides (Np, Am, Cm) produced (see Table 1.1).

Figure 1.1. Composition of spent nuclear fuel (standard PWR 33 GW/t, 10-year cooling)

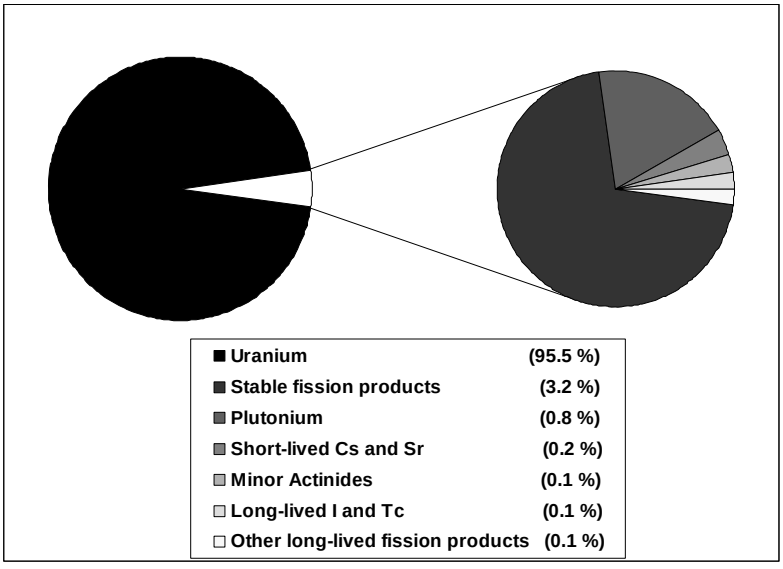

1 tonne of SNF contains:
955.4 kg U
8.5 kg Pu

Minor actinides (MAs)
0.5 kg ^{237}Np
0.6 kg Am
0.02 kg Cm

Long-lived fission products (LLFPs)
0.2 kg ^{129}I
0.8 kg ^{99}Tc
0.7 kg ^{93}Zr
0.3 kg ^{135}Cs

Short-lived fission products (SLFPs)
1 kg ^{137}Cs
0.7 kg ^{90}Sr

Stable isotopes
10.1 kg lanthanides
21.8 kg other stable

Table 1.1. MA build-up in various commercial reactors

Core type	PWR	PWR	PWR	PWR
Fuel material	UO_2	UO_2	MOX	MOX
Burn-up (GWd/t)	33	60	33	60
Cooling time (years)	5	5	3	3
MA build-up (kg/year/GWe)	22.2	26.3	77.9	78.0

Most of the hazard from the spent fuel stems from only a few chemical elements – plutonium, neptunium, americium, curium and some long-lived fission products such as iodine (half-life: 15.7×10^6 y) and technetium (half-life: 0.21×10^6 y) at concentration levels of grams per tonne.

These radioactive by-products (see Table 1.2), although present at relatively low concentrations in the spent fuel, are a hazard to life forms when released into the environment. As such, their disposal requires isolation from the biosphere in stable deep geological formations for long periods of time.

Table 1.2. Radioactive isotope characteristics

Nuclide	**Half-life (years)**	**Specific activity**			**Dose coefficients (10^{-7} Sv/Bq)**
		(Ci/g)	**(W/g)**	**(Neutron min^{-1} mg^{-1})**	
^{237}Np	2.14×10^6	7.07×10^{-4}	2.07×10^{-5}	$< 7 \times 10^{-6}$	1.1
^{238}Pu	87.404	17.2	0.570	155	2.3
^{239}Pu	2.4413×10^4	6.13×10^{-2}	1.913×10^{-3}	1.35×10^{-3}	2.5
^{240}Pu	6 580	0.227	7.097×10^{-3}	53.7	2.5
^{241}Pu	14.98	99.1	4.06×10^{-3}		4.7
^{242}Pu	3.869×10^5	3.82×10^{-3}	1.13×10^{-4}	95.3	2.4
^{241}Am	432.7	3.43	0.1145	3.55×10^{-2}	2.0
^{242m}Am	144	10.3	3.08×10^{-2}		1.9
^{243}Am	7 370	0.200	6.42×10^{-3}		2.0
^{242}Cm	0.445	3.32×10^3	122	1.21×10^6	0.13
^{244}Cm	18.099	80.94	2.832	6.87×10^{-5}	1.6
^{245}Cm	8 265	0.177	5.89×10^{-3}		3.0
^{252}Cf	2.64	537	38.3	2.3×10^{12}	0.98

A measure of the hazard of these elements is provided by the *toxicity* and in particular the *radiotoxicity* arising from their radioactive nature rather than their chemical form. A reference point is the radiotoxicity associated with the raw material used to fabricate 1 tonne of enriched uranium, including not only the uranium isotopes but also all their radioactive progenies. The radiotoxicity of the fission products dominates the total radiotoxicity during the first 100 years. Thereafter, their radiotoxicity decreases and reaches the reference level after about 300 years. The long-term radiotoxicity is solely dominated by the actinides, mainly by the plutonium and americium isotopes (see Figure 1.2). The dose coefficients (in Sv/Bq) for most actinides, used to calculate the radiotoxicity, are also given in Table 1.2.

Figure 1.2. Radiotoxicity evolution in time and its components

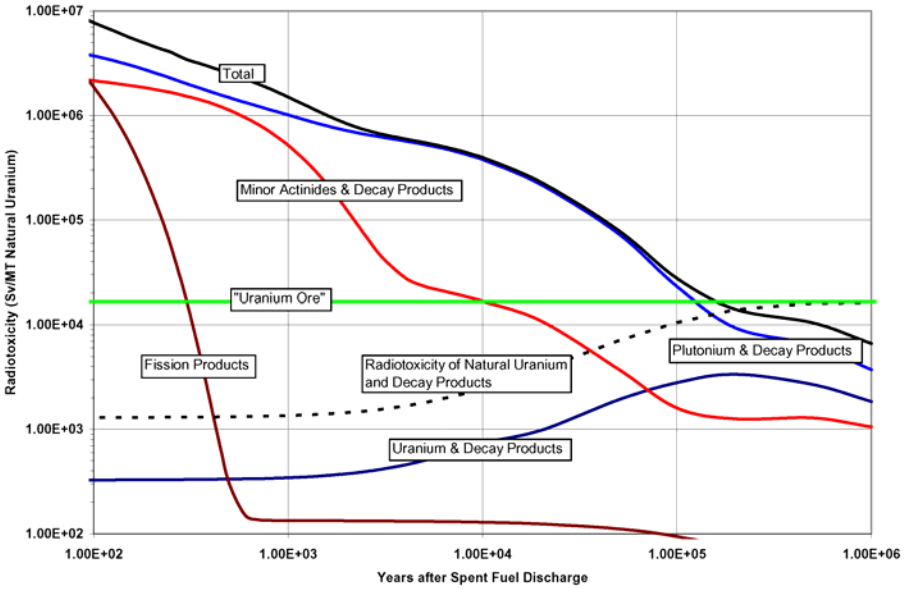

The reference radiotoxicity level is reached by spent nuclear fuel only after periods of more than 100 000 years.

Partitioning and transmutation is considered as a means of reducing the burden on a geological disposal. As plutonium and the minor actinides are mainly responsible for the long-term radiotoxicity, when these nuclides are removed from the waste (partitioning) and then fissioned (transmutation), the remaining waste loses most of its long-term radiotoxicity.

It can be shown (see Section 1.4), that the radiotoxicity inventory can be reduced up to a factor of 10 if all the Pu is recycled and fissioned. Reduction factors higher than 100 can be obtained if, in addition, the minor actinides (MAs) are burned. A prerequisite for these reduction figures is a nearly complete fissioning of the actinides, for which multi-recycling is a requirement. Losses during reprocessing and refabrication must be well below 1% and probably in the range of 0.1%.

Moreover, the partitioning and transmutation strategy allows in principle a combined reduction of the radionuclide masses to be stored, their associated residual heat, and, as a potential consequence, the volume and the cost of the repository (see Section 1.4).

Non-proliferation resistance of the overall fuel cycle, including the final repository, is also potentially enhanced by the same partitioning and transmutation strategies. In this field, although difficult to quantify, the proliferation risk is related to the mass of Pu in the overall fuel cycle and is a time-dependent function.

The drastic reduction of masses associated with partitioning and transmutation results in a drastic reduction of the proliferation risk, in particular if TRU are not separated from each other.

1.1.2 The physics basis of transmutation

The “transmutation” concept in a neutron field applies to the physical phenomena that transform a fresh fuel into an irradiated fuel.

The description of such phenomena is obtained by the solution of the set of Bateman equations (see Figure 1.3) which allow to obtain the vector of the nuclei densities $\overline{n}$ at a time $t = t_F$, starting from an initial value $\overline{n}_{t=t_0}$.

Figure 1.3. Paths of minor actinide formation in the U-Pu cycle

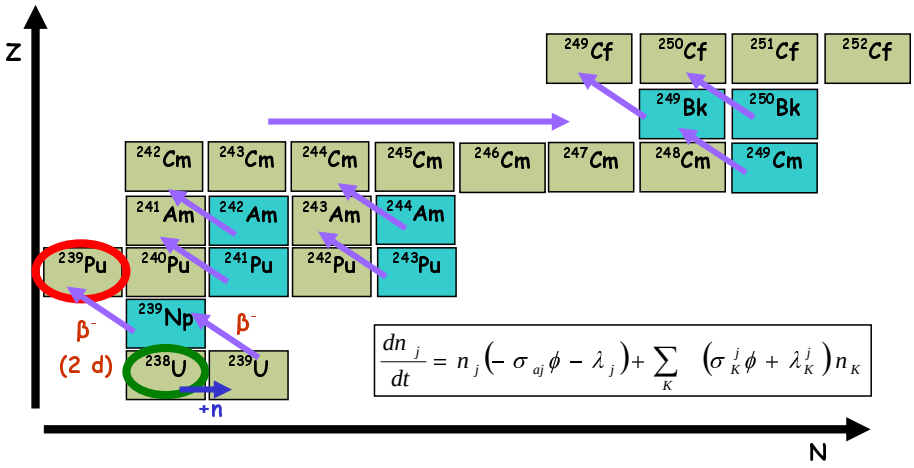

Any type of transmutation is a function of the neutron cross-sections and their spectral dependence. In the transmutation of nuclear wastes, the physics process to be privileged is obviously fission. The competition between the capture and fission processes is then of high relevance.

An inspection of ratios $\alpha = \overline{\sigma}_c / \overline{\sigma}_c$ of the average capture and fission cross-section of different isotopes (Table 1.3) shows the clear advantage of fast neutron spectra, where α values are the smallest.

Table 1.3. Average cross-section (barn): $\sigma = \int \sigma(E)\phi(E)dE \Big/ \int \phi(E)dE$

Isotope	PWR spectrum			Fast neutron spectrum		
	σ_f	σ_c	α	σ_f	σ_c	α
^{237}Np	0.52	33	63	0.32	1.7	5.3
^{238}Np	134	13.6	0.1	3.6	0.2	0.05
^{238}Pu	2.4	27.7	12	1.1	0.58	0.53
^{239}Pu	102	58.7	0.58	1.86	0.56	0.3
^{240}Pu	0.53	210.2	396.6	0.36	0.57	1.6
^{241}Pu	102.2	40.9	0.40	2.49	0.47	0.19
^{242}Pu	0.44	28.8	65.5	0.24	0.44	1.8
^{241}Am	1.1	110	100	0.27	2.0	7.4
^{242}Am	159	301	1.9	3.2	0.6	0.19
^{242m}Am	595	137	0.23	3.3	0.6	0.18
^{243}Am	0.44	49	111	0.21	1.8	8.6
^{242}Cm	1.14	4.5	3.9	0.58	1.0	1.7
^{243}Cm	88	14	0.16	7.2	1.0	0.14
^{244}Cm	1.0	16	16	0.42	0.6	1.4
^{245}Cm	116	17	0.15	5.1	0.9	0.18
^{235}U	38.8	8.7	0.22	1.98	0.57	0.29
^{238}U	0.103	0.86	8.3	0.04	0.30	7.5

For a full understanding of the transmutation potential of different neutron fields a new parameter has been defined [1], the neutron consumption/fission of isotope *J*, D_J.

The "neutron consumption/fission" D_J for nucleus *J* is defined as the number of neutrons needed to transform the nucleus and its reaction products into fission products.

To evaluate D_J, the following scheme can be set up for the nucleus *J* and its reaction products:

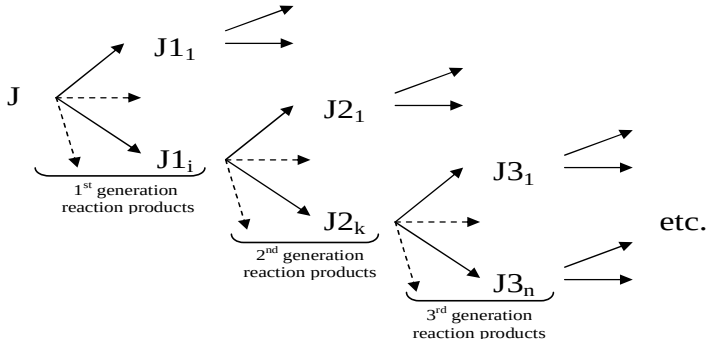

From that scheme, an algorithm [1] can be obtained:

$$D_J = \sum_{J1_i} P_{J \to J1_i} \left\{ R_{J1_i} + \sum_{J2_k} P_{J1_i} \to P_{J2_k} \; x \left[R_{J2_k} + \sum_{J3_n} P_{J2_k \to J3_n} x \ldots \right] \right\}$$

where $P_{JN_m \to J(N+1)_s}$ are probabilities (functions of neutron cross-sections) to transform JN_m into $J(N+1)_s$ and R_x is the neutron loss (or gain) due to the appearance of "*x*":

$$R_x = \begin{cases} 1 \text{ for a transmutation by neutron capture} \\ 0 \text{ for radioactive decay} \\ 1 - \nu \text{ for fission} \\ -1 \text{ for (n,2n) reactions} \\ \text{etc.} \end{cases}$$

Positive *D* means "consumption" and negative *D* means "production". For a mixture of isotopes:

$$D_{TRU} = \sum_J \varepsilon_J^{TRU} D_J^{TRU}$$

where ε_J^{TRU} are the fractions of the different transuranium isotopes present, e.g. in the irradiated fuel unloaded by a standard PWR. A D_{Pu} can be defined as:

$$D_{Pu} = \sum_J \varepsilon_J^{Pu} D_J^{Pu}$$

where ε_J^{Pu} and D_J^{Pu} are the corresponding fractions and *D* values for the Pu isotopes of, e.g. the same irradiated fuel.

The new "*D*" concept helps to understand if transmutation is feasible in a particular type of reactor. In fact, each reactor type is characterised by its neutron "energy spectrum" and by its neutron "economy balance" that we have defined as follows:

$$G = S_{ext} - D_{FUEL} - (L + CM)$$

where G is the neutron surplus (if $G > O$); S_{ext} is a potential external neutron source (e.g. in a source-driven system), expressed in neutrons/fission:

$$D_{FUEL} = \Sigma\, \varepsilon_i\, D_i$$

and i is the component of the nuclear fuel with ε_i fraction, $L + CM$ is the neutrons lost (per fission) due to leakage and "parasitic" captures in structural materials and fission products ($CM = C_{par} + C_{FP}$). If $G \geq O$, then transmutation is feasible in that particular system.

The hardest spectra are the most suitable, if, as we have indicated, fission is to be privileged. Inspection of Figures 1.4 and 1.5 makes this point clear. These figures show the fission cross-sections of the Am and Cm isotopes, respectively, most of them being of the threshold type.

1.1.3 The "equilibrium" e-method [2]

The standard Bateman equations can be generalised to account for the characteristics of specific fuel cycles and solved for the equilibrium concentrations of the actinide nuclides. This method computes the equilibrium composition and associated global neutron production potential of a simplified model of the nuclear reactor core if all "external" conditions (such as the neutron flux level, the fuel feed, the discharge and reprocessing rates) stay unchanged during sufficient time.

Figure 1.4. Fission cross-sections of americium isotopes in the mega-electron-volt region

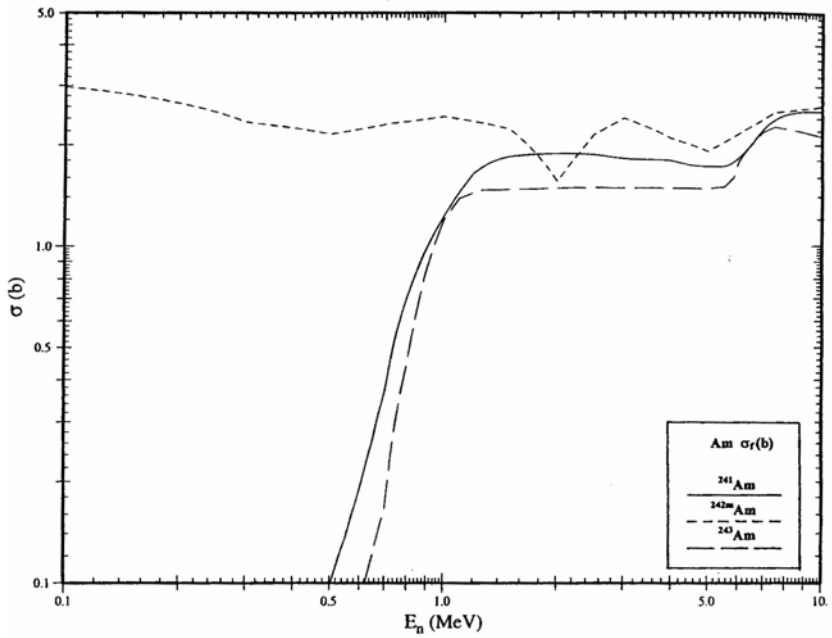

Figure 1.5. Fission cross-sections of curium isotopes in the mega-electron-volt region

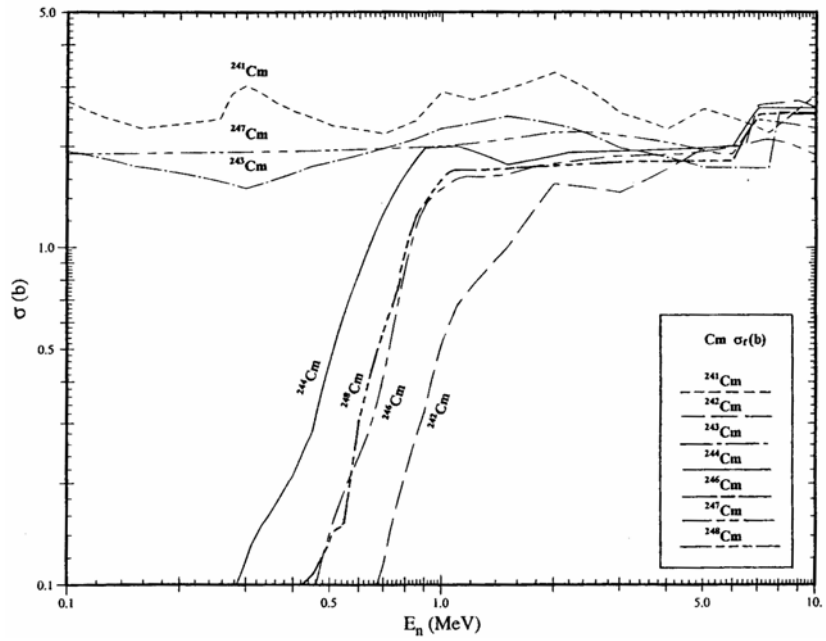

If a core is fed by a source S_j of *J*-nuclides, under neutron flux Φ, the fuel concentrations N_J the *J*-family are time-dependent and described by the following matrix-type GFC equation:

$$\frac{\overline{\partial N_J}}{\partial t} = \left(\hat{M} \times \Phi - \hat{\Lambda}_n - \hat{\Lambda}_{dl}\right) \overline{N}_J - \overline{S}_J \tag{1}$$

where $\overline{S}_J$ is the nuclei feed vector with a single non-zero component *J*, and $\overline{N}_J$ is the vector of the atomic concentrations of the *J*-family members, including its "father". $\hat{M}$ is the matrix related to all nuclear interaction processes, which is composed of the one-group absorption cross-section on the diagonal and off-diagonal terms representing the transmutation to different isotopes.

The $\hat{\Lambda}_n$ and $\hat{\Lambda}_{dl}$ terms in Eq. (1) are matrices of the family natural decays and of fuel discharge losses. The λ_{dl} elements of the matrix $\hat{\Lambda}_{dl}$ are defined by the ratio of nuclides loss (the transfer to a repository or reprocessing technology wastes, nuclear decay during fuel "cooling" time interval τ_{cool}) and it also depends upon the discharge "frequency" τ_{core}. A general expression λ_{dl} for each nuclide and for all fuel cycles is given by:

$$\lambda_{dl} = \frac{1}{\tau_{core}} \left\{ loss + (1 - loss)\left[1 - \exp\left(-\lambda_n \ \tau_{cool}\right)\right]\right\} \tag{2}$$

where "loss" could be assessed as the fraction of the nuclide inventory which is lost during reprocessing or sent to a repository (i.e. which does not return back to core) and the term $(1 - loss)\left[1 - \exp\left(-\lambda_n \ \tau_{cool}\right)\right]$ describes the isotopic decay during storage and processing. The asymptotic ($t \to \infty$) solution (if all operators are time independent) corresponds to the "equilibrium" case, i.e. when $\frac{\partial N}{\partial t} = 0$ in Eq. (1). This equilibrium solution can be presented in the following matrix

form: $\overline{N} = \hat{A}^{-1}\overline{S}$ where $\overline{S}$ includes all "father" nuclei contained in the core feed and $\hat{A} \equiv \hat{M} + \hat{\Lambda}_n + \hat{\Lambda}_{dl}$ as defined for Eq. (1). For this equilibrium actinide concentration in the core, the neutron balance can be computed for a specified composition consisting of *i*-components with proportions x_i:

$$-D_{eq}^{fuel} = \overline{\nu} - 1 - \overline{\alpha} \text{ (neutron/fission)} \tag{3}$$

where:

$$\overline{\nu} = \frac{\sum_i x_i\ \nu_i\ \sigma_i^f}{\sum_i x_i\ \sigma_i^f};\ \overline{\alpha} = \frac{\sum_i x_i\ \sigma_i^c}{\sum_i x_i\ \sigma_i^f}$$

The D_{eq}^{fuel} in Eq. (3) is consistent with the definition of Section 1.1.2.

1.1.4 Neutron balance (D-factor) intercomparison

The physics approach shown above can be used to compare standard PWRs (moderator-to-fuel ratio = 2) with MOX fuel with variation in the LWR moderator-to-fuel ratio, *r*, and also fast reactors with differing fuels and coolants. The *D* values for major actinides in Table 1.4 are for a closed fuel cycle for each individual TRU isotope with repeated recycle (no fuel cycle losses). In the case of LWRs, there is a significant dependence of the D_i on the level of the flux. This is also shown in Table 1.4, where the standard PWR D_i values are shown for two different flux levels (1×10^{14} and 2.5×10^{14} n/cm^2.s). This effect is due to the competition between absorption rates, which depend on the flux level, and decay (independent of the flux level).

Table 1.4. *D* (neutron consumption/fission) value for different isotopes in different systems

Isotope	MOX-LWR[1] r[2] = 1.4	MOX-LWR[1] r[2] = 2	MOX-LWR[4] r[2] = 2	MOX-LWR[1] r[2] = 4	He-cooled carbide fuel FR[3]	SUPER-PHENIX[3]	Lead-cooled nitride fuel FR[3]	Na-cooled oxide fuel FR[3]	Na-cooled metal fuel FR[3]
^{235}U	-0.31	-0.38	-0.43	-0.55	-0.84	-0.86	-0.92	-0.95	-1.04
^{238}U	0.104	0.068	-0.06	-0.007	-0.63	-0.62	-0.71	-0.79	-0.90
^{237}Np	0.91	0.93	0.75	0.96	-0.51	-0.56	-0.65	-0.73	-0.88
^{238}Pu	0.014	0.024	-0.16	0.038	-1.25	-1.33	-1.36	-1.41	-1.50
^{239}Pu	-0.60	-0.64	-0.79	-0.73	-1.44	-1.46	-1.58	-1.61	-1.71
^{240}Pu	0.65	0.56	0.14	0.38	-0.93	-0.91	-1.02	-1.13	-1.27
^{241}Pu	-0.26	-0.37	-0.80	-0.58	-1.25	-1.21	-1.26	-1.33	-1.39
^{242}Pu	1.27	1.22	0.73	1.13	-0.65	-0.48	-0.73	-0.92	-1.13
^{241}Am	0.92	0.93	0.71	0.95	-0.56	-0.54	-0.65	-0.77	-0.91
^{242m}Am	-1.55	-1.56	-1.66	-1.56	-2.03	-1.87	-2.08	-2.10	-2.16
^{243}Am	0.44	0.36	-0.15	0.25	-0.84	-0.65	-0.85	-1.01	-1.15
^{242}Cm	0.004	0.014	-0.18	0.026	-1.26	-1.34	-1.37	-1.41	-1.51
^{244}Cm	-0.51	-0.60	-1.12	-0.71	-1.54	-1.44	-1.53	-1.64	-1.71
^{245}Cm	-2.46	-2.46	-2.44	-2.44	-2.70	-2.69	-2.71	-2.74	-2.77

(1) ∅ = 1 × 10^{14} n/cm^2.s
(2) r = moderator-to-fuel ratio
(3) ∅ = 1 × 10^{15} n/cm^2.s – sodium-cooled burner configuration, GFR and LFR conventional concepts
(4) ∅ = 2.5 × 10^{14} n/cm^2.s

The results allow comparison of the feasibility of transmutation of the different isotopes in each reactor concept. As an example, in the case of the Am isotopes, the ^{241}Am transmutation is a neutron-consuming process in any LWR concept, relatively independent of the moderator-to-fuel ratio (r). For a flux value of 1×10^{14} n/cm^{2}s, ^{243}Am is also a neutron-consuming process in a LWR, but a higher r value is preferable because the corresponding D value is positive but smaller than with lower values of r. However, at $\phi = 2.5 \times 10^{14}$ n/cm^{2}s, the transmutation of ^{243}Am becomes a neutron production process. ^{242}Am transmutation is a neutron-production process, whatever the spectrum, with a slight advantage for fast neutron spectra.

Significant variations in the D-factor are observed between the fast reactor concepts. In general, a harder neutron spectrum leads to a more favourable neutron balance; thus, the metal-fuelled SFR provides the most excess neutrons for every actinide isotope. However, all of the fast reactor systems exhibit a significantly more favourable neutron balance compared to the MOX-LWR results.

1.2 Intercomparison of specific concepts and fuel cycle systems

The physics approach described in Section 1.1.3 allows comparing a large variety of fuel cycle strategies. Three significant scenarios are provided.

1.2.1 PU multi-recycling in LWRs

In this case, plutonium is multi-recycled in PWRs using the MOX-UE concept [3]. Minor actinides (MAs) are separated at the end of each cycle and sent to a repository, as illustrated in Figure 1.6. It is assumed that uranium is discharged and not further recycled. The mass of U + Pu loaded in the core is 2.0425 t/TWhe and the mass of fission product build-up is 0.125 t/TWhe. In this strategy, the average Pu content of fresh fuel is fixed at the maximum targeted value of 10% and ^{235}U is added to maintain criticality; the average burn-up is set at 60 GWd/MT. The feed requirement at equilibrium is chosen such that the fixed Pu content (10%) is preserved. The ^{235}U enrichment in the feed is determined by the criticality condition:

$$-D_{FUEL} - (L_{core} + C_{par} + C_{FP}) = 0$$

with a total loss of neutrons per fission ($L_{core} + C_{par} + C_{FP}$) estimated at 0.38; thus, $D_{fuel}^{eq} \simeq 0.38$ is needed.

Figure 1.6. Scheme for Pu multi-recycling in a PWR with burn-up equal to 60 GWd/t

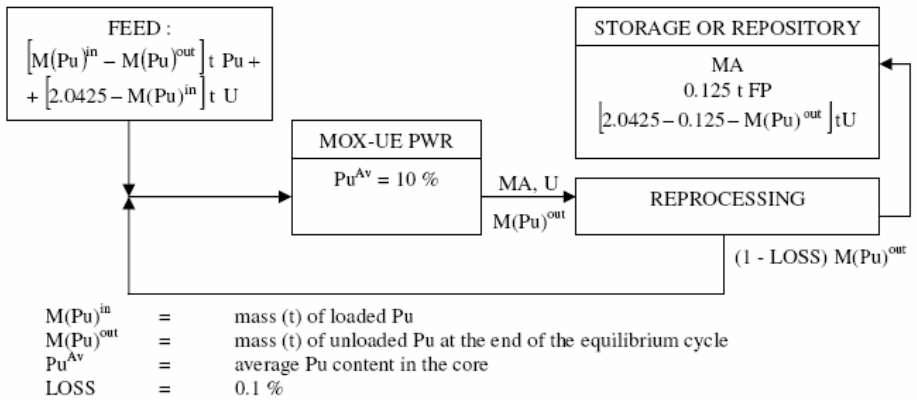

The neutron balance and mass flow results are shown in Table 1.5 for the same three moderator-to-fuel ratios evaluated in Table 1.4. The results show an increase in Pu consumption by a factor of ~3 from 38 kg/TWh to 108 kg/TWh as the moderator-to-fuel ratio is increased. However, the MA build-up roughly doubles from 13.9 to 24.8 kg/TWh as the moderator-to-fuel ratio is increased; the Cm build-up is particularly evident (10.6 kg/TWh) when the neutron spectrum is over-moderated (r = 4). Overall, the ratio of the quantity of Pu burned over that of MA produced is clearly in favour of high moderator-to-fuel ratio. The feed values also show the reduced need for ^{235}U enrichment in cores with high moderator-to-fuel ratios.

Table 1.5. Plutonium multi-recycling in MOX-UE PWRs

	Closed cycle for Pu – average Pu content 10%		
	***r* = 1.4**	***r* = 2**	***r* = 4**
Pu/U + Pu in feed	2.00%	3.03%	5.67%
U5/U in feed	5.90%	4.90%	2.53%
D_{fuel}	-0.380	-0.380	-0.380
D_{fuel}^{void}	-0.416	-0.316	+0.016
M(Pu)^{in} (kg/TWhe)	217	226	252
M(Pu)^{out} (kg/TWhe)	179	170	144
ΔM(Pu) (kg/TWhe)	38	56	108
Pu$^{(in)}$ (%)	10.6%	11.1%	12.3%
Pu$^{(out)}$ (%)	8.78%	8.30%	7.06%
MA$^{(in)}$ (kg/TWhe)	0	0	0
MA$^{(out)}$ (kg/TWhe)	13.9	17.1	24.8
Np$^{(out)}$ (kg/TWhe)	1.50	1.38	0.901
Am$^{(out)}$ (kg/TWhe)	8.40	9.89	13.4
Cm$^{(out)}$ (kg/TWhe)	3.97	5.87	10.6
ΔM(Pu)/ ΔM(MA)	2.73	3.27	4.35

r = moderator-to-fuel ratio

1.2.2 Pu and MA multi-recycling in LWRs

A similar fuel cycle approach to that shown in Figure 1.6 can be applied for multi-recycling of the minor actinide species in addition to the Pu in a MOX-UE PWR with moderator-to-fuel ratio of two. Successive cases are analysed with Pu + Np, Pu + Np + Am, and Pu + Np + Am + Cm recycle. In each case, the average content of Pu + MA in the core is set at 10% (7.7% Pu and 2.3% MA when all MA are recycled: 0.3% Np, 0.6% Am and 1.4% Cm). The results are shown in Table 1.6.

To counterbalance the "poison" effect of MA, a higher percentage of ^{235}U is needed with Np and Am recycle; the enrichment steadily increases from 4.9% with Pu recycle (Table 1.6) to 6.45% (Pu + Np) to 9.0% (Pu + Np + Am). A reverse trend is observed (down to 6.45% ^{235}U enrichment) when the Cm is also recycled. However, *note that the MA inventory is dominated by Cm when all MA elements are recycled;* and this fuel would be very difficult to handle. The Pu consumption is drastically reduced from 56 kg/TWh for Pu recycle to 43 with Np recycle to ~20 with Pu + MA recycle, and 0 with Pu + Np + Am. This behaviour is attributed to the transmutation of some of the MA isotopes (especially ^{241}Am and ^{237}Np) into Pu isotopes. The minor actinide production is reduced from 17 kg/TWh (Table 1.5) to 10 with Np recycle and 4 in the Am recycle case. However, only with full MA recycle can the MA inventory be stabilised, with the in-core destruction balanced by the ^{241}Pu decay source during recycle. However, as indicated previously the high Cm content of this case will severely complicate fuel handling.

Table 1.6. Pu + MA multi-recycling in MOX-UE PWRs

	Closed cycle for Pu + Np, avg. Pu + Np content ~10%, MOX-UE with r = 2	Closed cycle for Pu + Np + Am, avg. Pu + Np + Am content ~10%, MOX-UE with r = 2	Closed cycle for Pu + MA, avg. Pu + MA cont. 10%, MOX-UE with r = 2
Pu/(U + Pu + MA) in feed	2.31%	1.64%	1.10%
MA/(U + Pu + MA) in feed	0.17%	0.22%	0.16%
U5/U in feed	6.45%	9.0%	6.45%
D_{fuel}	-0.380	-0.380	-0.380
D_{fuel}^{void}	-0.343	-0.397	-0.299
$M(Pu)^{in}$ (kg/TWhe)	211	190	163
$M(Pu)^{out}$ (kg/TWhe)	168	189	142
ΔM(Pu) (kg/TWhe)	43	1	21
$Pu^{(in)}$ (%)	10.3%	9.3%	8.0%
$Pu^{(out)}$ (%)	8.2%	9.3%	6.9%
$MA^{(in)}$ (kg/TWhe)	10.5	26.2	47.7
$MA^{(out)}$ (kg/TWhe)	20.4	30.4	44.5
$Np^{(in)}$ (kg/TWhe)	10.5	10.1	7.2
$Np^{(out)}$ (kg/TWhe)	7.1	7.7	5.6
$Am^{(in)}$ (kg/TWhe)	0.0	16.2	13.1
$Am^{(out)}$ (kg/TWhe)	8.4	14.2	11.8
$Cm^{(in)}$ (kg/TWhe)	0.0	0.0	27.3
$Cm^{(out)}$ (kg/TWhe)	4.9	8.5	27.1
ΔM(Pu)/ΔM(MA)	4.34	0.24	-6.56

r = moderator-to-fuel ratio

Another important indicator of the feasibility of the different recycling options is given by the Pu vector at equilibrium, as shown in Table 1.7. An inspection of the results indicates a strong increase of the ^{238}Pu content when any MA is recycled; and the fuel cycle consequences of associated increases in decay heat must be investigated.

Table 1.7. Plutonium vectors at equilibrium (%) in MOX-UE cases with r = 2

Pu isotope	Closed cycle for Pu	Closed cycle for Pu + Np	Closed cycle for Pu + Np + Am	Closed cycle for Pu + MA
^{238}Pu	7.5	12.8	16.6	15.1
^{239}Pu	34.3	32.7	33.9	35.6
^{240}Pu	24.9	22.2	22.0	22.5
^{241}Pu	16.1	14.1	13.6	13.6
^{242}Pu	17.2	14.5	13.9	13.1

1.2.3 PU and PU + MA recycling in fast reactors

The following cases can be compared in the case of fast reactors:

- Pu and Pu + MA multi-recycling in a sodium-cooled oxide-fuelled burner reactor, as considered in Section 1.1.4. The feed is a mixture of Pu and natural U.

- Pu and Pu + MA multi-recycling in the sodium-cooled SUPERPHENIX-type reactor self-sustaining regime with a Pu (or Pu + MA) recycle. The feed is natural U.

The results are summarised in Table 1.8. Significant Pu burning (53 kg/TWhe) is obtained in the burner case together with a limited MA production (6.75 kg/TWhe). These features can be compared with the LWR cases (Table 1.5). In the case of standard MOX-UE, a comparable Pu consumption (56 kg/TWhe) induces a much higher (factor ~3) MA production, in particular Cm. The higher Pu consumption of a MOX-UE with r = 4 (108 kg/TWhe), induces an even higher MA production, and Cm production is increased by more than a factor 10 compared to the Pu-burner fast reactor case.

Table 1.8. Pu and Pu + MA multi-recycling in fast reactors

	Oxide Na-cooled burner, avg. Pu content 35%	Oxide Na-cooled burner, avg. Pu + MA content 35%	SUPERPHENIX-type, self-sustaining Pu regime, avg. Pu content 16.1%	SUPERPHENIX-type, self-sustaining Pu + MA regime, avg. Pu + MA content 16.9%
Pu/(Pu + U + MA) in feed	54.3%	42.1%	0	0
MA/(Pu + U + MA) in feed	0%	6.0%	0	0
D_{fuel}	-1.162	-1.089	-0.796	-0.801
D_{voided}	-1.252	-1.190	-0.914	-0.919
$M(Pu)^{in}$ (kg/TWhe)	286	247	127	124
$M(Pu)^{out}$ (kg/TWhe)	233	206	127	124
$\Delta M(Pu)$ (kg/TWhe)	53	41	0	0
$Pu^{(in)}$ (%)	36.2%	31.3%	16.1%	15.7%
$Pu^{(out)}$ (%)	29.5%	26.2%	16.1%	15.7%
$MA^{(in)}$ (kg/TWhe)	0	35.8	0	4.69
$MA^{(out)}$ (kg/TWhe)	6.75	29.9	1.36	4,69
$Np^{(in)}$ (kg/TWhe)	0	7.19	0	0.939
$Np^{(out)}$ (kg/TWhe)	0.354	4.27	0.389	0.939
$Am^{(in)}$ (kg/TWhe)	0	18.4	0	2.77
$Am^{(out)}$ (kg/TWhe)	5.47	16.0	0.875	2.77
$Cm^{(in)}$ (kg/TWhe)	0	10.1	0	0.979
$Cm^{(out)}$ (kg/TWhe)	0.930	9,69	0.097	0.979
$\Delta M(Pu)/\Delta M(MA)$	7.85	-6.96	0	0

In the case of a Pu + MA burner, the fast reactor considered can burn 41 kg/TWhe of Pu and 5.9 kg/TWhe of MA. In the corresponding case, a MOX-UE with r = 2 (Table 1.6), the Pu consumption is drastically reduced (21 kg/TWhe) and the MA consumption is only 3.2 kg/TWhe. The Cm inventory is higher by a factor of ~3 in the MOX-UE with respect to the fast burner case.

An important distinction of the second set of fast reactor cases (self-sustaining) is the ability to operate at equilibrium with a natural uranium-only feed. This is possible due to the large neutron surplus, -0.8 to -1.2 in a fast spectrum, avoiding the need for fissile make-up. Furthermore, the build-up of minor actinides is quite small, roughly an order of magnitude less than the thermal reactor cases in Table 1.5.

1.2.4 Homogeneous and heterogeneous recycling and their consequences on the fuel cycle

1.2.4.1 Homogeneous recycling [4]

The "homogeneous" recycling mode consists of a system capable to recycle not-separated Pu and minor actinides (MA), to reach equilibrium, stabilising both Pu and MA mass flows, and sending to the wastes only a very small fraction of the radiotoxic isotopes (losses at reprocessing).

The appealing aspects of the "homogeneous" recycle are:

- The concept is mainly designed to produce energy, making an optimised use of resources and using a robust reactor and fuel cycle layout.
- The fuel cycle does not imply the separation of Pu and MA.
- The concept can accommodate in principle several options in terms of reactor size and fuel, reactor coolant, waste forms, etc.

In general, homogeneous recycling has equivalent performances for whatever the type of fuel in the fast reactor. In fact, if the losses at reprocessing are assumed to be of the order of 0.1%, homogeneous recycling allows to reach a reduction of the potential radiotoxicity with respect to the open cycle scenario by a factor of 200 and more, and this over the entire time scale ($10^2 \rightarrow 10^6$ years), as will be shown in Section 1.4.2. This reduction is such that the radiotoxicity in deep geological storage becomes comparable to that of the initial uranium ore, after less than a thousand years

One can also envisage a multi-recycle of both Pu and MA in PWRs. However, even if a specific core assembly design can in principle allow acceptable core performances, the impact on the fuel cycle (e.g. at fuel fabrication) should be taken into account. In fact nuclei evolution under irradiation has to be evaluated, accounting for very high mass nuclei production.

Table 1.9 shows the increase of decay heat, γ and neutron doses, when a multiple recycle is performed in a LWR, loaded with Pu and minor actinides. The presence of Cm in the fuel is at the origin of the observed results, and this effect is related to the very high capture cross-sections of actinides in a thermal neutron spectrum. In fact, most of the neutron source comes from the build-up of ^{252}Cf, which is much higher in a thermal spectrum reactor with respect to a fast spectrum one, as shown in Figure 1.7.

To overcome this potential difficulty, a compromise must be reached in terms of minor actinides to be recycled, the number of recyclings and the mode of recycling.

The obvious first step is to limit the recycling to Am and Pu. The Cm initially produced in UOX-PWRs and further produced during the multi-recycling of Pu and Am should be managed separately.

Table 1.9. Impact on some fuel cycle parameters of the multiple recycle of all TR in an LWR

Fuel cycle parameter(1)	**Increase factor**(2)	**Comments**(3)
Decay heat	~10	^{244}Cm ~70%; ^{238}Pu ~30%
Neutron source	~5 000	^{252}Cf ~90% – if cooling time = 20 years, ^{252}Cf ~40%, the rest is due to ^{244}Cm; ^{250}Cf, ^{250}Cm, ^{246}Cm, ^{248}Cm
Gamma source	~10	^{241}Am, ^{244}Cm, ^{238}Pu, ^{252}Cf, ^{243}Cm are major contributors

(1) *At fuel loading of seventh cycle, after fabrication and 5 years cooling.*
(2) *Increase in parameter, taken as the ratio to the corresponding parameter in a Pu-only MOX-LWR.*
(3) *When Pu only is multi-recycled in MOX-LWR, ^{238}Pu is the major contributor to all parameters.*

Figure 1.7. ^{252}Cf inventory comparison

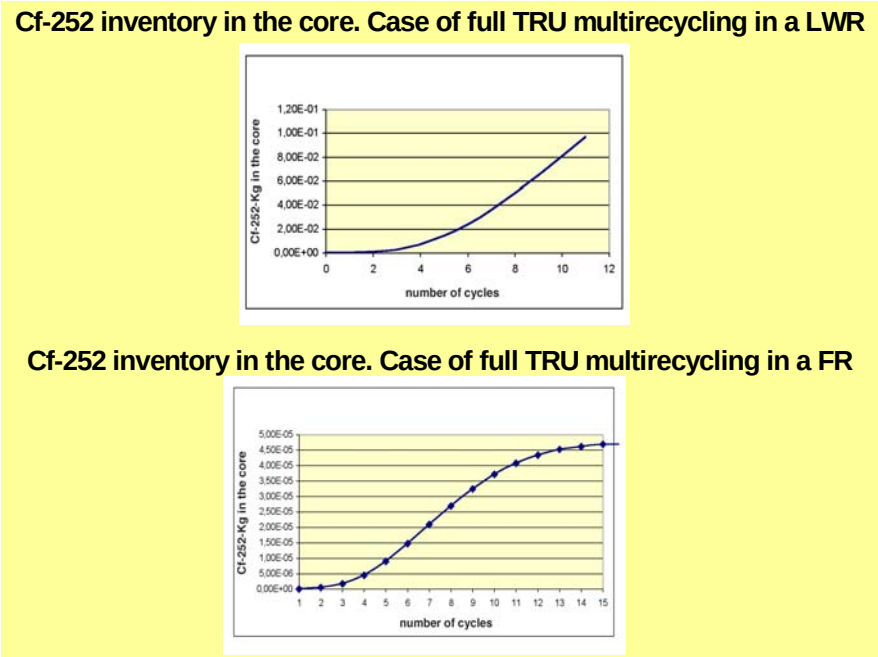

One possibility, explored several years ago and reported in *Evaluation of Possible P&T Strategies and Means to Implement Them* [EUR 19128 EN (2000)], is to store the Cm temporarily, waiting for its decay in order to process it further to separate the Pu produced by decay (see Figure 1.8), which can be successively transferred to future fast reactors or future dedicated systems. We will come back to this scenario in Section 1.4.

Figure 1.8. Cm decay in intermediate storage

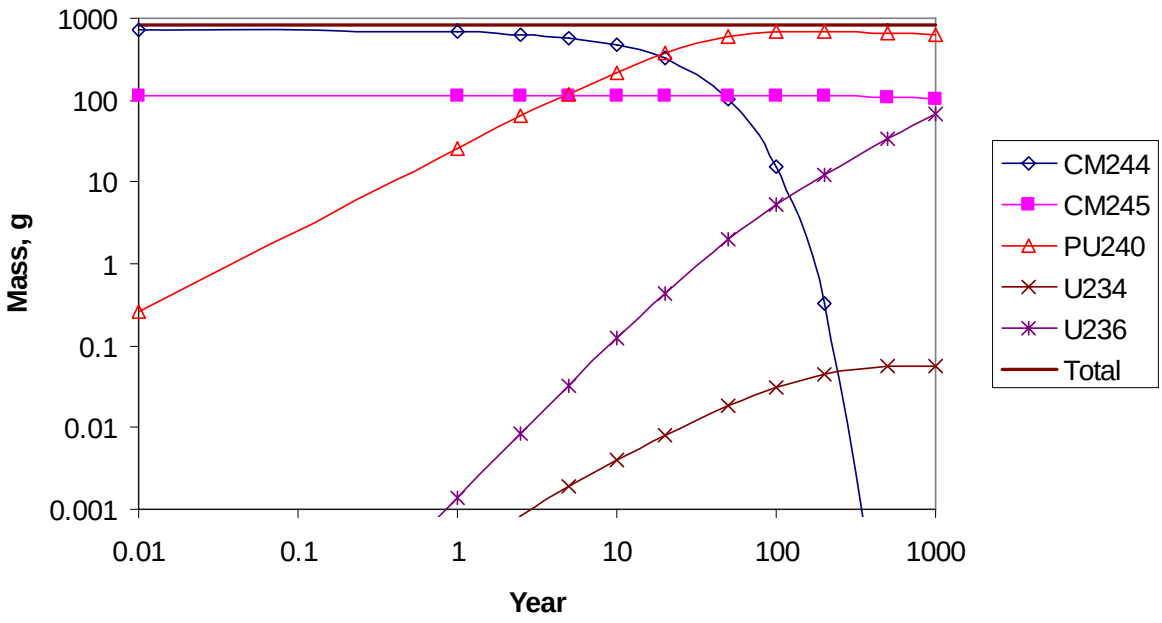

1.2.4.2 Heterogeneous recycling

That option, explored, mainly in Europe [5] and at JNC in Japan [6], consists in performing the transmutation of MA in the form of targets to be loaded in critical cores of a "standard" type. The mode of recycling has been called "heterogeneous", the potential advantage being to concentrate in a specific fuel cycle the handling of a reduced inventory of MA (separated from plutonium). The major obstacles to this approach are:

- The very high irradiation time needed to fission a significant ($> 90 \div 95\%$) amount of MA (which implies very high damage rates).
- The need to separate Am and Cm from Pu and to keep them (Am and Cm) together, in order to reach high values (~30) for the radiotoxicity reduction.
- The need to load the MA targets in a very large fraction ($\sim 30 \div 50\%$) of the reactor park, possibly made of fast reactors, which provide high neutron fluxes and can be easily tailored in energy to increase fission rates.
- Control of the power distributions and their evolution with time. In fact, local variations of the power can be significant, creating high gradients which can evolve strongly with time.
- As far as targets, the minor actinide matrix support can be U-free (e.g. MgO) or can be U itself. This last approach could be the most favourable one, in terms of target fabrication and, if needed, reprocessing.

The most relevant point is represented by the fact that, for heterogeneous recycling the limiting factor is the fission rate value which can be reached under realistic conditions, and for homogeneous recycling the limiting factor is the separation chemistry performance.

Finally, the presence of Cm in the targets will have a strong impact on the target fabrication, as is shown in Table 1.10.

Table 1.10. Influence of Cm for target fabrication

Material in the target	100% Am	90% Am + 10% Cm	80% Am + 20% Cm
Heat	1[(a)]	× 2.3	× 3.6
γ dose at 1 m	1	× 1.5	× 2
Neutronic source	1	× 120	× 240

[(a)] *Reference value.*

1.3 Dedicated systems and the role of ADS [7]

A possible approach to keep the MA fuel cycle and the transmutation technology separated from the electricity production, is the one which calls for the use of "dedicated" cores, where the fuel is heavily loaded with MA, the rest being plutonium. In principle critical "dedicated" cores can have difficulties related to the degradation of safety parameters. In particular, these cores can present a very low delayed neutron fraction ($< 0.2\%$ $\Delta k/k$) due to the low delayed neutron fraction of Am, Cm, Np (see Table 1.11), and a reduced Doppler effect (due to the absence of a fertile isotope like ^{238}U). These characteristics have helped to promote the concept of accelerator-driven subcritical systems (ADS)

Table 1.11. Delayed neutron fractions β for selected nuclei

Nuclide	β
^{238}U	0.0172
^{237}Np	0.00388
^{238}Pu	0.00137
^{239}Pu	0.00214
^{240}Pu	0.00304
^{241}Pu	0.00535
^{242}Pu	0.00664
^{241}Am	0.00127
^{243}Am	0.00233
^{242}Cm	0.000377

and the so-called "double strata" fuel cycle concept which will be described in Section 1.4. In fact, ADS systems offer the feature of the subcriticality ($k_{eff} \simeq 0.95 \div 0.99$), to overcome some of the drawbacks due to low β_{eff} and low Doppler effect.

In order to develop an idea of the characteristics of a typical ADS, certain simplified considerations can be made as discussed below.

Hypothesis

- Proton beam energy E_p = 600 MeV.
- Heavy metal spallation target providing $z = \frac{\text{neutrons}}{\text{proton}} = 16$.
- Γ (number of neutrons/fission produced in the core due to the external source, if all the energy produced in it is used to feed the accelerator) = 1.06.
- Thermal power of the accelerator-driven core W = 500 MWt.
- Minor actinide/Pu ratio in the fuel ~1, to which corresponds a Δk/cycle $\simeq$1%/Δk/k/year and $\beta_{eff} \simeq$ 0.15%/Δk/k
- φ* (ratio of the importance of the source neutrons to the importance of fission neutrons) $\simeq$1.

Energy requirements

The fraction f of energy produced in the subcritical core used for feeding the accelerator depends on the subcriticality level:

$$f \simeq \frac{\nu}{\Gamma}\frac{1-k}{k}$$

If ν (average number of prompt fission neutrons per fission) = 2.8, one has:

f = 2.6% if 1 – k = 0.01
f = 5.3% if 1 – k = 0.02
f = 13% if 1 – k = 0.05

Current (power) of the proton beam i_p (W_p)

If E_f (energy released/fission) ~200 MeV, then:

$$i_p \simeq \frac{\Gamma}{z} W \frac{1}{E_f} \begin{cases} 4.3 \text{ mA} & \text{if } 1-k = 0.01 \\ 8.6 \text{ mA} & \text{if } 1-k = 0.02 \\ 22 \text{ mA} & \text{if } 1-k = 0.05 \end{cases}$$

which correspond, respectively, to:

$$W_p = \begin{cases} 2.5 \text{ MWt} \\ 5 \text{ MWt} \\ 12.5 \text{ MWt} \end{cases}$$

A few comments on the outcome of these simplified evaluations:

- The subcriticality level choice is a crucial parameter.
- In fact, it is probably difficult to envisage a deep subcriticality level (e.g. k < 0.95), in view of the demanding characteristics of the required accelerator (> 12.5 MWt in the beam) and the cost of the energy to feed it.
- The appropriate choice of the minor actinide/Pu ratio can help to optimise the reactivity swing during irradiation (down to ≤ 1%/Δk/k), and reduce the accelerator current requirement.
- The stringent requirements in terms of accelerator reliability have to be met whatever the type of the accelerator-driven system.
- If the subcritical level is chosen in the range k = 0.97 ÷ 0.98, it will be very relevant to demonstrate the safe operation of an accelerator-driven system in the “transition” from “source-dominated” to “feedback-dominated” regime.
- The continuous and effective monitoring of the subcriticality level will be mandatory, and appropriate experimental techniques should be developed and demonstrated.

1.4. Implementation of P&T

1.4.1 Major scenarios

One can define four major scenarios to implement P&T:

a) Sustainable development of nuclear energy with waste minimisation. One type of reactor, one fuel type, one reprocessing process (see Figure 1.9).

b) "Double-strata" fuel cycle [8]: 1) commercial reactors with Pu utilisation 2) separate MA management. Two separate fuel cycles (see Figure 1.10). This is the typical scenario using ADS.

c) Temporary scenario using existing reactors with a partial management of MA (e.g. in case of delay in implementation of scenario a) [see Figure 1.11].

All three previous scenarios imply the continuous use of nuclear energy, the stabilisation of the TRU stocks in the fuel cycle and the minimisation of wastes in a repository.

d) Reduction of TRU stockpiles (e.g. as a legacy from the past operation of power plants; see Figure 1.12).

All four scenarios go beyond the strategy of "once-through" ("open") fuel cycle (i.e. the final storage of irradiated fuel), and imply fuel reprocessing.

As far as scenario a), it can be implemented in Gen-IV fast reactors, with homogeneous recycling of not-separated TRU (Pu *and* MA). It allows a drastic minimisation of ultimate wastes in terms of volume, radiotoxicity and heat load (see Section 1.4.2). It preserves resources (Pu is an essential resource) and provides enhanced resistance to proliferation (Pu and MA are kept together).

As far as scenario b), the main interest is to keep the management of MA independent from the commercial fuel cycle. The expected reduction of radiotoxicity is similar to that expected in scenario a), if the separation performance (e.g. losses during reprocessing, or TRU recovery rate) is approximately the same in the two scenarios. The implementation of this scenario will be described in detail in Chapter 2.

Figure 1.9. Scenario a): Reference scenario for sustainable development of nuclear energy with waste minimisation

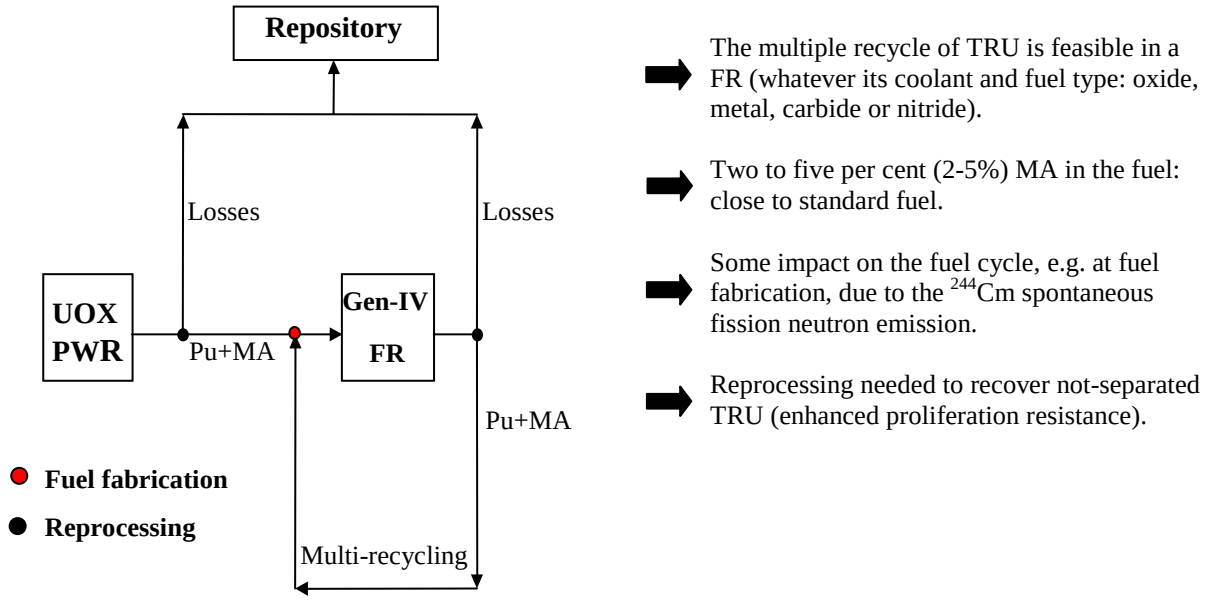

Figure 1.10. Scenario b): "Double strata" – Pu still a resource, Gen-IV FR deployment delayed

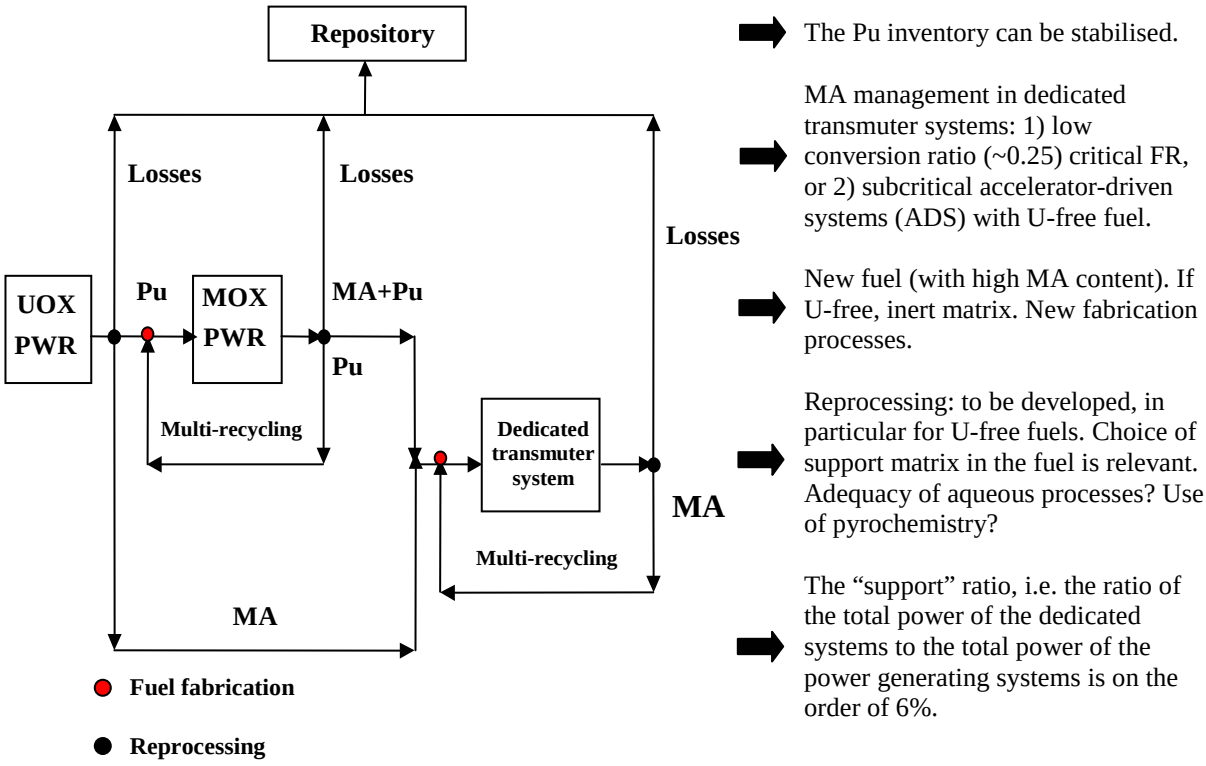

Figure 1.11. Scenario c): Temporary scenario before Gen-IV FR deployment

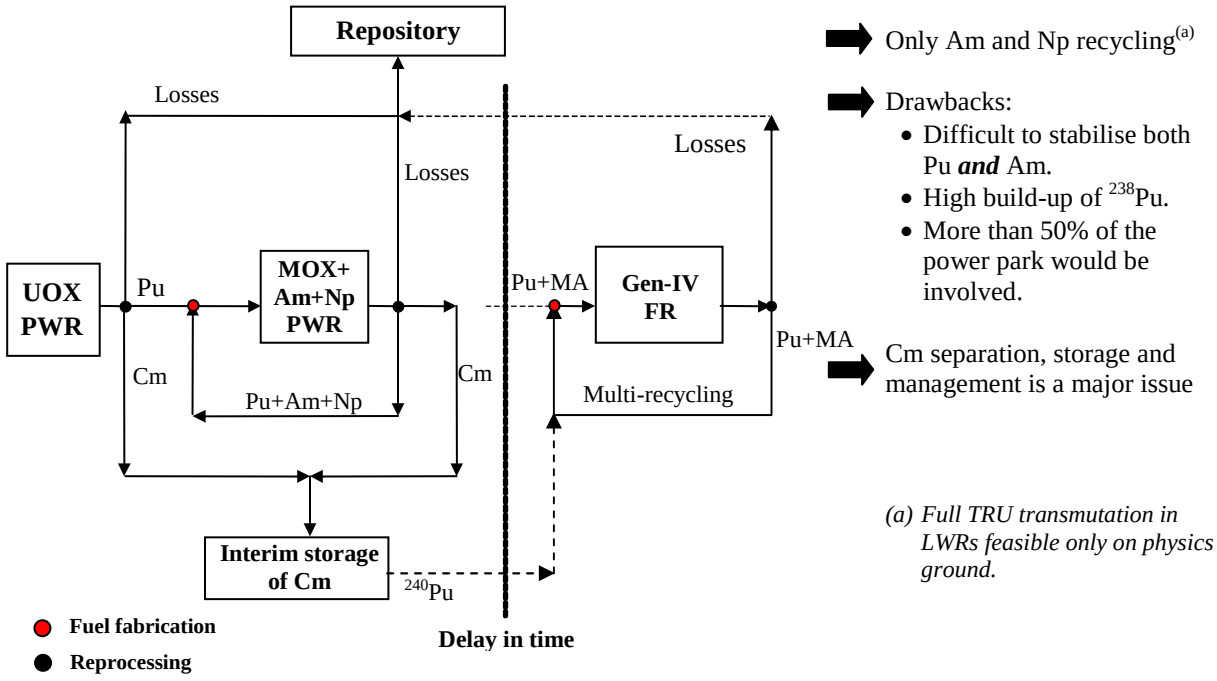

Figure 1.12. Scenario d): Reduction of Pu + MA stockpile (Pu considered as waste)

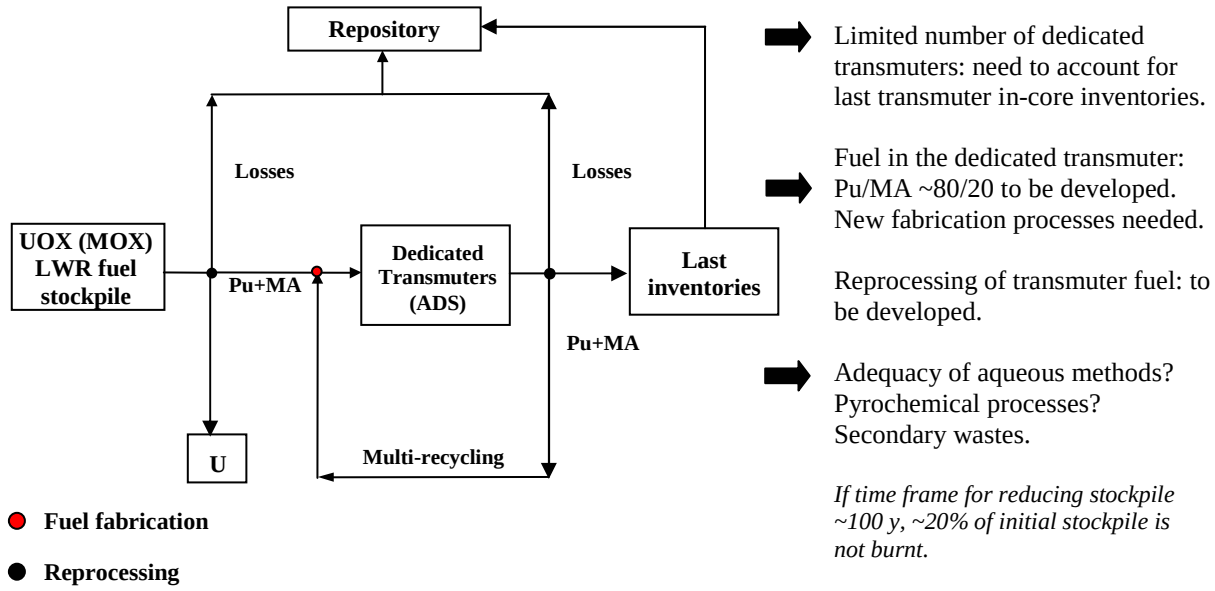

In fact, the "second" strata transmuter will have a core with a U-free, MA-dominated fuel. Such a type of core can present unacceptable safety features, and core subcriticality can offer a potential solution.

As far as scenario c), two major points have already been underlined (see Section 1.2.4.1):

1. The recycling of MA should be limited to Np and Am, since the full TRU recycling (i.e. including Cm), even if theoretically possible from the physics point of view, has an unacceptable impact on the fuel cycle, e.g. at fuel refabrication. In fact, the build-up of ^{252}Cf (see Figure 1.7, where the ^{252}Cf build up is compared in a LWR and in a FR) gives rise to a neutron source (due to its spontaneous fissions, see Table 1.2) which is ~10^4 times higher than the neutron source at the refabrication of standard MOX fuel.

2. If Cm is not recycled, it is necessary to implement the separation of Am and Cm (both at valence III) and to manage the storage of Cm, which should last more than hundred years, to allow it to decay (in ^{240}Pu). These extra installations of the fuel cycle are not straightforward to design and can have relevant cost and environmental impact.

Finally, scenario d) offers a potential means of reducing stockpiles of Pu and MA in spent fuel, e.g. in the case of phase-out of nuclear power plants. However, this scenario implies a substantial deployment of new installations (fuel reprocessing and fabrication, ADS). This point will be illustrated in Chapter 2.

1.4.2 Potential benefits of P&T

P&T offers significant potential benefits to the fuel cycle:

- Reduction of potential source of radiotoxicity in deep geological storage ("intrusion" scenario).
- Reduction of the heat load: larger amount of wastes can be stored in the same repository.
- If TRU are not separated (e.g. in the homogeneous recycling in a fast neutron reactor), improved proliferation resistance is expected.

Examples related to each point are given in Figures 1.13, 1.14 and 1.15.

Figure 1.13 shows that, as for as radiotoxicity, the same reduction is obtained with a reactor park where homogeneous recycling is performed (in fast reactors or in thermal reactors) or with a reactor park of the double-strata type, if the same performance of the chemical separations (e.g. recovery factors at all reprocessing steps and installations, of the order of 99.9% for Pu and $\leq$ 99.5% for MA) is assumed. The reduction is such that, at equilibrium, the potential radiotoxicity of the wastes sent to a repository is reduced to the level of the radiotoxicity of the initial uranium ore, after <1 000 years.

Figure 1.13. Radiotoxicity reduction

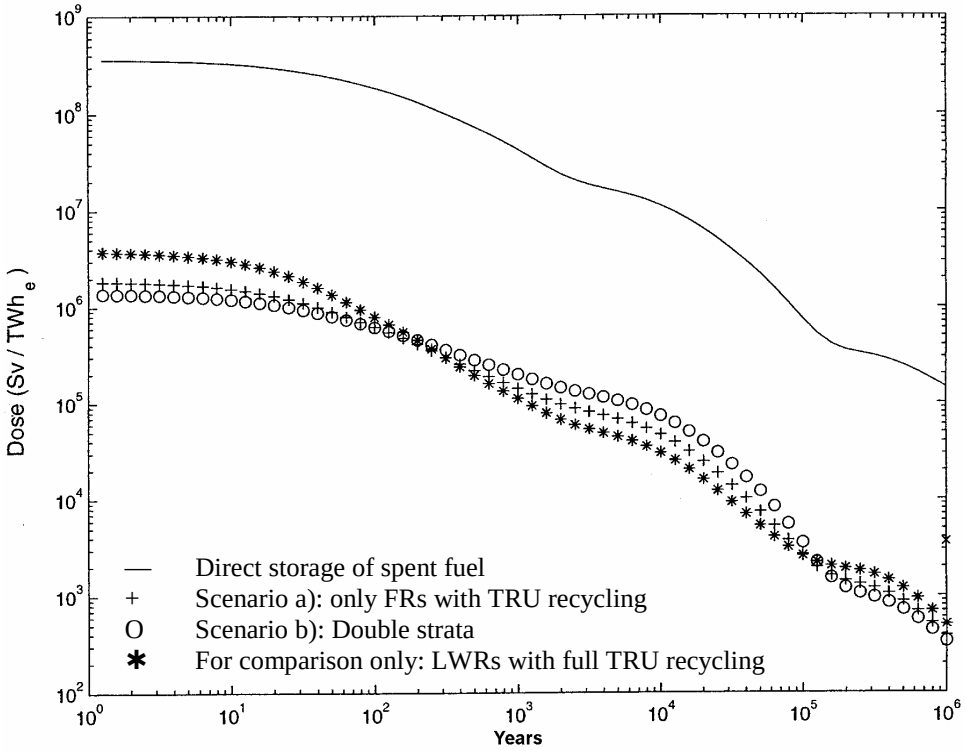

- *Radiotoxicity reduction is comparable (i.e. higher than a factor 100) in transmutation scenarios a), b), and depends on losses during reprocessing. In cases presented here a 0.1% value is taken for all TRU.*
- *However, the impact on the fuel cycle is different. It becomes unacceptably high if all TRU is recycled in LWRs, due to the high neutron doses at fuel fabrication.*

In the case of the homogeneous recycling, all the reactors can be loaded with MA. In the Pu case of the double strata power park, the MA are loaded in a very limited number of dedicated reactors (e.g. corresponding to ~5% of the overall power fleet, as will be shown in Chapter 2).

Figure 1.14 shows the expected reduction of heat load in a repository. The multiple Pu recycling and MA disposal has limited benefits (factor ≤ 2). The multiple Pu and Am recycling associated with Cm disposal has a more favourable impact (e.g. factor ~5-6 at 1 000 years after disposal). If Cm is stored and not disposed, the heat load theoretical reduction is comparable to what is achievable when TRU are fully recycled in a fast reactor.

Figure 1.14. Heat load in a repository

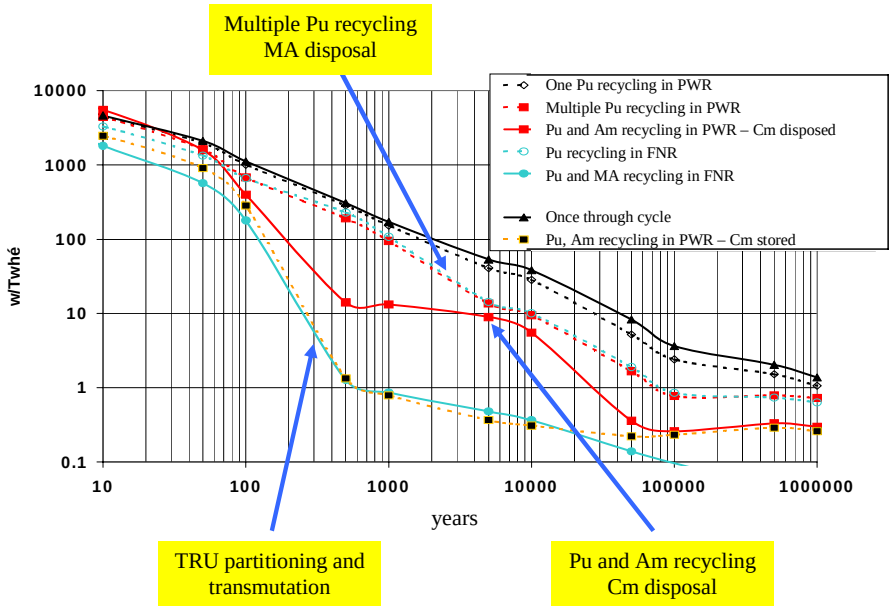

Finally, Figure 1.15 (provided by R. Wiegland and co-workers at Argonne National Laboratory) shows the benefits of P&T in terms of loading increase in a repository of the Yucca Mountain type. As expected from the results quoted above, the separation of Pu and Am allows an increase by a factor of ~6. The further separation of Cm, Cs and Sr allows for the reaching of a loading increase factor ~50 and higher.

Figure 1.15. Potential repository drift loading increase

Courtesy of R. Wiegland and T. Bauer, Argonne National Laboratory

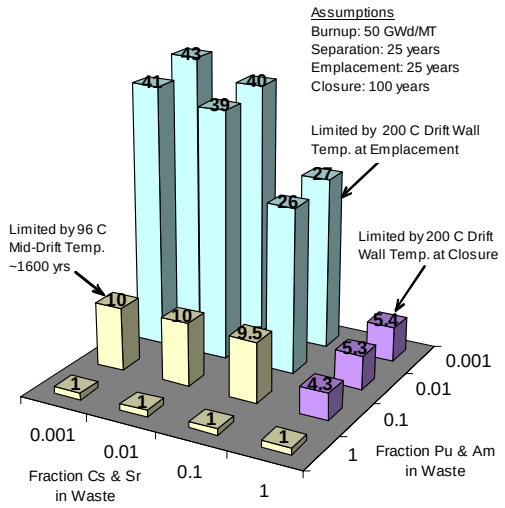

- Separation of Pu & Am allows for denser loading of the repository
  - up to a factor of 6 with 99.9% removal
- Subsequent separation of Cs & Sr provides for much greater benefit
  - up to a factor of 50 with 99.9% removal
- Removal of Cm further increases the potential benefit (with Pu & Am)
  - greater than a factor of 100 with 99.9% removal
- Appropriate waste forms are needed to take advantage of this potential

1.4.3 Challenges associated with P&T

The physics of transmutation is well understood; experiments have been performed irradiating pure TRU isotope samples in power reactors, and transmutation rates have been compared successfully to calculations.

As far as technical challenges to actinide separations, it should be recalled that:

- Concentrations in either spent fuel or in tank high-level wastes (HLW) will vary widely; separation processes must be robust enough for a wide range of feeds.
- Feed characterisation requires significant analytical capability.
- Chemistry of actinides is complex; actinides form multiple valence states, similar to that of lanthanides. The separation of trivalent Am and Cm from lanthanides is a challenging task.
- "Grouped" separation of TRU has to be demonstrated.
- Processing of the U-free fuels foreseen in ADS or of the targets of a heterogeneous recycle; the impact of the choice of the support/matrix on dissolution and extraction has to be carefully evaluated.
- Production and management of secondary wastes is also a concern related to the previous point.

Aqueous and dry (pyrochemical) processes can be used and are being developed, mainly in the USA, Europe, Japan and Russia. Significant results have been obtained mostly at laboratory scale, but have to be translated to industrial plants.

There are technical challenges to fuel development:

- Large decay heat and high neutron emission of several higher-mass TRUs (see Table 1.2) present new problems with respect to standard fuel manufacturing.
- However, problems are smaller if the fuel contains U and small amounts of MAs [(as in the case of scenario a)] with respect to U-free fuels [as in the case of scenarios b) and d)] with large amounts of MA.
- The presence of a significant amount of Am induces a high He production (see Figure 1.16), and should be accommodated to avoid a too-large pressure and swelling of the fuel pin.
- In the case of U-free fuels, the choice of the support/matrix (e.g. for oxide fuels: MgO, ZrO_2, Mo...) is crucial for a good thermal behaviour under irradiation.
- Fabrication processes are challenging (should avoid contamination, etc.), in particular for a significant content of Cm.
- In any case, remote handling is needed.

Figure 1.16. Helium production during Am irradiation

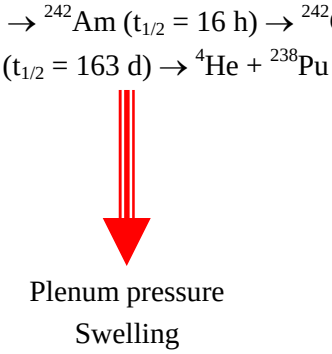

Finally, in the case scenarios b) and d), the implementation of ADS requires the validation of this new concept: high intensity proton accelerators with $5 \div 20$ MW in the beam and high reliability, spallation target with solid or liquid metal, and a full coupling of the different ADS components, to validate the dynamic behaviour at power of a subcritical system in the presence of an external source, the subcriticality monitoring and control, etc. Some of these aspects will be discussed in Chapter 3.

Finally, no P&T strategy can be implemented without a careful cost/benefit evaluation.

1.4.4 Conclusions

- P&T technologies offer the potential for a significant radioactive waste minimisation.
- P&T can be applied to widely different fuel cycle strategies:
  - Sustainable development of nuclear energy.
  - Minimisation of the waste arising from a legacy of spent nuclear fuel.
- P&T does not eliminate the need for deep geological storage whatever the strategy, but allows increasing its capacity, drastically reducing the burden and potentially improving public acceptance.
- Fast reactors offer the most flexible tool in order to implement P&T. The use of ADS can be seen as an option or a potential back-up solution, and Chapter 2 will provide quantitative examples of their implementation.
- Demonstration of P&T implies the demonstration of all the “building blocks” of the strategy: adapted fuels, adapted reprocessing techniques, reactor behaviour when loaded with significant quantities of MA.

REFERENCES

[1] Salvatores, M., *et al*., "A Global Physics Approach to Transmutation of Radioactive Nuclei", *Nucl. Sci. Eng*., 116, 1 (1994).

[2] Salvatores, M., R. Hill, I. Slessarev, G. Youinou, "The Physics of TRU Transmutation – A Systematic Approach to the Intercomparison of Systems", *Proceedings of the Intern. Conf. PHYSOR 2004*, Chicago, 25-29 April (2004).

[3] Youinou, G., F. Varaine, A. Vasile, "Plutonium and Americium Multi-recycling in EPR Using Slightly Over-moderated U-235 Enriched MOX Fuel Assemblies", *Proceedings of GLOBAL '03 Conference on Advanced Nuclear Energy and Fuel Cycle Systems*, New Orleans, LA, 16-20 November 2003.

[4] Salvatores, M., "Waste Transmutation Schemes in Different Nuclear Power Deployment Scenarios", *Proceedings of GLOBAL'03 Conference on Advanced Nuclear Energy and Fuel Cycle Systems*, New Orleans, LA, 16-20 November 2003.

[5] Klosterman, J.L., *et al*., "Strategies for the Transmutation of Am", *Proceedings of GLOBAL'97*, Yokohama (1997).

[6] Ozawa, M., T. Wakabayashi, "Status on Nuclear Waste Separation and Transmutation Technologies in JNC", *Ibidem*.

[7] Mukayama, T., *et al*., "Partitioning and Transmutation Program OMEGA at JAERI", *Proceedings of GLOBAL'95*, Versailles (1995).

[8] Salvatores, M., *et al*., *Nucl. Inst. and Methods*, A414, 5-20 (1998).

Chapter 2

SCENARIO STUDIES FOR P&T

The relevance of scenario studies to assess the performance of a particular transmutation strategy was discussed in Chapter 1.

Two major approaches can be used, namely a steady-state approach, relevant to an equilibrium situation, or a full dynamic, time-dependent approach. The relevance of the time-dependent approach is extensively discussed in Section 2.1 in the context of P&T studies. Section 2.2 presents an overview of available software. Section 2.3 is devoted to the application of the scenario studies to the ADS-based transmutation. In this section, parametric scenario studies at equilibrium are first presented, in order to characterise the use of ADS-based transmutation from two different perspectives: a) the use of ADS in a "double-strata" strategy in order to transmute essentially minor actinides, b) the use of ADS in a "double-component" strategy, in order to transmute both Pu and minor actinides. Successively, two "images" of ADS are presented in more detail, the first representative of a "minor actinide" burner (as relevant to the double-strata strategy) and the second of a "TRU burner" (as relevant to the double-component strategy).

Finally, Section 2.3 presents time-dependent scenarios in order to analyse the practical implementation of ADS-based transmutation, according to the two strategies mentioned above.

2.1 Time-dependent P&T studies

2.1.1 Introduction

Steady-state studies can yield a useful initial guide to the performance of a particular P&T scenario and are relatively easy to construct [1,2]. As they do not consider start-up or shutdown of various reactors within the cycle they are therefore valid only when continuously operating reactor parks are considered over long time scales.

There are, however, some shortcomings in using a steady-state approach, the most important of which is the fact that long time scales and multiple recycling are required to validate the approach and to produce the desired reduction in radiotoxicity. This essentially means that no account is taken of the scenario shutdown in this infinite steady-state approach. If the assumption is made that at some point operations must end then the total reduction factor achieved by P&T must take into consideration what is in the cycle in addition to waste already generated. Under equilibrium operating conditions this can represent a significant inventory which will seriously erode the toxicity reduction factor achieved for the cycle as a whole. Given these shortcomings it seems sensible to perform time-dependent P&T studies to allow explicitly for shutdown and to allow for a physically correct comparison of inventories from a common time origin.

In addition to fully accounting for shutdown scenarios there are further advantages to considering time-dependent P&T scenarios. Studies have shown that if a finite total operation time is considered

and that a uniform cycle operation is adopted, the time taken to achieve a given reduction factor is typically several thousands of years [3]. If, however, a more optimal approach is made, where P&T requirements are tailored to specific inventory evolution, then a similar reduction can typically be made in an order of magnitude less time. This requires reactor operations to be a function of time and cannot be considered in a steady-state approach. Further, if losses are considered it has been demonstrated that maximum reduction factors exist that can never be exceeded. There is therefore a trade-off between overall operation time and process losses which require dynamic analyses to evaluate.

There are further advantages to be gained when considering the composition of the fuel material for practical manufacturing. For example, curium recycle is problematic due to the high heat production and high spontaneous neutron emission. The introduction of recycle delays would allow for significant decay to plutonium which is easier to convert to fuel. Again, such a delay will have an impact on the inventory at shutdown. In addition, the progressive change in inventory composition may have an impact on reactor operation and performance. This will limit loading possibilities for current designs, or may point to essential requirements for future reactor designs.

As a final addition to the advantages of a time-dependent scenario, it is also worth noting that commercial nuclear power stations have been operational since the mid 1950s. There is, therefore, already a significant inventory of spent nuclear fuel in existence. A time-dependent explicit inventory tracking approach allows this material to be considered in addition to the inventories that will be generated from future power production, thus taking into account any material "backlog".

2.1.2 Theoretical studies

The commonly used fuel cycle scenario for analytic P&T studies consists of a closed loop system in which a nuclide or actinide of interest is continually manufactured into fuel, irradiated and reprocessed for recycling, as shown in Figure 2.1. Note, this figure depicts the situation after the initial core transients (see Section 2.1.2.1). Let an actinide store hold an instantaneous mass, M_S, of a single actinide. Let this feed a manufacturing plant of efficiency of ε_m, meaning that for every tonne of actinide fed to the manufacturing plant, a mass ε_m is processed into fuel and the fraction $(1 - \varepsilon_m)$ is lost from the system and ultimately is disposed of. The manufactured fuel batch feeds a reactor at f tonnes per year, where a burn-up of B% is achieved. The spent fuel is cooled and reprocessed with an efficiency ε_r, which is analogous to ε_m, and then returned to the store for recycling.

Figure 2.1. Idealised mass flow diagram

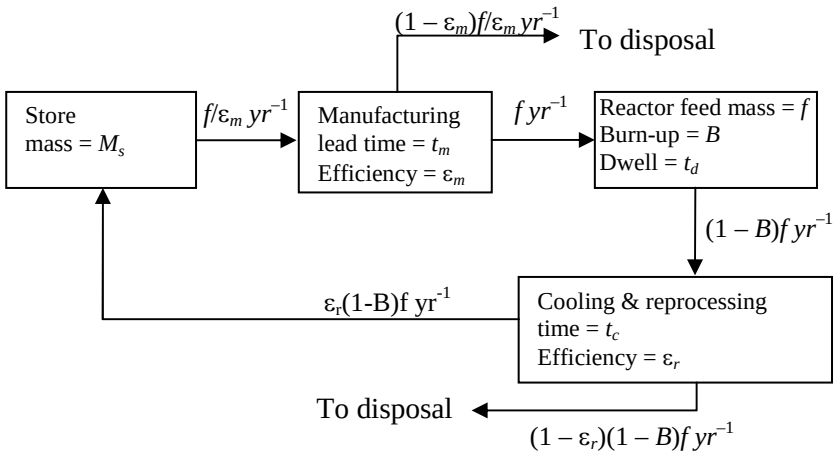

The exact performance of a system is dependent upon the exact nature of operations, with the prime variable being the amount of material fed to the reactor per year, *f*. In theory this may be continuously variable, however in practice an engineered design will usually specify a fixed amount determined by the physics of the reactor. Two simple extremes may be considered: a uniform deployment and a variable size deployment. In the former, a single reactor design is fixed and run for its operational life. Upon shutdown it is replaced by an identical unit. This continues until a prescribed reduction factor is obtained. In the variable size deployment scenario an initial reactor is constructed to run for a fixed number of years. At shutdown, this is replaced by a potentially different design that is optimised for the inventory existing at that time. These scenarios are analysed and compared below. No assumption is made as regards the details of the reactor type – only that some reduction in mass is achieved during irradiation.

2.1.2.1 Single nuclide model with uniform reactor deployment

Consider a single nuclide example, in which decay is assumed to be slow compared with operational timescales. Further, let the only destruction mechanism for the actinide be by fission to produce short-lived fission products. The number of batches is N_B, so that the refuelling fraction of the core is $(1/N_B)$ of its inventory. The burn-up is assumed to accumulate linearly so that an incremental burn-up of $b = B/N_B$ is achieved in each year of dwell. Defining the total time for which reactors operate as T_F and the equilibrium refuelling mass as f tonnes per year, the total mass of material removed from the store over T_F years of operation is given by:

$$M_r = \frac{f}{\varepsilon_m}\left(N_B + T_F - 1\right) \tag{1}$$

which is an initial core of $N_B f$ tonnes in the first year followed by $(T_F - 1)$ reloads of mass f each year. The mass fraction that is irrecoverably lost from the fuel cycle over T_F years of operation due to manufacturing, M_{Lm}, is given by:

$$M_{Lm} = \frac{f}{\varepsilon_m}\left(1-\varepsilon_m\right)\left(N_B + T_F - 1\right) \tag{2}$$

Defining the total time required for material leaving the store to return in a useable form as T_R, where T_R is the sum of the manufacturing lead time, t_m, the reactor dwell time, t_d, and the cooling and reprocessing time, t_c:

$$T_R = t_m + t_d + t_c \tag{3}$$

the mass of material returned to the store up to year T_F, M_R, is given by:

$$M_R = \left(T_F - T_R\right)\left(1-B\right) f\varepsilon_r + \sum_{i=1}^{N_B-1}\left(1-ib\right) f\varepsilon_r \tag{4}$$

where the first term represents fuel that has achieved full burn-up, while the second accounts for the partial burn-up of discharged batches from the initial core. Note, this expression allows for the manufacturing lead time so that t years of reactor operation is accompanied by exactly t years of manufacturing time, although the two operations may be offset in time. Simplifying the second term yields:

$$\sum_{i=1}^{N_B-1}(1-ib)f\varepsilon_r = f\varepsilon_r(N_B-1)\left(1-\frac{B}{2}\right) \tag{5}$$

The mass left in the reactor and cooling ponds after T_F years, M_E, is given by:

$$M_E = (T_R - N_B + 1)(1-B)f\varepsilon_r + f\varepsilon_r(N_B-1)\left(1-\frac{B}{2}\right), \tag{6}$$

where the first term represents fuel that has had a full burn-up, while the second represents part-burned fuel discharged at shutdown. Note the symmetry with the start-up fuel.

Assuming all fuel is cooled and reprocessed, the total irrecoverable losses due to reprocessing over T_F years of operation, M_{Lr}, is:

$$M_{Lr} = (T_F - N_B + 1)(1-B)f(1-\varepsilon_r) + 2f(1-\varepsilon_r)(N_B-1)\left(1-\frac{B}{2}\right) \tag{7}$$

It can be argued that fuel that could not be returned to the reactor should not be reprocessed, however this study considers all mass left after operations and as such expressions (2), (6) and (7) will be summed. By not reprocessing, expression (6) will be altered by an equal and opposite correcting amount to (7) as mass is conserved. It is therefore not necessary to complicate the algebra with this refinement.

If the store has an initial mass M_0, the mass in the store after T_F years is given by:

$$M_S = M_0 - M_r + M_R \tag{8}$$

Substituting for terms gives:

$$\varepsilon_m(M_0 - M_S) = f\{T_F\Lambda + \Gamma\} \tag{9}$$

where:

$$\begin{aligned}\Lambda &= 1-(1-B)\varepsilon_m\varepsilon_r \\ \Gamma &= (N_B-1)\left[1-\varepsilon_m\varepsilon_r\left(1-\frac{B}{2}\right)\right] + (1-B)T_R\varepsilon_m\varepsilon_r\end{aligned} \tag{10}$$

Physically, Λ may be interpreted as the total removal fraction from the cycle through irreversible process inefficiencies and burn-up destruction, i.e. the fraction of material leaving the store that cannot return after a single complete run through the fuel cycle. The expression Γ represents the combined effects of delays in the cycle which delays material from re-entering the store in time for manufacture of fuel, and the effects of batch operation in which some initial core fuel does not achieve a full irradiation. It therefore represents the start-of-operations penalty for batch-operated start-up.

The residual material in the system after shutdown of the last operating reactor, M_u, is:

$$M_u = M_{L,m} + M_E + M_{L,r} + M_S \tag{11}$$

where the mass of unused material remaining in the store is included along with irrecoverable losses and material resident in process plant and the reactor.

Introducing the reduction factor, α, as the total residual fraction of the initial mass, i.e. $\alpha = M_0/M_u$, expression (11) can be re-written as:

$$\frac{\varepsilon_m M_0}{\alpha} = f\{T_F(\Lambda - \varepsilon_m B) + \Gamma\} + \varepsilon_m M_S \tag{12}$$

Eliminating f from (9) and (12) yields the time T_F required to achieve a specified reduction factor as:

$$T_F = \frac{M_0\Gamma(\alpha - 1)}{M_0\{\Lambda - \alpha(\Lambda - \varepsilon_m B)\} - M_S\alpha\varepsilon_m B} \tag{13}$$

M_S and T_F must be positive real to be physical, therefore T_F is minimised in Eq. (13) when the denominator is as large as possible, which occurs when $M_S = 0$. This makes physical sense as this indicates that all the material in the store at the end of reactor operations is just used for the last reload. It also maximises the reload mass f, through Eq. (9), i.e. the reactor is taking as much material as possible per year to achieve the given reduction factor. This gives the final expression for T_F as:

$$T_F = \frac{\Gamma(\alpha - 1)}{\Lambda - \alpha(\Lambda - \varepsilon_m B)} \tag{14}$$

A plot of Eq. (14) for a target reduction factor of $\alpha = 50$ and various batch operation and efficiency values is shown in Figure 2.2. In this figure, Γ has been expanded to allow plotting of T_F versus the number of reactor batches. A one-batch scheme burn-up of 10% is assumed, which gives a three-batch burn-up of 15% when constant end-of-cycle $k_{effective}$ is assumed (see Appendix 2.1); the value used for the multi-nuclide numerical case. Manufacturing lead time was taken as one year and post-irradiation cooling was taken as two years [1]. It is noted that the derived times are several thousands of years, and arguably much too long to be feasible. The reason for the behaviour is the single-sized reactor assumption. The reactor refuelling size must be such that the recoverable residual in the system does not result in more that $1/\alpha$ of the starting inventory. This means small reloads over many years. However, this has the drawback that irrecoverable losses accumulate over a longer period, which requires a smaller recoverable residual to compensate. The optimal balance between the two effects results in the time given by Eq. (14).

Figure 2.2. Time taken to reach a 50-fold reduction in inventory for a uniformly sized reactor deployment

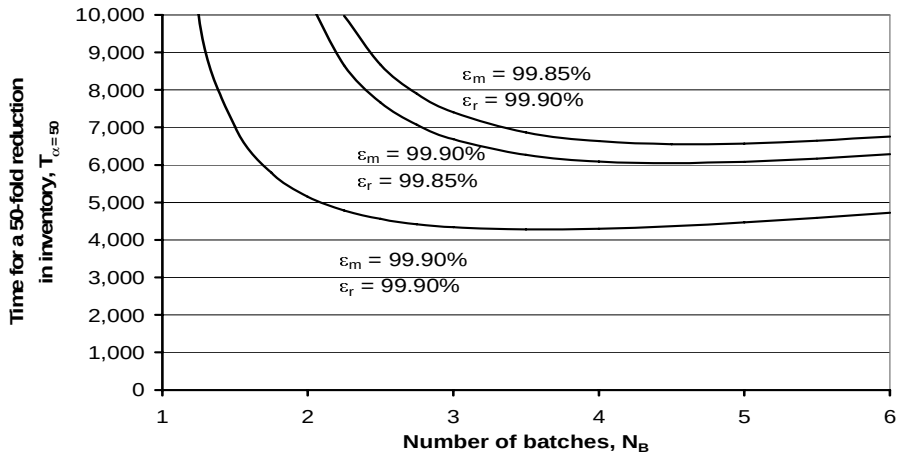

Figure 2.2 also shows that the value of T_F is very sensitive to small changes in process efficiencies and, further, that high efficiencies are required. It is also observed that the curves demonstrate a tendency to go to infinity for some value of batches, or, equivalently, burn-up. To analyse this behaviour, Eq. (14) is re-written in terms of α to give:

$$\alpha = \frac{T_F \Lambda + \Gamma}{T_F \left(\Lambda - \varepsilon_m B\right) + \Gamma} \tag{15}$$

With all parameters positive real it is obvious that Eq. (15) approaches an asymptotic limit as $T_F \to \infty$ of:

$$\alpha\big|_{T_F \to \infty} \to \frac{\Lambda}{\Lambda - \varepsilon_m B} \tag{16}$$

while for $T_F \to 0$, it is seen that $\alpha \to 1$. This implies that for given process parameters the maximum reduction factor achievable has an upper limit which cannot be exceeded over any time scale. The variation of the upper limit on, α_{max}, is compared for the three process efficiency cases above in Figure 2.3. It can be seen that manufacturing efficiency has a greater impact than reprocessing efficiency as any manufacturing losses are applied to the pre-irradiated mass which is by definition larger than the post-irradiated mass. It is also noted that with the burn-ups and efficiencies used in these examples, $\alpha_{max} < 100$, the stated target reduction factor for many P&T study cases [1].

Figure 2.3. Sensitivity of maximum theoretical reduction factor to changes in process efficiency for a uniformly sized reactor deployment

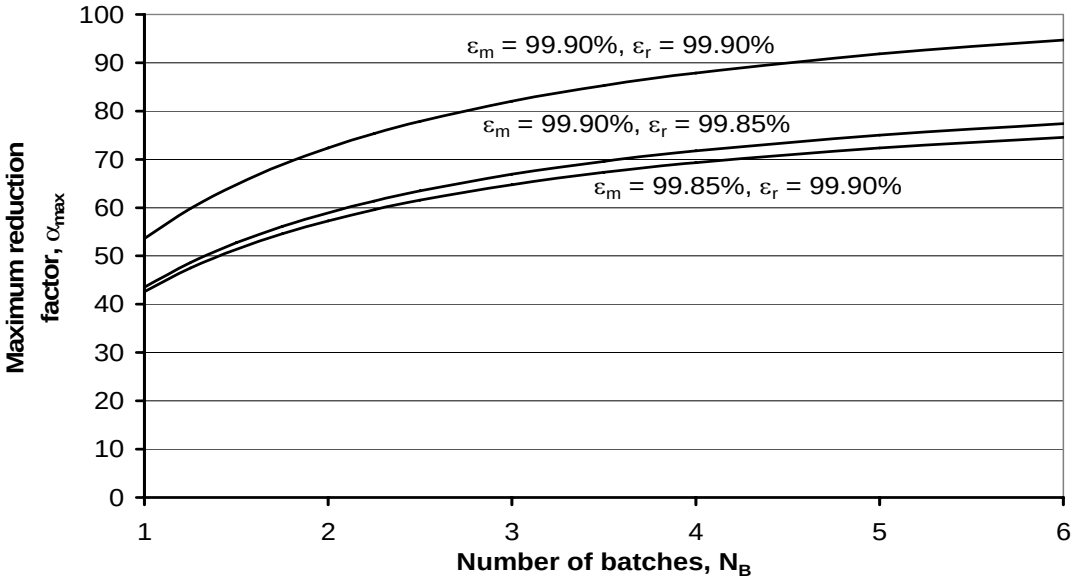

We now seek to prove that α approaches the above limiting value monotonically with time to ensure that it is a global maximum. Finding the first derivative of α with respect to operating time from Eq. (15) gives:

$$\frac{d\alpha}{dT_F} = \frac{\Gamma\left(\varepsilon_m B\right)}{\left(T_F \left(\Lambda - \varepsilon_m B\right) + \Gamma\right)^2} \tag{17}$$

The denominator is always positive. Inspecting the numerator and using the bounds, $0 \le \varepsilon_m, \varepsilon_r, B \le 1$, it is seen that the derivative follows the sign of Γ, which is always positive. This means that $d\alpha/dT_F$ is positive for all T_F and so the limiting value of α is reached monotonically.

2.1.2.2 A more optimal variable size reactor deployment scenario

The above calculations have studied a single reactor (or repeated identical units operating one after the other) operating on a fixed reload mass over a given period of time. Example calculations show that operation times can be very long for this approach due to the requirement to keep the residual material at the end of operations to a suitable level in order to prevent unusable material from violating the desired reduction factor. A more optimal approach is to assume that a number of separate reactor generations operate, each being optimised for the material available to that generation and to specify that only the material left after the end of operation of the last generation meets the reduction criteria, as shown in Figure 2.4.

Figure 2.4. Schematic of mass flow individual P&T loop generation scenario

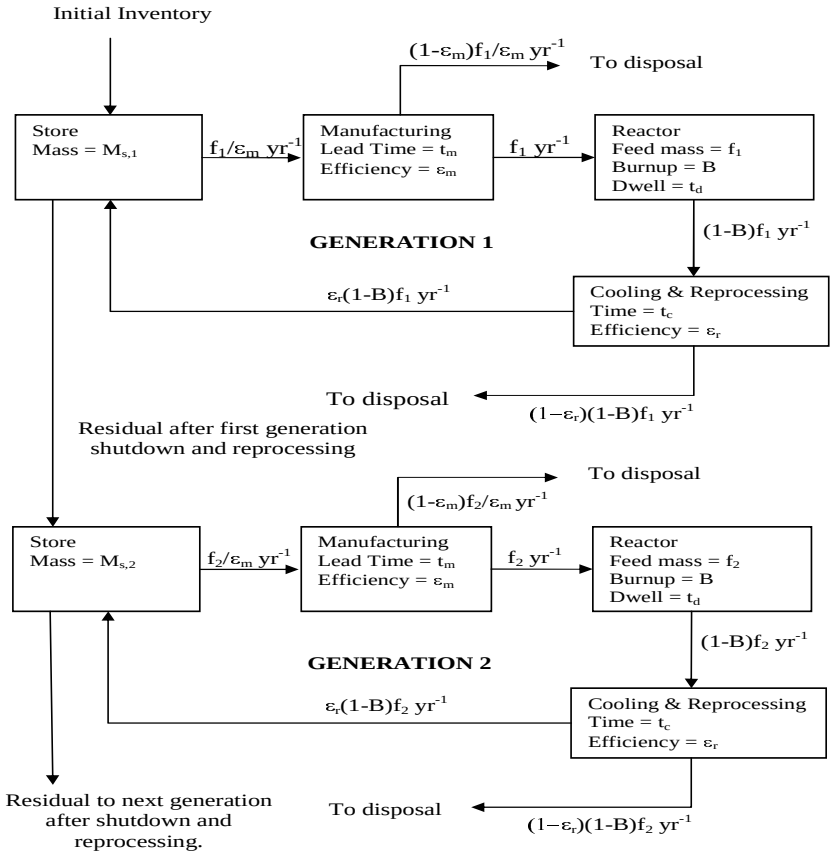

To formulate a more optimal operation, consider the scenario where a reactor generation operates for a fixed time $T_A < T_F$, and that over this time the reactor just uses all the material available to it, i.e. $M_S(t = T_A) = 0$. Further, assume that each generation of reactor has the same burn-up and that process efficiencies are constant throughout operations. Eq. (9) can then be used to determine the equilibrium feed mass for the fist generation of reactors as:

$$f^{(1)} = \frac{\varepsilon_m M_0}{T_A \Lambda + \Gamma} \tag{18}$$

The mass left for use in a second-generation reactor is given from Eq. (6) as:

$$M_E^{(1)} = f^{(1)} \Delta \tag{19}$$

where:

$$\Delta = T_R \varepsilon_r (1 - B) + \varepsilon_r (N_B - 1) \frac{B}{2} \tag{20}$$

Eliminating *f* from Eq. (20) using Eq. (18) yields:

$$M_E^{(1)} = \frac{\varepsilon_m M_0 \Delta}{(T_A \Lambda + \Gamma)} \tag{21}$$

which then becomes the initial inventory for the second generation. By induction it can be shown that the equilibrium feed mass for the N^{th} generation reactor is given by:

$$f^{(N)} = \frac{\varepsilon_m^N M_0 \Delta^{N-1}}{(T_A \Lambda + \Gamma)^N} \tag{22}$$

and the residual mass useable for fuel in the next generation will be:

$$M_E^{(N)} = \frac{M_0 (\varepsilon_m \Delta)^N}{(T_A \Lambda + \Gamma)^N} \tag{23}$$

The total irrecoverable material arising in generation *N* is given from Eqs. (2) and (7) with the substitution of Eq. (22) as:

$$M_L^{(N)} = \frac{D M_0 (\Delta \varepsilon_m)^{N-1}}{(T_A \Lambda + \Gamma)^N} \tag{24}$$

where:

$$D = T_A (\Lambda - \varepsilon_m B) + (N_B - 1)(1 - \varepsilon_m \varepsilon_r) \tag{25}$$

The total residual material after *N* generations is given by:

$$M_U^{(N)} = M_E^{(N)} + \sum_{i=1}^{N} M_L^{(i)} \tag{26}$$

The summation is evaluated by noting that Eq. (24) is a geometric progression of the form $M_L^{(i)} = ar^{i-1}$ with:

$$a = \frac{DM_0}{(T_A\Lambda + \Gamma)} \qquad r = \frac{\Delta\varepsilon_m}{(T_A\Lambda + \Gamma)} \tag{27}$$

so that the sum is given by:

$$\sum_{i=1}^{N} M_L^{(i)} = \frac{a(1 - r^N)}{1 - r}$$

Substituting into Eq. (26) gives:

$$M_u^{(N)} = \frac{M_0(\Delta\varepsilon_m)^N}{(T_A\Lambda + \Gamma)^N} + \frac{DM_0}{(T_A\Lambda + \Gamma - \Delta\varepsilon_m)}\left(\frac{(T_A\Lambda + \Gamma)^N - (\Delta\varepsilon_m)^N}{(T_A\Lambda + \Gamma)^N}\right) \tag{28}$$

Recalling the definition of the reduction factor α, $\alpha = M_0/M_u$, the number of generations required to achieve the reduction factor is then given by:

$$N = \ln\left[\frac{\alpha(T_A\Lambda + \Gamma - \Delta\varepsilon_m - D)}{T_A\Lambda + \Gamma - \Delta\varepsilon_m - \alpha D}\right] \Big/ \ln\left[\frac{T_A\Lambda + \Gamma}{\Delta\varepsilon_m}\right] \tag{29}$$

The total time is then simply given by:

$$T_F = N(T_A + T_R) \tag{30}$$

Solutions to Eq. (29) exist if:

$$T_A\Lambda + \Gamma - \Delta\varepsilon_m - \alpha D > 0 \tag{31}$$

as a limiting case. Expanding Γ, Δ and D in Eq. (31) and solving gives:

$$\alpha < \frac{T_A\Lambda + (N_B - 1)(1 - \varepsilon_m\varepsilon_r)}{T_A(\Lambda - \varepsilon_m B) + (N_B - 1)(1 - \varepsilon_m\varepsilon_r)} \tag{32}$$

which is similar to the single-sized reactor case. This limit is slightly less than the single-sized reactor case due to the fixed fraction of batches that do not achieve full burn-up. For a single batch case this limit reduces to the single-sized reactor limit. It is also noteworthy that Eq. (32) indicates that $\alpha \to 1$ as $N_B \to \infty$, suggesting that high batch numbers are not the most efficient for this operational approach. Any penalty on operating limits imposed by the adoption of an optimal reducing reactor size approach is offset by the vastly reduced times required to achieve a given target, as discussed in the following paragraph.

Assuming that each reactor has a fixed operational life of 60 years and that the burn-up achieved is a function of the number of batches, Figure 2.5 shows a comparison of the predicted T_F values for the stated number of batches and process efficiencies to achieve a target reduction factor of $\alpha = 50$. The values may be compared directly with those in Figure 2.2 for a single-sized reactor case. It is seen that the times required are reduced by an order of magnitude.

Figure 2.5. Time taken to reach a 50-fold reduction in inventory for an optimised reactor deployment

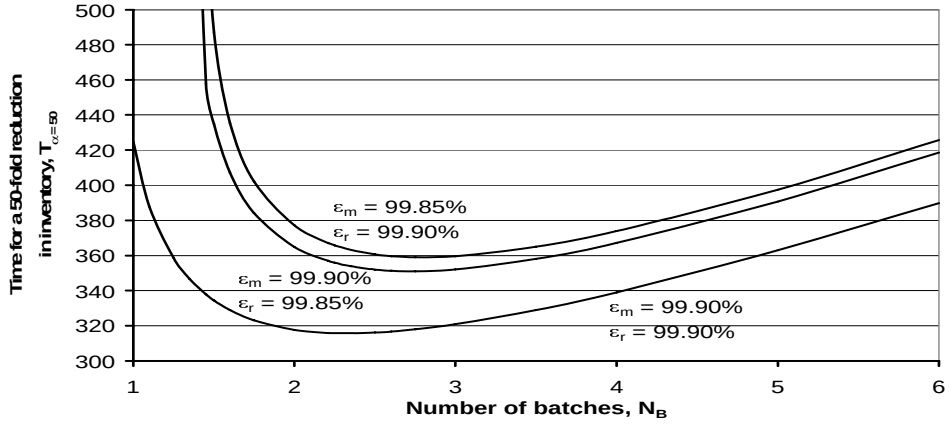

An analysis of the sensitivity of T_F with process efficiencies is also shown in Figure 2.5 for combinations of ε_m and ε_r. These plots show that the value of T_F is sensitive to small changes in process efficiencies, however as the magnitudes of the time scales are smaller, the absolute impact is less than the uniform-sized case. It is also apparent that there exists an optimal number of batches which is a function of the process parameters.

In Figure 2.6, the variation of the upper limit, ε_{max}, is compared for the three process efficiency cases. As in the uniform reactor case it can be seen that manufacturing efficiency has a greater impact than reprocessing efficiency.

Figure 2.6. Sensitivity of maximum theoretical reduction factor to changes in process efficiency for an optimised reactor deployment

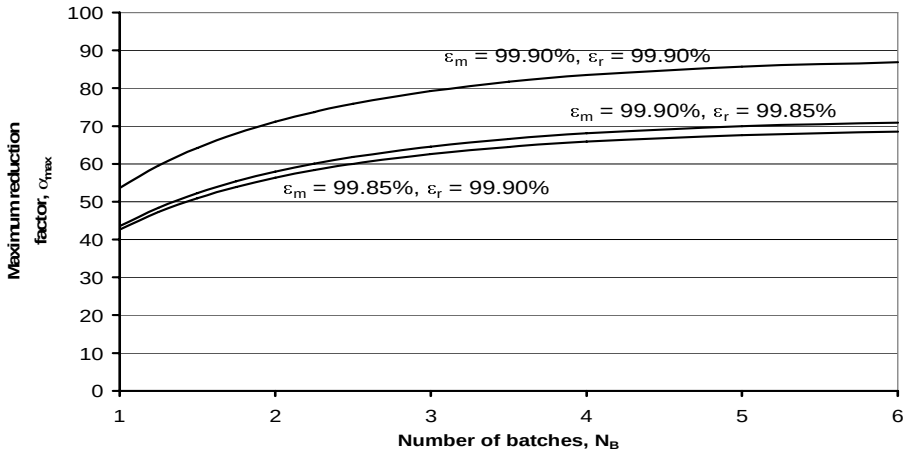

2.1.2.3 Impact on performance due to reactor operations

The evolution of the reduction factor for different numbers of batches is shown in Figure 2.7, where end-of-generation statepoints are plotted. This demonstrates that the bulk of the reduction is carried out by generations 4 to 8 for the chosen parameters. Generations 1, 2 and 3 have too large a residual inventory to have a large impact on the reduction factor, while generations 9 and later use small reloads so the incremental reduction is less. The batch scheme that gives the best performance at a particular point in time changes throughout the comparison, i.e. any performance optimisation must take into account the planned time horizon of operations.

Figure 2.7. Variation of cumulative reduction factor for each successive generation in an optimised reactor deployment

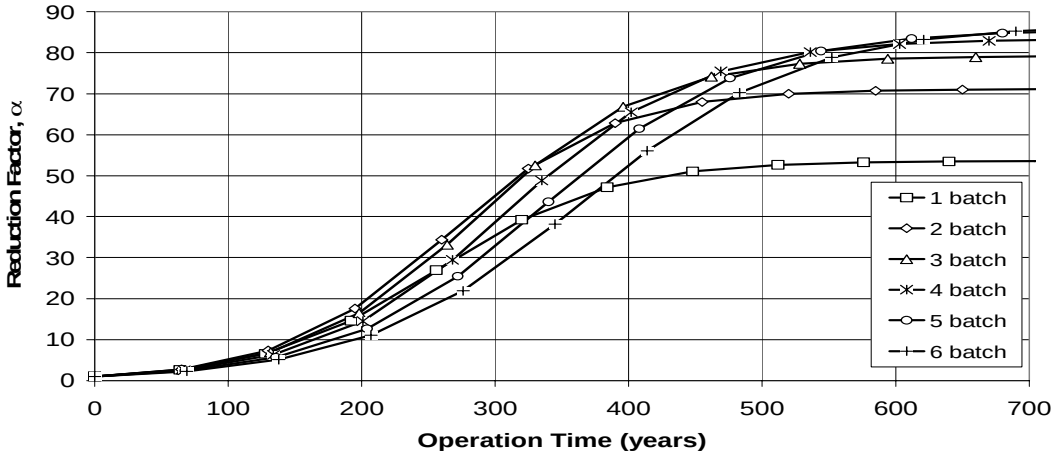

An example of the variation in required reactor size for each of the generations and the accumulated destruction observed is shown in Table 2.1 for the parameters $\varepsilon_m = \varepsilon_r = 99.90\%$, $T_R = 9$ years, $B = 17.1\%$, $T_A = 60$ years, $N_B = 6$ and an initial actinide inventory of 100 tonnes. This table shows that the last generation of reactor is on a scale of approximately 67 times less than the first generation and loads only 81 kg per year. There could be technical and commercial difficulties when designing and operating a plant to operate over such a variation of through-put requirements, although to some extent these could be ameliorated by deploying a large number of small units to handle large early-stage mass throughput requirements.

Table 2.1. Multi-generation characteristics

Generation	Reload mass (kg)	End of generation reduction factor (α)
1	5 469	2.3
2	2 357	5.1
3	1 015	11.0
4	438	21.9
5	189	38.2
6	81	56.1

Another aspect of performance that is of operational importance is the behaviour of the reduction α over a fixed overall operating time, T_F, with variations in the number of generations employed. The

variation of α with N for parameters $\varepsilon_m = \varepsilon_r = 99.90\%$, $T_R = 3 + N_B$ years, $T_F = 300$ years and a variation in number of batches is shown in Figure 2.8. It is observed that there is an optimal number of generations for a given number of batches.

Figure 2.8. Variation of reduction factor over a fixed operating period with the number of generations used

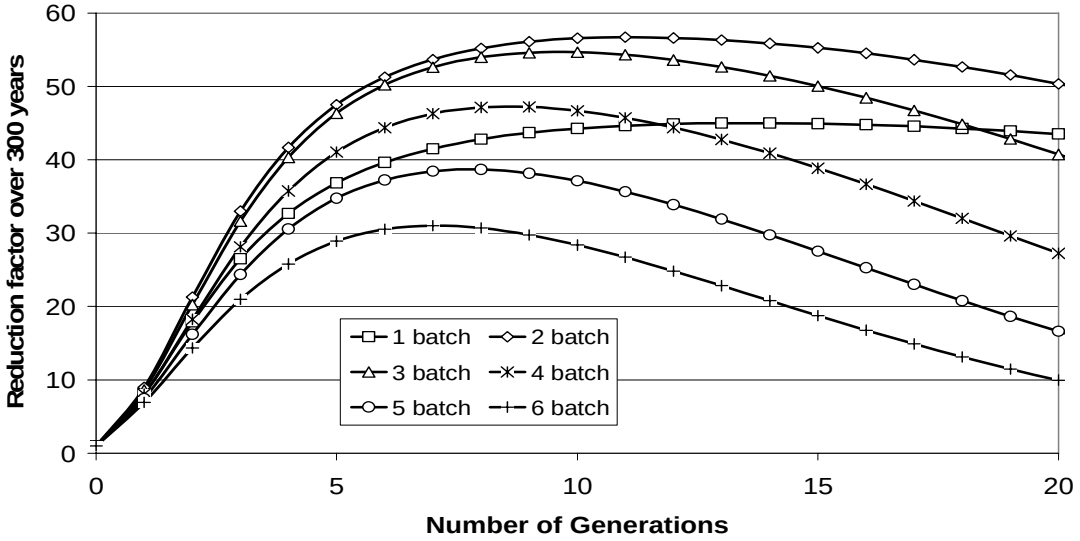

Figure 2.8 also indicates that the optimal reduction over a 300-year operation time is achieved for a two-batch scheme operating over 11 generations. This equates to an individual reactor generation operation time of ~22 years, which is much shorter than typically quoted reactor lifetimes of 60 years and will have a detrimental impact on economic performance.

2.1.2.4 Impact on performance due to manufacturing and reprocessing operations

Both the single-sized reactor scenario and the more optimal approach show that upper limits on the performance of the system are set by the three basic removal mechanisms from the fuel cycle: burn-up, manufacturing efficiency and reprocessing efficiency. The ultimate upper limit on reduction factor possible for both the uniform deployment and a variable size deployment is given by Eq. (16). Given this relationship, the important question "what process and cycle characteristics need to be achieved in order to obtain a destruction factor of…?" may be asked. The answer may be plotted as a three-dimensional surface of constant α where burn-up, manufacturing efficiency and reprocessing efficiency provide the three axes. If the simple assumption is made that manufacturing efficiency and reprocessing efficiency are equal, then the plot shown in Figure 2.9 is obtained. This figure indicates that tight control on process efficiencies must be maintained if the target reduction factor of $\alpha = 100$ is adopted [1], with a minimum manufacturing and reprocessing efficiency of 99% required. If it is noted that average irradiation beyond 15% has not been proven using known fuel technologies [1], the efficiencies increase to the more stringent value of at least 99.92%. While current separation techniques can achieve this performance for uranium and plutonium, further development work is required to meet this target for other actinides [1]. Conversely, any development work that enables increased burn-up will allow some relaxation of required process efficiencies.

Figure 2.9. Variation of burn-up and process efficiencies required to achieve a stated maximum reduction factor

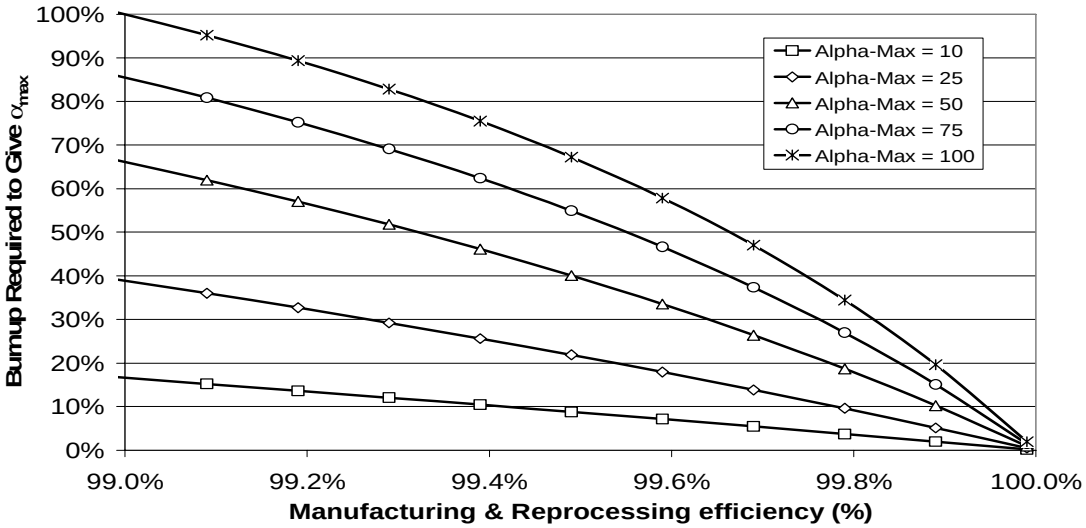

2.1.2.5 Examination of the mixed reactor case

The previous cases describe the situation where a P&T scenario is detached from the primary power production of the initial reactor. It is unlikely that the potentially useful generating capacity of the P&T cycle would be unaccounted for. Where P&T is used in a waste management scenario for phase-out, this additional power generation could be seen as a useful byproduct that helps offset the cost. For an ongoing mixed-generation scenario, this capacity must be accounted for as an integral part of the total generation potential installed. In this case, the P&T loop is modified to include the arisings from a co-running LWR, as show in Figure 2.10.

Figure 2.10. Idealised continuous mixed production mass flow

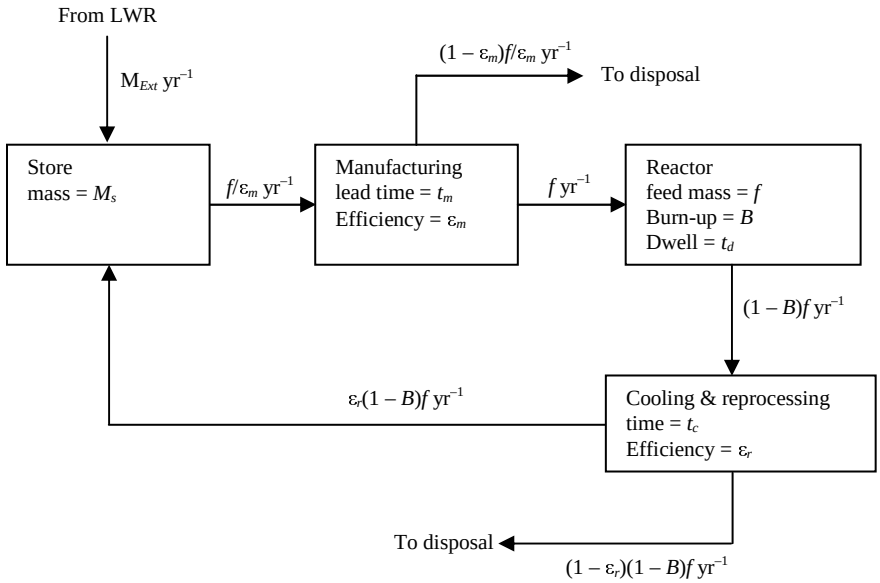

To account for a mixed scenario the fractions of the total generation due to LWR and P&T operations must be determined. Let the PWR have an annual loading of M_{LWR} tonnes and let the specific power density of the LWR be $\rho_{LWR.}$ If the number of fuel batches in the LWR is $N_{B,LWR}$, the total inventory of the LWR is $N_{B,LWR} \times M_{LWR}$ tonnes, and the total power due to the LWR is P_{LWR}, given by:

$$P_{LWR} = N_{B,LWR} M_{LWR} \rho_{LWR} \tag{33}$$

The fraction of the fuel loaded into the LWR that becomes the external feed for the P&T cycle is ϕ, so that:

$$M_{Ext} = \phi M_{LWR} \tag{34}$$

As stated previously, the reactor in the P&T loop loads f tonnes per year. For $N_{B,P\&T}$ batches then the total core inventory is $N_{B,P\&T} \times f$, and this operates at a power density of $\rho_{P\&T}$ MW/t, giving the power due to the P&T loop as:

$$P_{P\&T} = \varepsilon_{P\&T} N_{B,P\&T} f \rho_{P\&T} \tag{35}$$

where $\varepsilon_{P\&T}$ is the fraction of the P&T reactor that is not used to operate any dedicated plant such as a beam accelerator.

The equivalent reload mass of an LWR only system, M'_{LWR}, (of equal generating power) is given by P_T. Balancing the installed generating capacity means that:

$$P_T = N_{B,LWR} M'_{LWR} \rho_{LWR} = N_{B,LWR} M_{LWR} \rho_{LWR} + \varepsilon_{P\&T} N_{B,P\&T} f \rho_{P\&T} \tag{36}$$

For such a system, the reduction factor is calculated as the ratio of the arisings from an LWR only system with those from an LWR and P&T system. In general, the LWR only system will run for at least one generation to account for current operating practices. This means that there is a pre-existing stockpile of material for the P&T loop.

The behaviour of this system is complicated and is not trivially susceptible to generalised analysis. The principal causes of the complication arise from the requirement for a continuous supply of generation and that start-up and shutdown cores are of different mass than the reload mass. When considering the P&T loop, there are two critical times at which material inventory limits the size of the P&T loop reactor: the manufacturing of the first core and the manufacturing of the last reload.

The first core is $N_{B,P\&T}$ times larger than the reload mass, *f*, and so sufficient material must be available to meet this. As material from both the LWR and the P&T reactor take a finite amount of time to become available, the final few reloads of both reactor types and the larger final core cannot be relied on to supply the start-up mass for the first core of the next generation of P&T reactor. This consideration provides the first limit of *f*.

The second limit on *f* arises from the requirement to run for a fixed number of years. The reload must be sized, therefore, to ensure that the P&T mass store does not empty prior to the end of the operation of the current P&T generation.

A numerical analysis using a spreadsheet to track mass flow and accumulation for an example mixed reactor case with constant, uniform power production and scenario parameters, given in Table 2.2 [1], predicts the reload mass and reduction factor shown Figures 2.11 and 2.12, respectively.

Table 2.2. Example mixed generation parameters

Parameter	Value
P_T	4 000 MW
ρ_{LWR}	40 MW/t
$N_{B,LWR}$	4
T_A	60 years
ε_m	99.90%
ε_r	99.90%
$\varepsilon_{P\&T}$	90.00%
B	15.00%
t_m	1 year
t_d	3 years
t_c	2 years
$N_{B,P\&T}$	3
$\rho_{P\&T}$	250 MW/t (metal fuel)
ϕ	1.40%

Figure 2.11. Variation of reload mass for an example mixed reactor case

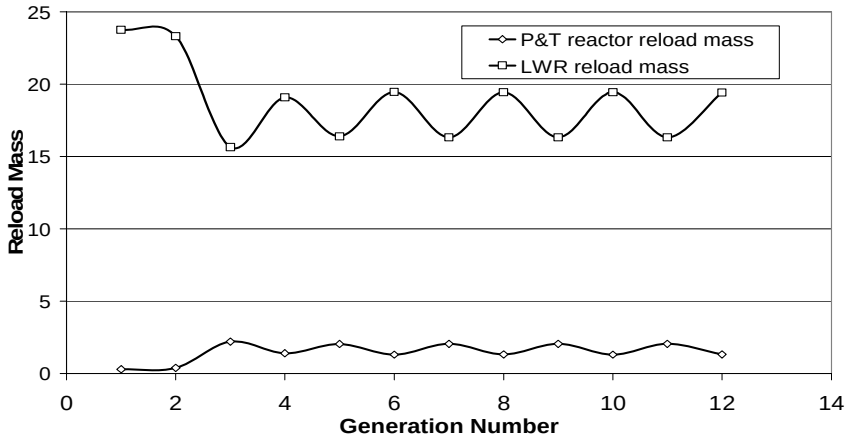

Figure 2.12. Evolution of reduction factor for an example mixed reactor case

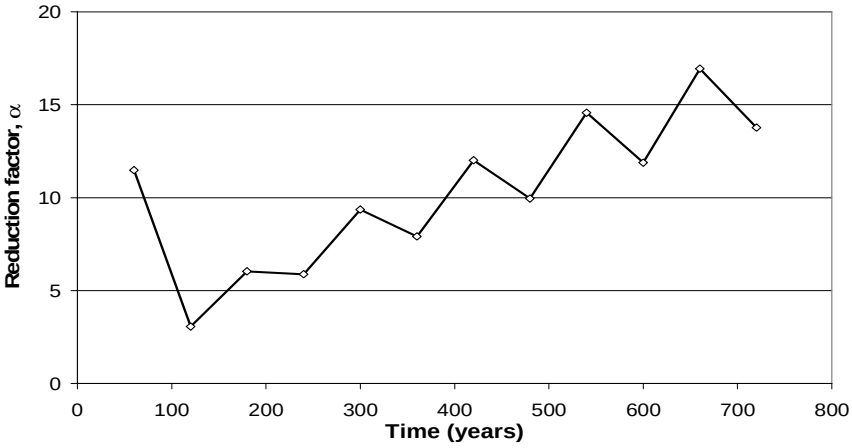

Figure 2.11 shows that the sizes of the LWR and P&T reactor oscillate between two fixed values after an initial transition of about six generations (360 years in this example). The reason for this is that the two limits on the P&T reactor reload size, *f*, tend to exclude each other. Where there is a sufficiently large initial mass of material, the initial core can easily be manufactured and *f* is limited by the requirement to manufacture the final reload. This strategy minimises the end of generation inventory and so in the following generation the production of the initial core becomes limiting on *f*. However, this does not minimise the end of generation material left over so that in the following generation the requirements for the initial core can easily be met and it is again the final reload that limits *f*. This cycle continues into equilibrium.

The different operating approaches for the odd and even generations have a significant impact on the reduction factor achieved, as depicted in Figure 2.11. Where the final reload is limiting on *f*, the reduction factor is minimised. Where the initial core is limiting on *f*, there is a larger inventory of material at the end of a generation and the reduction factor decreases. In equilibrium, alternating between the two states, the fractional change between any two adjacent generations remains constant. However the absolute value oscillates with increasing amplitude while the mean increases.

The question arises as to whether the mass oscillations could be smoothed out. Analysis shows that if this is done by forcing a reload mass that is the average of the odd and even generations, the system is stable in the future but with a reduced performance. The performance can be improved by increasing the P&T loop reload mass; however, this does not ensure steady-state performance into the future – at some point in time the material store for the P&T loop runs dry. Further, the alternate generation reload masses appear to be basins of attraction; any variation after an arbitrary set of reload conditions that seeks to maximise performance will bring the system back to the alternating reload mass scenario shown in Figure 2.10.

The mixed generation scenario places constraints on the operation of the P&T loop. As a result, the scenario operates in a similar manner to the fixed size reactor scenario described in Section 2.1.2.1, i.e. long time frames are required to achieve a useful reduction factor. This is clearly seen in this example where a reduction factor of less than 20 is achieved only after ~700 years of operation.

An alternative strategy could be to use the cascade approach described in Section 2.1.2.2. For this scenario the first level P&T loop could be sized to use just the material from the previous generation of LWR. The arising from this at the end of operations is fed to a smaller second level P&T loop, and so on until enough loops have been implemented to achieve a desired reduction factor. In this scenario, for the parameters used in the above example, the first level P&T loop will contribute ~5% to the total generation, the second level ~0.8% with subsequent loops generating ever decreasing amounts. Such a scenario would require a number of generations of the order of the number of P&T loops to reach equilibrium. Also, an eventual future shutdown of LWR generation may require running of the P&T loops several generations further to obtain a target reduction factor.

2.1.3 Example behaviour of a time-dependent scenario

The previous sections have demonstrated that a simple model predicts bounds on performance for P&T schemes. The next step is use simulation software to perform a similar analysis for the more realistic multi-nuclide case that incorporates decay. In this case, MEEMS software was used.

In a real waste inventory there will be a mixture of a number of actinides which will all decay at some natural rate while being processed and which in general will be part of a family of decay chains

leading to potential for in-growth as well as decay. Furthermore, while in the single nuclide case mass and toxicity may be interchanged as a reduction measure, this is not true for a nuclide mixture, where a reduction of mass does not necessarily equate to an identical reduction in toxicity.

The example considered here is a multi-generation P&T loop with a fixed initial inventory. The starting inventory may be taken, for example, as the transuranic arisings of a PWR burning UO_2 fuel [1]. A normalisation to 100 tonnes of material was made which represents the arisings from ~3.84×10^3 TWh(e) operation. This initial inventory is shown in Table 2.3.

Table 2.3. Initial inventory [1]

Nuclide	Initial mass (*t*)
^{237}Np	6.63853E+00
^{238}Pu	2.87797E+00
^{239}Pu	4.87721E+01
^{240}Pu	2.29087E+01
^{241}Pu	9.28626E+00
^{242}Pu	5.06523E+00
^{241}Am	2.34075E+00
^{243}Am	1.45817E+00
^{244}Cm	6.13968E-01
^{245}Cm	3.83730E-02
TOTAL	1.00000E+02

The operational approach adopted was the use of optimised generations, as shown previously in Figure 2.4, where each generation of P&T reactor is sized to use the inventory available to it. After a short inter-generation time to allow material in the system to return to the store, the next generation of P&T reactor is brought online. This next generation will be smaller that the previous as burn-up in the reactor will have reduced the nuclide store available. A three-batch fast neutron reactor (FNR) operating for 60 years and loading inert matrix fuel was considered with a fixed flux of 1.5×10^{15} $ncm^{-2}s^{-1}$, which gave a full-dwell burn-up of ~15% depending on the exact fuel mixture. This is taken as a sensible upper bound for known fuel technologies [1]. Depletion was performed using a one-group fast model integral to MEEMS. Initially all transuranic nuclides were recycled through the system and no limits were set on the composition of the fuel materials. No fission product effects were considered. Manufacturing lead time was taken as one year. Post-irradiation cooling was taken as two years [1].

2.1.3.1 Performance results

The predicted reduction factors for both mass and toxicity (calculated using ICRP 68 dose coefficients [4]) are shown in Figure 2.13 for a range of manufacturing and reprocessing efficiencies (it is assumed that the manufacturing and reprocessing efficiencies are numerically equal). In this plot the comparison is made with the reference case in which the initial inventory is aged naturally to an equivalent time. This prevents any over-prediction of the reduction factor from decay that would have occurred naturally, ensuring all effects are due to FNR irradiation only.

Figure 2.13 shows that, as predicted in the simple single nuclide case, even small changes in process efficiencies can have large impacts on performance. It also shows that the toxicity reduction is less that the mass reduction. This is to be expected as the FNR will not only destroy material by fission, it will also shift the distribution of surviving nuclides towards heavier nuclides, which tend to have higher toxicities.

Figure 2.13. Comparison of cumulative mass and toxicity reduction factors for 99.85%, 99.90% and 99.95% process efficiencies

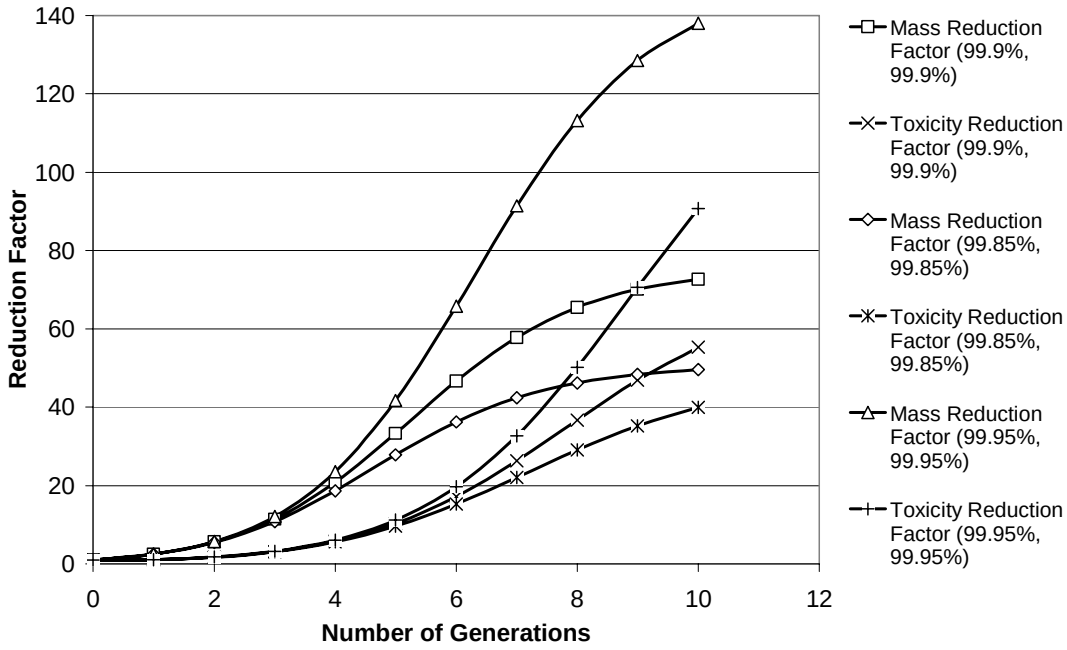

The plot for mass reduction at 99.9% process efficiencies indicates an asymptotic approach to a maximum value approaching 80. The theoretical single nuclide limit on the mass reduction factor given a burn-up of 15% and 99.9% manufacturing and reprocessing efficiency is 79. Similar agreement between the theoretical single nuclide limit is seen for the other two mass reduction cases. This indicates that, if mass reduction is considered, the idealised single nuclide analytical results can give a good indication on performance limits, sensitivity to parameter variation and the order of time scales required.

The long-term behaviour of the inventory, post FNR operations, is shown in Figure 2.14 for times up to 1×10^6 years. The mass reduction factor is constant to about 1×10^5 years after which it increases slightly. This increase is due to ^{242}Pu, which is present in slightly elevated proportions in the FNR scenarios due to neutron capture during irradiation. The toxicity plot shows an even more marked variation in reduction factor, where the value increases over ~1×10^4 years followed by a reduction. This increase is initially due to the decay of the higher actinides curium and americium. The peak occurs when ^{240}Pu is the dominant contributor in the FNR scenarios. Note that the absolute values for the mass of these species are lower in the FNR cases than the reference case, however the distribution is shifted towards the heavier and more toxic species.

The nominal process efficiencies of 99.9% quoted as achievable for uranium and plutonium (but ambitious for other actinides [1]) give an overall reduction factor of less than 80 for both mass and toxicity over the 1×10^6 year time horizon considered here. It is clear that if the often quoted target reduction factor of 100 [1] is to be met, then higher performance is required for process efficiency, and/or methods for improving net burn-up must be demonstrated. With the assumed burn-up, a quadratic interpolation indicates that efficiencies of at least 99.937% must be achieved on both manufacturing and reprocessing in order to produce a factor 100 reduction in mass at the end of FNR operations.

Figure 2.14. Comparison of long-term mass and toxicity reduction factors for 99.85%, 99.90% and 99.95% process efficiencies

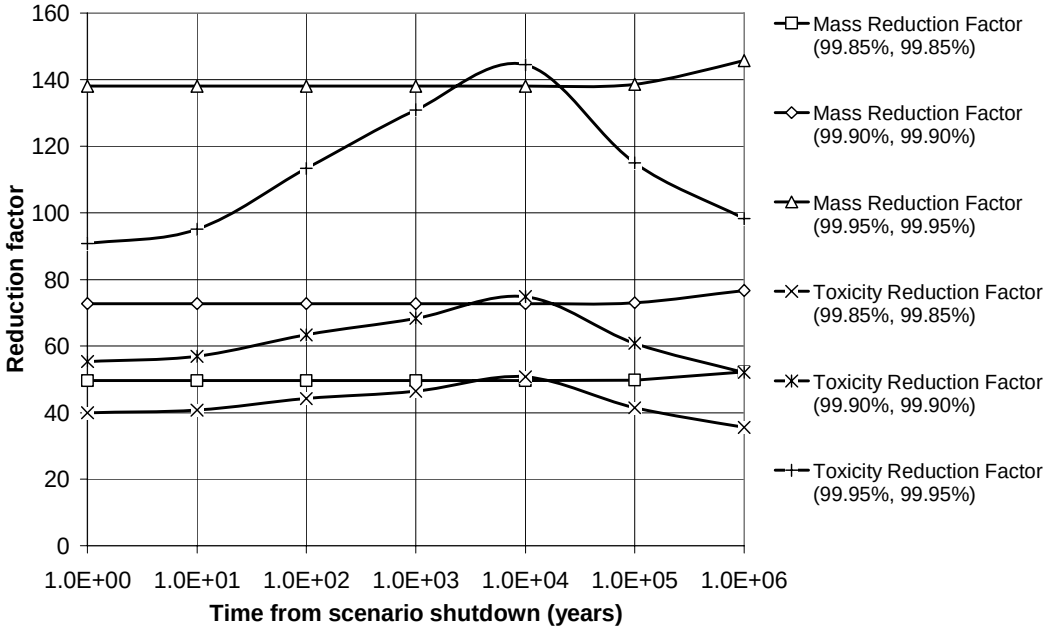

2.1.3.2 Impact on operation

The results presented so far have been based on the prompt recycle of all materials. While this is optimal in terms of material irradiation it may not be practical in terms of manufacturing, handling and storage. Specifically, the trend in nuclide distribution towards curium in multi-recycle schemes leads to highly active feed materials that produce both large amounts of decay heat and spontaneous neutrons.

To prevent difficulties arising from curium, two additional curium management techniques can be considered. The first is the most straightforward and involves the removal of curium from the cycle as it is produced. The second involves the storage of the curium for the life of a single generation of FNR for introduction into the next generation. This allows for the decay of curium to plutonium for 66 years (the inter-generation time) before being reintroduced into the cycle. A comparison of the effects these management strategies have on spontaneous neutron emission and heat production of fresh fuel is shown in Figures 2.15 and 2.16, respectively.

Figure 2.15 shows that specific neutron emission rate from fresh fuel is reduced by two orders of magnitude when curium is excluded from the cycle. However, even when curium is excluded the promotion of even isotopes of plutonium due to extensive multi-recycle leads to emission rates that are an order of magnitude higher than current LWR MOX fuels which have typical upper limits of 1×10^5 $ns^{-1}kg^{-1}$ [1]. When curium is delayed, the neutron emission rate is between the full curium and no curium values. There is, however, a steady increase as the re-introduction of curium into the cycle allows for build-up of other neutron emitting species, for example ^{242}Pu. Significant shielding would be required for manufacturing and transport of any fuel described in this study. The very high emission rates where curium is fully recycled would also lead to concerns for criticality during transport and storage.

Figure 2.15. Comparison of spontaneous neutron emission for various recycling options

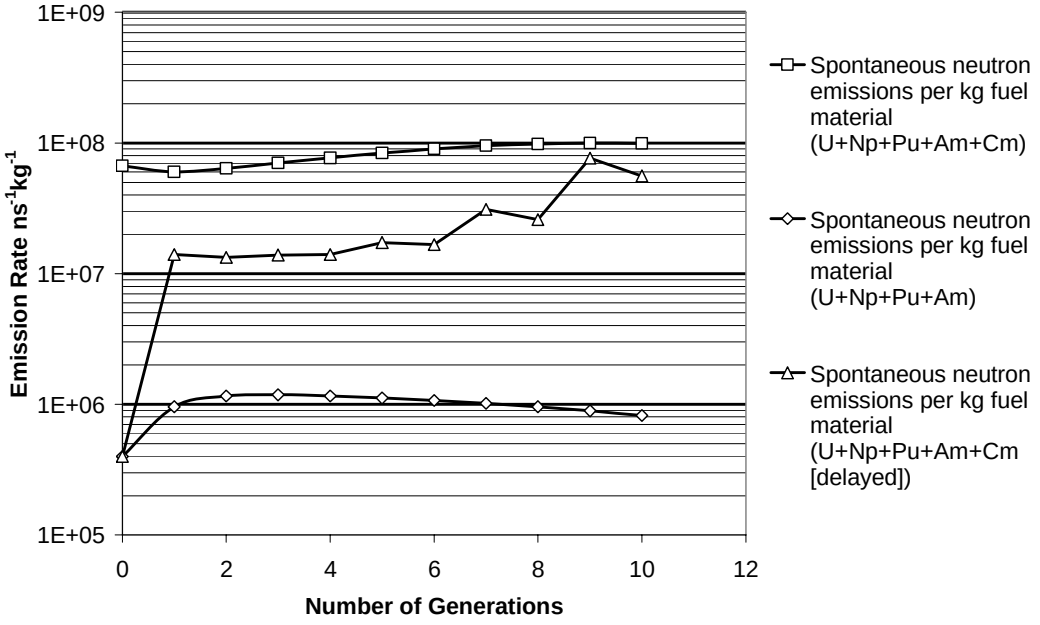

The variation of heat production of in the fresh fuel is compared for the three curium management strategies in Figure 2.16. It is seen that delaying the re-introduction of curium into the cycle can remove virtually all the heat production associated with curium, reducing heat production by up to almost 50% in later generations. Typical heat production for LWR MOX is 2 W/kg, so even the best case scenario with no recycled curium is 10 times higher when multi-recycle FNR operations are considered. Given the high levels of heat production predicted, special care would be required during handling and transport to ensure safe working temperatures are maintained. This may necessitate the use of active cooling techniques.

Figure 2.16. Comparison of decay heat production for various recycling options

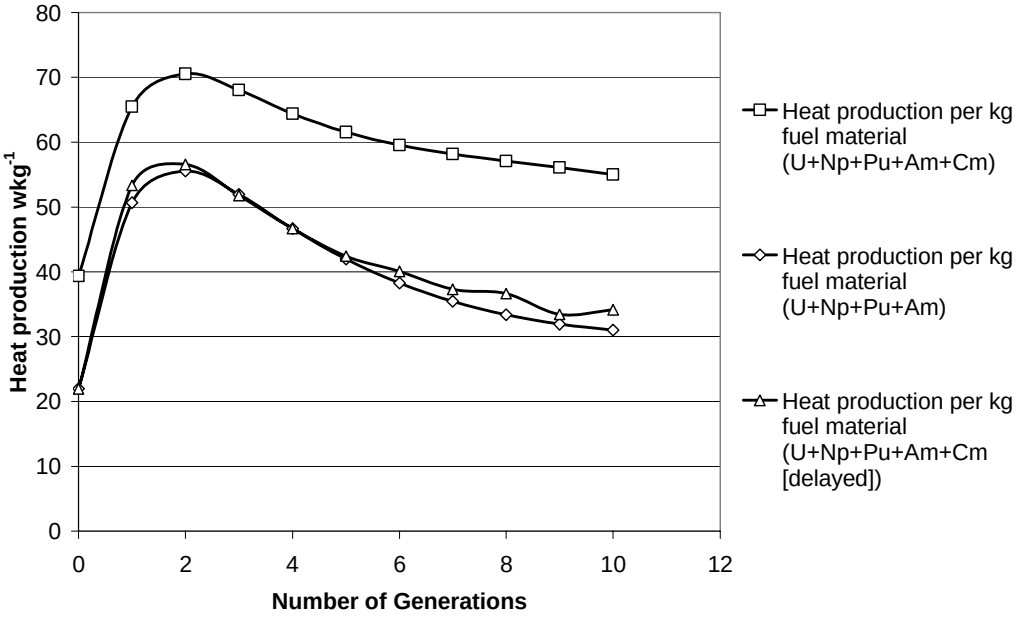

It is obvious that while the use of different curium management techniques has an impact on operational viability of manufacturing, handling and transport, it will also have an impact on overall performance. A comparison of the mass and toxicity reduction factors during operation for the three curium management strategies is shown in Figure 2.17. It is seen that the delayed re-introduction of curium into the cycle has a slight detrimental effect on performance. This is to be expected as the curium fractions of the fuel will have one less generation of irradiation and so proportionately less will be destroyed by fission. When curium is excluded from the cycle entirely, the performance of the scenario falls by more than a factor 2, giving an upper limit of about 30 on mass reduction and of 25 on toxicity reduction. These values are much lower than the commonly stated target of a factor 100 reduction [1], and demonstrate that some form of curium recycle is vital if P&T is to be an effective method of inventory reduction.

Figure 2.17. Comparison of cumulative mass and toxicity reduction factors for various recycling options

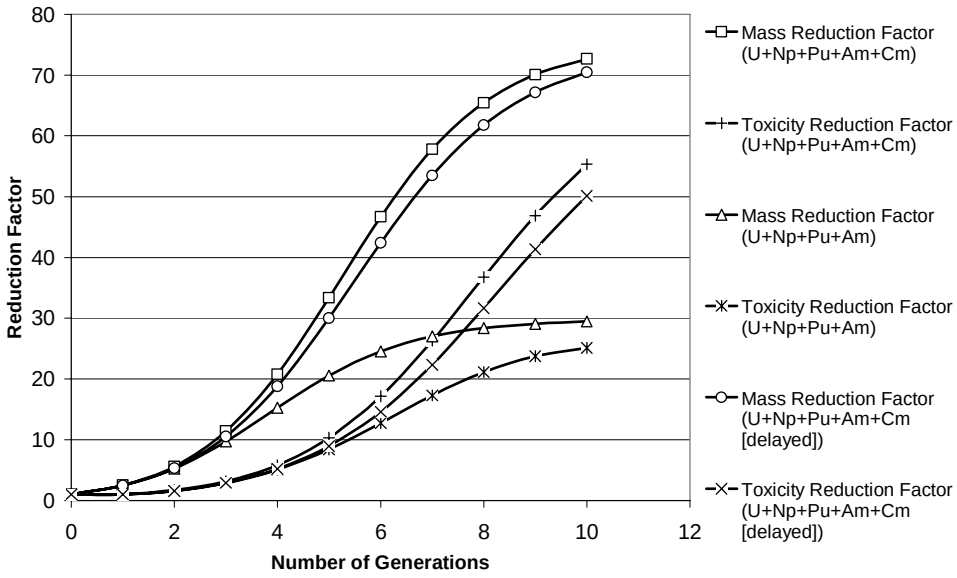

2.1.4 Summary

Time-dependant fuel cycle analysis gives insights into the key parameters required for P&T of nuclear fuel waste. While steady-state P&T studies can provide a useful guide to the likely performance and mass-flow characteristics of particular scenarios, they show some limitations when compared with the engineering realities of implementation.

The general treatment of the topic in this chapter has shown that the achievable reduction factor (either in terms of mass or radiotoxicity) is a sensitive function of fuel manufacturing or recycling process efficiencies, P&T reactor burn-up and P&T reactor operating strategy. In addition these factors determine the time scale required to implement the required reduction factor which could be several centuries. This has a further political implication in the establishment of the required institutional control over relatively long time scales.

Therefore time dependence, along with reduction factor requirements imposed by technical or political restrictions, can help define development targets for manufacturing loss, reprocessing separation factors and P&T reactor burn-up. Optimisation of reactor management factors such as refuelling strategy and operational lifetime must also take the planned time horizon of operations into account.

A further important aspect of time dependence is the ability to study transitions from current nuclear generation to future scenarios. These will indicate deployment scales for P&T based on the process and operating parameters chosen or targeted over a given period of time, and will also indicate how current stockpiles of actinide materials will behave over such transition periods.

2.2 Scenario studies for P&T: Overview of software available to perform analyses

The simplified analysis given in the previous section can provide indications of performance and useful analytic tools. While detailed physics analyses are used to generate reactor loaded to discharge mass ratio these are generally for equilibrium conditions and so do not explicitly take into account the large fuel composition variations that are characteristic of higher order multi-recycle schemes. In particular, nuclear decay chain relationships are not explicitly accounted for within the mass flow calculation. Further, when operational performance is evaluated, it is obvious that for a nuclide mixture a reduction in mass does not equate to an equivalent reduction in toxicity due to differences in specific toxicity values. Thus, in order to evaluate more realistic models, numerical simulation using software is required. A number of organisations are presently active in the development of such software. A brief overview of some of the systems currently available is provided below.

2.2.1 MEEMS (BNFL)

MEEMS is a software package designed to simulate the operations of general nuclear fuel cycles with a view to assessing both short- and long-term impact [5,6]. The software is designed around a graphical user interface that allows "dragging and dropping" of various plants and rapid connection of the plant items. This is intended to allow an intuitive approach to complex scenario modelling. Component details may be inspected, defined or updated through an edit window that "pops up" as required. MEEMS tracks 26 actinides and 22 long-lived fission products on an individual nuclide basis. Implementation of the decay chains is used to allow accurate prediction of inventory change during storage. This is particularly important for plutonium-based fuels, where significant changes to ^{241}Pu and ^{241}Am can occur over relatively short time scales, and also for systems that consider curium recycle. Material flow is tracked through a number of process nodes, which have the ability to store, alter and delay material, and which are connected via user-defined streams. Process components can either force material into the system, a feed source for example, or pull material through as required, a reactor for example. Material change and diversion within a process to simulate chemical/mechanical separation or nuclear transmutation is generally captured through the use of transformation coefficients that are derived from either experiment or higher-definition calculations. In addition, MEEMS contains a one-group reactor model to allow for explicit nuclear transformation calculations to be made where flux and cross-section data are available. This is particularly useful for studying multi-recycle scenarios where material compositions may undergo considerable evolution during operations. Streams may either be mixed as a feed to a process or kept separate to allow tracking of different downstream pathways. Streams may be inspected to give an indication of nuclear characteristics such as activity, toxicity, neutron emission and heat production, all of which help characterise the viability for use of material and an indication of likely safety, shielding or criticality implications. MEEMS runs scenarios on a discrete year-by-year basis and calculates storage and stream evolution both during scenario operation and to any future year after shutdown. The primary metric used is mass, although toxicity, activity, neutron emission and heat production data may also be requested. Results can be presented as a combination of a number of nuclides or given individually. All output is graphical, though the data may be exported for numerical analysis. Execution is relatively quick with a typical example taking of the order of minutes to run. Each case constructed in MEEMS can be used to produce a thorough QA document that lists all the physical parameters and linkages to allow verification that a model has been correctly defined.

2.2.2 DANESS (LISTO/ANL)

DANESS [7] is an integrated nuclear process model intended for the dynamic analysis of today's and future nuclear energy systems on a fuel batch, reactor, and country, regional or even worldwide level. The model allows simulating up to 20 different reactor types and up to 20 different fuel types in one simulation. The fuel cycle consists of 21 steps in the fuel cycle chain wherein several fuel cycle facility technologies can be characterised in the model. In its current version, DANESS v1.0, it is intended to deliver a systems view on future nuclear development paths. It therefore emphasises the actinide and fission product mass flows in the system and the economics of the components and the system as a whole. Detailed isotopic compositions of fuels are not calculated but are based on associated databases of typical fuel isotopic compositions. Starting from today's nuclear reactor park and fuel cycle situation, DANESS will simulate energy-demand-driven nuclear energy system scenarios over time and allows the simulation of changing nuclear reactor parks and fuel cycle options. The energy demand is given as an energy-demand scenario for electricity or any other energy form demanded from nuclear, e.g. hydrogen production. New reactors are introduced based on the energy demand and the economic and technological ability to build new reactors. The technological development of reactors and fuel cycle facilities is modelled to simulate the delays in technology availability. Levelised fuel cycle costs are calculated for each nuclear fuel batch for each type of reactor over time and are combined with capital cost models to arrive at bus-bar costs per reactor and, by aggregation, into a cost of energy for the whole nuclear energy system. More detailed cost analysis is performed to obtain an evolution of expenses for utilities, taking into account taxes, depreciation policies, average cost of capital and other factors. A utility sector and government-policy model may be activated to simulate the decision-making process for new generating assets and new fuel cycle options. The government policy model is still under development and will allow simulating different actions that governments may exert through, for instance, tax rates, regulation, R&D funding and others. Extension to life cycle analysis data, non-proliferation metrics and ecological impact for the system as a whole and/or subelements of the system is foreseen in future versions of DANESS. An additional advantage of DANESS is the implementation on standard PC/Mac platforms. A typical full-scale DANESS simulation covering a timespan of 100 years calculated in time steps of one month takes about 15 to 30 minutes on a modern PC or Mac. Shorter calculation times of the order of a minute are obtained with reduced problem sizes. DANESS is currently implemented using the IThink-Analyst software of High Performance Systems. DANESS has been extensively verified with other calculations of nuclear energy systems and this verification has indicated error margins inferior to a few per cent, depending on the quality and detail of data delivered by the user.

2.2.3 ICECAT (AEN/NEA)

The ICECAT (Integrated Costs and Needs of Fuel Cycle Analysis Tool) model is designed to simulate installed nuclear capacity. It operates under the IThink commercial software environment (supplied by High Performance Systems Inc.). Visual programming of IThink allows the user to manage the flow of materials, cash, personnel, etc. Provision of a graphical interface makes the model invisible to the user, thereby creating a simple but powerful tool. Data can be processed either under IThink using tables and graphs available on the interface, or under Excel by means of semi-automatic links. ICECAT is driven by energy demand, that is to say the construction of new reactors and fuel production/consumption is based on a scenario of demand for nuclear energy which the model must accommodate as well as possible. The installed capacity and fuel cycle chosen are semi-independent, which offers users considerable freedom of choice. Data on existing reactors and scenarios for energy demand are stored in a database (MS Access format) and are therefore easy to consult or modify, even on a computer without IThink. To allow the model to be updated with the most recent data available

(for example annual updates), the database output files are formatted in Excel. These Excel files are therefore linked to the tables in ICECAT. ICECAT has limited, coarse splits for material flow; for example, the number of elements separated in reprocessing is fixed to three (U, Pu, actinides).

2.2.4 NFCSim (LANL)

The NFCSim model [8] simulates complex nuclear fuel cycle (NFC) scenarios characterised by a large array of interacting components of the NFC. A nuclear economy in NFCSim may consist of any number of reactors. The model's reactor and fuel cycle modelling capabilities include fuel cycles oriented toward water reactors with the option of actinide recycling and a suite of fast reactors or accelerator-driven systems for closure of the NFC. A demand function for nuclear energy is specified, and NFCSim deploys new facilities as needed, subject to additional exogenously specified constraints such as limitations on the capacity of reprocessing facilities. Using a database of the current US nuclear infrastructure (mines, conversion, fabrication and enrichment plants) as the point of departure, NFCSim determines the time-dependent demand for these services. Unit costs for individual processes plus amortised capital costs for new facilities are assessed; a default cost database is provided. With the aforementioned information NFCSim calculates a system-wide time-dependent annual cost of electricity (COE) as well as a discounted life-cycle cost. LACE is a criticality and burn-up engine developed to provide life-cycle material balances for the diverse, mutually interacting, evolving reactor fleets treated by NFCSim. Given the appropriate cross-section libraries, LACE obtains fluence-dependent burn-ups as well as neutron production and destruction rates for each actinide present in the initial fuel. Given these data, a piecewise linear, reactor-specific reactivity model is formulated with fluence, rather than burn-up, as the independent variable. The model generalises to arbitrary reactor types and initial fuel compositions. These cycle-by-cycle capabilities are used to determine reactor fuel compositions upon charge and discharge and at various times after discharge (e.g. upon entering separations, fuel fabrication or a repository). LACE operates under transient and equilibrium fuel management regimes at the refuelling batch level and invokes ORIGEN2.x for burn-up and decay calculations.

2.2.5 COSI (CEA)

COSI, a software developed by the Nuclear Energy Direction at CEA, the French Atomic Energy Commission [9], is a code simulating a pool of nuclear electricity generating plants with its associated fuel cycle facilities. This code has been designed to study various short-, medium- and long-term options for the introduction of various types of nuclear reactors and for the usage of associated nuclear materials, with due consideration for the isotopic composition essentially of uranium, plutonium, minor actinides and some fission products.

The simulation that can be performed with the COSI code is shown schematically in Figure 2.18, and includes:

- Facilities that are part of the fuel cycle (mines, enrichment, fabrication, reactors, reprocessing, stockpiles, waste storage).
- Input data for the simulation (energy demand, fuel and nuclear materials requirements).
- Transfer of nuclear materials.
- Steps in which the change in the isotope composition of the fuel is important (irradiation, cooling time, aging time).

Figure 2.18. Schematic structure of the COSI code

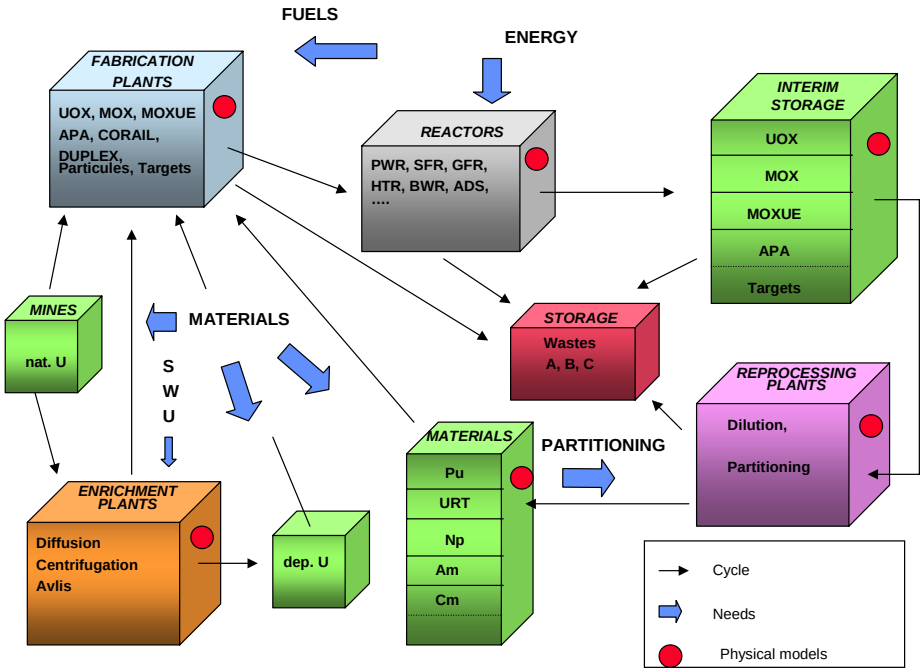

The general mechanism is illustrated by the requests; the study is supervised by the date of commissioning of reactors.

From this, the requests of the upline fuel cycle (fuel elements, nuclear materials, and so on) can be deduced.

For the downline cycle, the results are then evaluated (irradiated stockpiles, reprocessing flux, plutonium, uranium from reprocessing, wastes, and so on).

The request of plutonium, uranium or minor actinides from reprocessing closes the cycle.

The main features of the COSI code are:

- A detailed analysis of the fuel cycle with the possibility of taking into account:
  - Conversion, enrichment (natural and/or reprocessed uranium), fuel fabrication (uranium oxide, MOX, fuel with minor actinides, targets) and reprocessing plants, each with its technical characteristics: operating time, annual capacity, losses.
  - The various types of reactors (gas-graphite, PWRs, SFRs, GFRs, advanced reactors, incinerator reactors) together with their technical characteristics: date of commissioning, electrical power, load factor, lifetime, core management: time history, reload fuel management, type of fuel (UOX, UOX+MOX, MOX ...), characteristics of reload (mass, cycle path).
  - Stockpiles before and after each operation.
  - Transport.

- A detailed analysis of nuclear materials, taking into account:
  - Isotopic content: ^{232}U, ^{234}U, ^{235}U, ^{236}U, ^{238}U, ^{237}Np, ^{239}Np, ^{236}Pu, ^{238}Pu, ^{239}Pu, ^{240}Pu, ^{241}Pu, ^{242}Pu, ^{241}Am, ^{242m}Am, ^{243}Am, ^{242}Cm, ^{243}Cm, ^{244}Cm, ^{245}Cm, ^{99}Tc, ^{127}I, ^{129}I, ^{134}Cs, ^{135}Cs, ^{137}Cs.
  - Constraints in the operation of the fuel cycle facilities: ^{241}Am maximum acceptable concentration in MOX fuel fabrication, reprocessing plant capacity in heavy metal and in plutonium, minimum cooling down period prior to spent fuel reprocessing.
  - The possibility of alternative choices by the user for the reprocessing of spent fuel: "first in", "first out"; burn-up min, burn-up max; ^{241}Pu min, ^{241}Pu max; Pu content min, Pu content max.
  - The selection by the user of the various dilutions available in the reprocessing of the irradiated fuels.
  - Partitioning of minor actinides.
- A detailed computation of the materials balances including:
  - Computation of the plutonium content or ^{235}U enrichment entering fuel fabrication is based on: composition of the various batches of plutonium used, the origin of uranium (natural, depleted or reprocessing uranium), core management and burn-up.
  - Computation of the fuel isotopic content in and out of the reactor at any time and for each step in the fuel cycle. The evolution calculations are performed for the following systems:

PWR (UOX): 1.4% < ^{235}U < 9%	0 < burn-up < 100 GWd/t
PWR (MOX): 5% < Pu content < 12%	0 < burn-up < 70 GWd/t
PWR (MOXUE) 5%< Pu content < 12%, 0.25% < ^{235}U < 5%	0 < burn-up < 70 GWd/t
SFR (core and blanket): Phénix, SPx1, EFR, CAPRA	
GFR	
Np, Am and Cm transmutation in PWR, SFR or GFR	

- An economic balance on reactors and fuel cycle facilities in order to obtain a levelised cost for the kWh.

For each scenario, COSI allows to obtain:

- A material balance (mass, isotopic composition) at any time and for each step of the fuel cycle.
- An economic balance with decomposition for cycle cost, reactor operation cost, KWh cost.
- A waste radiotoxicity inventory (ingestion and inhalation).

Finally, the COSI code allows for the exploration of different electronuclear scenarios involving:

- A pool of reactors (PWRs, SFRs, HTRs, GFRs …).
- The full set of the fuel cycle facilities.
- The different types of fuels (UO_2, MOX, fuels with minor actinides, targets …).

Treatment of the isotopic content of nuclear materials (U, Pu, minor actinides) allows for the calculation of the following:

- Evolution of initial Pu content or ^{235}U enrichment entering in fuel fabrication.
- Evolution of fuel composition.
- Material balance at any time and for each step in the fuel cycle.

2.3 Scenario studies for P&T: Applications to ADS

2.3.1 Introduction

Innovative fission systems able to efficiently burn plutonium and/or minor actinides (MAs) are investigated here. There are two basic means of achieving a massive transmutation: either to perform multiple irradiation runs with limited burn-up for each run, and reprocessing, topping and re-fabrication between each run (this will be called multiple recycling) or to perform a single irradiation run with a very high burn-up, in order to limit as much as possible the amounts to be reprocessed and fabricated into fuel elements (this will be called once-through recycling). Only the first way is investigated here.

In this section "equilibrium" scenarios are analysed, i.e. to assess the asymptotic proportions of the different reactor types in the reactor fleet, the asymptotic composition in the burner reactors and in the waste stream (a given loss level at reprocessing being assumed).

2.3.2 Scenarios at equilibrium

Multiple recycling of actinides is considered in all the parametric studies presented in what follows. In that way, only reprocessing losses go to the waste. These losses are assumed here to be 0.1% for all actinides. The core concepts studied are dedicated to the transmutation of actinides, i.e. their fuel is made only of plutonium and minor actinides, and they can be critical or subcritical reactors (ADS).

In the so-called "double-strata" scenarios (see Chapter 1), a first stratum of reactors is devoted to plutonium (and neptunium) recycling, and a second stratum of reactors is dedicated to burn the other minor actinides, i.e. Am and Cm (see Figure 2.19). The "double-component" scenarios involve two types of reactors: standard reactors to produce electricity, based on PWR and uranium fuel, and innovative reactors burning Pu and MA together (see Figure 2.20). In both cases, the burner reactor compositions are given at equilibrium, i.e. at the asymptotic regime when isotopic compositions are stabilised from a loading to the next one.

The innovative concepts used to compare critical reactor and subcritical reactors (ADS) are based on fast reactors using different coolant technologies: sodium (Na), lead or lead-bismuth (Pb, Pb/Bi) or gas (He). The critical cores for MA transmutation in double-strata scenarios cooled by heavy metal are small units (150 MWth, see Table 2.4). The choice of a small core size is suggested in order to improve reactivity coefficients strongly affected by the large MA fraction in the fuel (see Table 2.5). The ADS systems are medium size (1 500 MWth) for all types of scenarios. However, "twin" ADS with respect to critical cores (i.e. same core volume and power) have been studied in order to allow for a comparison due to subcriticality alone.

All calculations were performed using the ERANOS neutronic code system [10], with nuclear data based on JEF2 evaluations.

Figure 2.19. Double-strata scenario

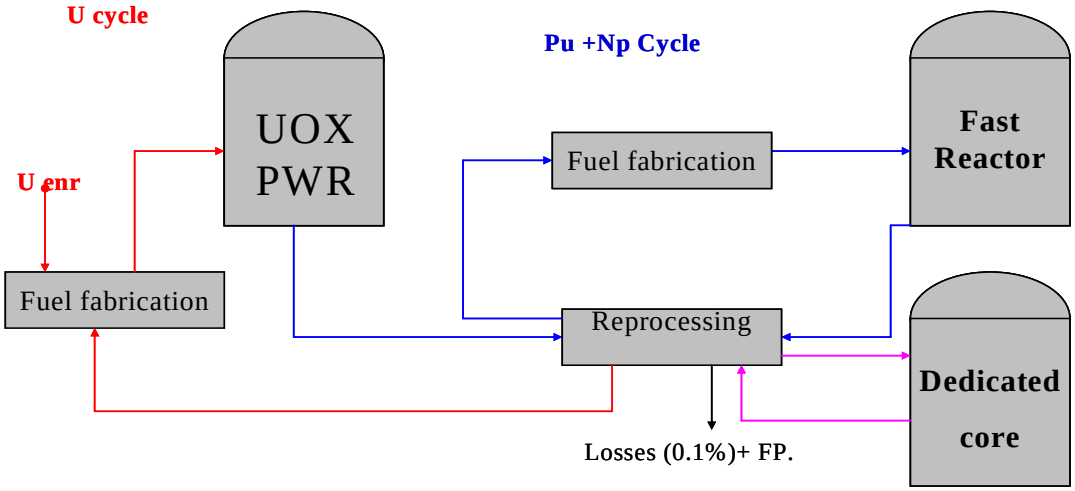

Figure 2.20. Double-component scenario

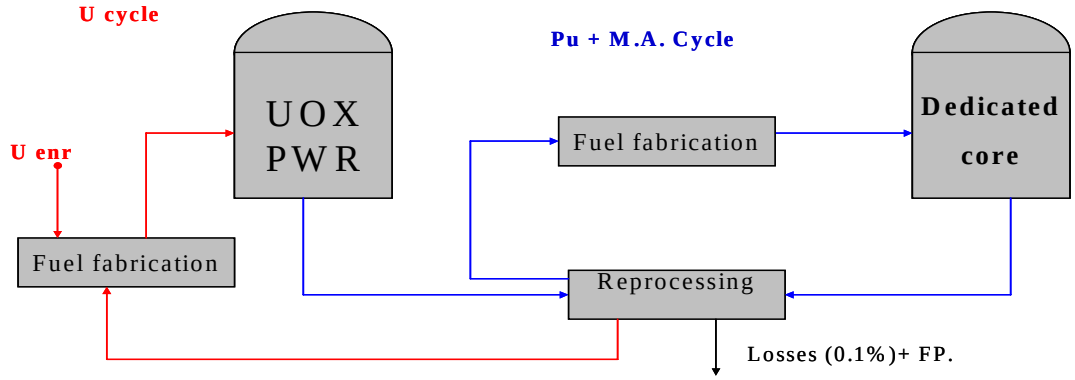

Table 2.4. General data for double-strata cores

Core type	Critical			"Twin" ADS			ADS		
Coolant	Na	Pb	He	Na	Pb	He	Na	Pb	He
Core power (MWth)	156	138	1 000	156	138	1 000	1 500	1 500	1 500
Fuel volume fraction (%)	22.7	22.0	14.4	22.7	22.0	14.4	14.4	11.9	15.4
Actinide load (kg)	1 267	1 116	3 336	1 378	1 213	3 497	6 376	5 422	4 798
Fuel residence time (efpd)	1 500	1 500	900	1 500	1 500	900	1 500	1 500	900
Average power (W/cm^3)	274	243	441	276	244	442	406	406	407
Average BU (%)	18.3	18.3	26.7	17.0	17.0	25.5	34.6	40.4	27.8

Table 2.5. Reactivity coefficients for double-strata cores

Core type	Critical			"Twin" ADS			ADS		
Coolant	Na	Pb	He	Na	Pb	He	Na	Pb	He
$\Delta\rho_{coolant}$ (pcm)	2 060	1 290	–	2 540	2 950	–	4 360	5 440	–
$K_{Doppler}$ (pcm)	-211	-181	-253	-178	-119	-311	-422	-393	-485
β_{eff} (pcm)	162	155	148	213	142	121	121	140	133

2.3.2.1 Double-strata scenarios

The first stratum is made of UOX PWRs and standard, EFR-type, sodium-cooled fast reactors (FR); the PWRs feeding the FRs with the plutonium they produce. The second stratum is made of MA burners fed by the MA output of both PWRs and FRs, and possibly with some amount of plutonium which is diverted from the Pu stream directed to the fast reactors, in order to support the reactivity level if needed. The asymptotic composition for the MA burner fuel results in a non-negligible plutonium content due to both the Pu feed (if any) and the transmutation of minor actinides (mainly captures on ^{237}Np, capture + decay on ^{241}Am, and decay of ^{244}Cm). Table 2.6 shows the Pu content in the fuel, characterised by a very degraded isotopic composition, i.e. high content in even Pu isotopes: ^{238}Pu and ^{242}Pu (due to the capture + decay on ^{241}Am) and ^{240}Pu (due to the decay of ^{244}Cm).

Table 2.4 gives some general data on the double-strata cores. The main assumptions concern core power (global and specific) and fuel residence time. The low power for liquid-metal-cooled critical cores and their associated twin ADS is motivated by reactivity coefficient mitigation; it is worth noting then that the critical core contains some amount of hydrogenated moderator such as ZrH_x (a volume fraction roughly 5%) in order to reduce the coolant void reactivity and increase the Doppler feedback, and that the particle fuel for the gas-cooled reactors is placed within graphite-based subassemblies that provide some moderation as well. Residence times are assumed to lie between three and five calendar years. The fuel volume fraction results directly from the subassembly geometry for the critical cores. It was adjusted for ADS in order to obtain the prescribed reactivity level (k = 0.98 at beginning of cycle); some dilution of the fuel with an inert matrix is then assumed.

The main reactivity coefficients are given in Table 2.5. This table shows that with a degraded Pu + MA fuel composition, the coolant void reactivity is high, even for very small liquid-metal-cooled cores; the absolute value of the Doppler constant is low despite the presence of moderator; and the delayed neutron fraction is very small. In order to have a reference for comparisons, typical values for a standard LMFBR core, such as Super Phénix or EFR are approximately 2 200 pcm for the sodium void reactivity, -800 pcm for the Doppler constant and 360 pcm for the delayed neutron fraction. The advantage of ADS is to be much better able to cope with very the poor reactivity coefficients due to Pu + MA fuel than the corresponding critical cores.

Table 2.6 shows how the plutonium content in the fuel, the reactivity loss and the accelerator requirements (intensity, fraction of the gross electrical power of the ADS devoted to feed the accelerator) are correlated. The lower reactivity level for ADS with respect to critical reactors allows for the decrease of plutonium content; this reduction is amplified by a size effect (leakage reduction for larger cores). The larger size should in principle lead to a reduction of the reactivity loss, but this effect is somewhat offset by the increase in specific power (for the liquid metal cooled cores). The reactivity evolution vs. time, characterised by an increase at low burn-ups followed by a decrease at higher burn-ups, may lead to very small accelerator requirements for the equilibrium batch.

Table 2.6. Pu content, reactivity loss and accelerator requirements for double-strata cores

Core type	**Critical**			**"Twin" ADS**			**ADS**		
Coolant	**Na**	**Pb**	**He**	**Na**	**Pb**	**He**	**Na**	**Pb**	**He**
Pu/(Pu+MA) (w%)	55.5	48.5	38.6	44.0	39.2	36.0	32.5	29.7	37.7
Δρ (pcm/efpd)	-6.2	-4.2	-2.4	-2.8	-1.1	-1.4	-4.2	-6.0	-1.4
I_{acc}/P_{th} (mA/GW)	–	–	–	11.5	11.6	11.7	3.7	~0	11.7
P_{acc}/P_{elec} (%)	–	–	–	7.2	7.2	7.2	2.3	~0	7.3

Finally, Table 2.7 shows global scenario parameters for a fixed-size reactor fleet, i.e. 60 GWe installed power, producing 400 TWhe a year. These parameters are the fraction of the reactor fleet electricity produced by the second stratum burner reactors, the TRU inventory in reactors and cycle plants (i.e. for reprocessing and fuel fabrication), the annual amount of TRU wastes when an elementary loss rate of 0.1% is assumed, and finally the reduction in TRU waste inventory or radiotoxicity, taken at 10 000 years after storage, with respect to what is called the "open cycle", i.e. a reactor fleet of the same global power made only of (once-through) PWRs. The figures show that there is very little difference between scenarios involving critical or ADS TRU burners. This is not surprising, since the basic spectrum average reactions (capture, fission) are very similar in both cases.

Table 2.7. Scenario data for double-strata cores

Core type	**Critical**			**"Twin" ADS**			**ADS**		
Coolant	**Na**	**Pb**	**He**	**Na**	**Pb**	**He**	**Na**	**Pb**	**He**
Fraction of electricity prod. (%)	5.3	4.3	3.6	3.5	3.2	3.2	3.5	3.7	3.4
Inventory (t)									
Pu	492	492	473	499	498	478	471	466	474
Np	10.8	11.0	10.5	11.3	11.2	10.6	10.5	10.4	10.5
Am	44.8	43.6	26.2	44.1	43.5	26.2	24.7	22.6	24.5
Cm	14.5	14.1	10.8	14.9	14.7	11.6	10.9	9.7	11.5
Wastes (kg/y)									
Pu	37.9	37.7	36.5	38.2	38.1	36.8	35.9	35.5	36.5
Np	0.84	0.84	0.80	0.9	0.9	0.8	0.8	0.8	0.8
Am	3.50	3.40	2.25	3.5	3.5	2.4	2.0	1.8	2.2
Cm	1.19	1.15	1.10	1.2	1.2	1.1	0.9	0.8	1.1
Waste TRU mass reduction	271	273	290	269	270	287	308	313	328
Radiotox. reduction at 10^4 y	228	228	239	225	225	236	271	255	264

The ADS detailed nuclide inventories are given in Appendix 2.3.

2.3.2.2 Double-component scenarios

These scenarios involve PWRs that send their TRU output into burners, plutonium not being recycled in separate units as in the double-strata scenarios. In these scenarios, plutonium represents roughly 90% of the feed to TRU burners. As a consequence the fuel is much more reactive (fissile), and a further reduction in the fuel volume fraction is required (see Table 2.8). In these scenarios, the TRU burners are He-cooled reactors, either based on pin or particle fuel design. For pin design, no moderator is present, while for the particle fuel design, the main subassembly support material is graphite. The fuel is made only of plutonium and minor actinides (no uranium).

Table 2.8 shows that the fuel volume fractions have to be decreased dramatically in order to maintain an acceptable reactivity level. This means that an inert matrix would have to be used. Due to a smaller core volume and correlatively a higher specific power for the same fuel residence time, the burn-up is much greater for the particle fuel design.

Table 2.8. General data for double-component cores

Core type / Fuel design	ADS	
	Pin	Particle
Core power (MWth)	1 500	1 500
Fuel volume fraction (%)	7.6	8.8
Actinide load (kg)	6 094	2 828
Fuel residence time (efpd)	900	900
Avg. power (W/cm^3)	176	407
Average BU (%)	21.3	43.4

Table 2.9 shows that in the pin fuel ADS core, with no moderator inside, the Doppler constant is quite low, while it is high for the particle fuel core due to the large amount of graphite present. On the contrary, the delayed neutron fraction is much lower in the particle fuel core, which has the softest spectrum, due to the higher degradation of the plutonium isotopic composition, while it remains fairly high in the non-moderated core which allows the lowest degradation of the Pu isotopic composition.

Table 2.9. Reactivity coefficients for double-component cores

Core type / Fuel design	ADS	
	Pin	Particle
$\Delta\rho_{coolant}$ (pcm)	–	–
$K_{Doppler}$ (pcm)	-99	-845
β_{eff} (pcm)	238	70

The plutonium content is much higher than for the double-strata core, as shown in Table 2.10, due to the very large content of the Pu + MA feed (roughly 90%). This means a higher reactivity loss (effect mitigated in the pin fuel design by the lower specific power), due to a lower Pu (re)generation from captures on minor actinides. Consequently higher beam intensities are needed for a given core energy output than in double-strata cores.

Table 2.10. Pu content, reactivity loss and accelerator requirements for double-component cores

Core type / Fuel design	ADS	
	Pin	Particle
Pu/(Pu + MA) (wt.%)	80.8	79.3
$\Delta\rho$ (pcm/efpd)	-8.56	-21.4
I_{acc}/P_{th} (mA/GW)	36.5	63.5
P_{acc}/P_{elec} (%)	22.8	39.7

Since the ADS have to fission all TRU nuclides coming from PWRs, the fraction of electricity in the overall reactor fleet produced by the TRU burners is much greater than it was for the MA burners in the double-strata scenarios. The mass inventories are clearly dependent on the average burn-up achieved in the core: the greater the burn-up, the lower the inventory and the waste produced by reprocessing, as shown in Table 2.11. For the double-strata scenarios, this effect was somewhat masked by the inventory and waste stream due to the Pu burners in the first stratum, operating at fixed burn-up for all the scenarios.

Table 2.11. Scenario data for double-component cores

Core type / Fuel design	ADS	
	Pin	**Particle**
Fraction of electricity prod. (%)	18.4	16.1
Inventory (t)		
Pu	387	206
Np	19.7	8.8
Am	44.6	17.8
Cm	11.5	18.8
Wastes (kg/y)		
Pu	36.4	18.9
Np	1.8	0.7
Am	4.3	1.6
Cm	1.1	1.7
Waste TRU mass reduction	302	514
Radiotox. reduction at 10^4 y	252	455

The ADS detailed nuclides inventories are given in Appendix 2.3.

2.3.2.2 Conclusions

In conclusion, the parametric scenario studies presented in this section indicate the size of the "transmuter" reactor fleets needed to stabilise (at equilibrium) the minor actinide or minor actinide plus plutonium inventories. In the double-strata strategy, a fraction of 3 to 5% (in terms of the total reactor fleet power) of transmuter cores is needed. In the case of the double-component strategy, under the most favourable conditions, a fraction of 25% of transmuter cores is needed. These results are relatively independent of the type of transmuter core, and in particular of the core coolant.

In the parametric scenario studies, small (i.e. ~150 MWth) or relatively large (i.e. ~1 500 MWth) ADS cores have been used. This choice does not affect the order of magnitude of the main results. However, in the international community there has been the tendency to focus on a somewhat intermediate core size (~800 MWth) with liquid-metal cooling, and in the next paragraph two typical ADS core images of that class will be described.

2.3.3 Two examples of ADS of intermediate size with liquid-metal cooling

The characteristics of two ADS cores are described here. The first one is a ~800 MWth ADS core, Pb/Bi cooled, devoted to TRU transmutation (Pu/MA ratio in the fuel ~4), developed at the Royal Institute of Technology of Stockholm (KTH) [11]. The second is a Na-cooled ADS core of similar power, also devoted to TRU transmutation, developed at Argonne National Laboratory [12]. The KTH core has a nitride fuel, and the ANL core a metal fuel.

2.3.3.1 The "KTH" Pb/Bi-cooled ADS

The following tables from Ref. [11] display the major characteristics. Table 2.12 gives the pin and pellet specifications of the (TRU,Hf)N fuel, Table 2.13 gives the core specifications and Table 2.14 gives a summary of the core performances. Finally, Figure 2.21 shows a core layout.

Table 2.12. Reference system, pin, and pellet design specifications

A triangular pin lattice is adopted. Maximum allowed internal gas pressure in the fuel pin is 20 MPa.

Pellet density (% TD)	0.85
Pellet outer radius Rfuel (mm)	2.4
Cladding inner radius Rgap (mm)	2.5
Cladding outer radius Rpin (mm)	3.0
Active pin length (cm)	100
Length of upper fission gas plenum (cm)	150
Length of lower fission gas plenum (cm)	10
Length of bottom plenum spacer (cm)	10
Length of radial reflector SAs (cm)	140
Thickness of radial reflector (cm)	150
Length of upper reflector (cm)	200
Length of lower reflector (cm)	230
Spallation target radius (cm)	20
Radius of accelerator beam tube (cm)	15
Distance of target window from centre plane (cm)	20

Table 2.13. Design specifications of the conceptual core

Parameter conceptual design	
SA outer flat-to-flat (cm)	10.8
SA pitch (cm)	11.0
Duct thickness (cm)	0.25
Pins per SA	91
Pitch-to-diameter ratio	1.75
Number of core SAs	294
Thermal power (MW)	800
Averaged linear power (kW/m)	29.9
Pb/Bi spallation target outer radius (cm)	22.5
Radius of accelerator beam tube (cm)	15

Table 2.14. Neutronic, safety and burn-up performance of the conceptual core design. A capacity factor of 0.75 is assumed.

Parameters	**Unit**	**Conceptual design**
En ($1^{st}/2^{nd}/3^{rd}$ enrichment zone)	keV	164/183/166
Proton efficiency ϕ* (BOC/EOC)		26.9/26.0
Coolant void worth at BOL	pcm	-270
Cladding and duct worth at BOL	pcm	+6 390
Flooding of the accelerator tube	pcm	+200
Doppler $T\Delta k/\Delta T$	pcm	-47
Axial fuel expansion $\Delta k/(\Delta H/H)$	$Pcm/10^{-5}$	-0.21
Grid expansion $\Delta k/(\Delta P/P)$	$Pcm/10^{-5}$	-0.52
Coolant density change $\Delta k/\Delta T$	pcm	+0.13
β_{eff} at BOL pcm	pcm	230
M_{act} at BOL	kg	2 140
Burn-up rate	%FIMA/fpd	0.036
Reactivity loss	pcm/batch	-3 300

Table 2.14. Neutronic, safety and burn-up performance of the conceptual core design. A capacity factor of 0.75 is assumed (*cont.*).

Parameters	Unit	Conceptual design
Δk_{eff}/%FIMA	pcm/%	-850
Doubling of the accelerator power Ip	fpd	100
^{242}Cm fraction in fuel	%/%FIMA	0.12
Number of batches		5
Batch length	days	100
Average burn-up without initial core reshuffle	%FIMA	~20
Maximum radiation damage at EOL	dpa-NRT	100
Net Pu consumption	kg/efpy	188
Net MA consumption	kg/efpy	21

Figure 2.21. Cross-section of the conceptual core design

The core consists of three enrichment zones with different matrix fractions. Radial steel reflector subassemblies are depicted in grey. The thickness of the radial reflector was optimised so that the coolant void reactivity is minimised.

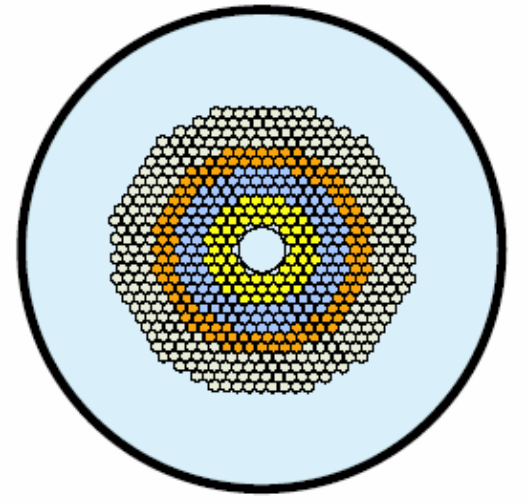

2.3.3.2 The "ANL" Na-cooled ADS [12]

A sodium-cooled blanket system point design was developed based on the results of a series of parametric studies. The proposed SubCritical MultiplyerSCM core layout, shown in Figure 2.22, consists of an LBE target/buffer that occupies the space equivalent to the 19 central assemblies along with 132 fuel assemblies. The fuel assemblies are surrounded by two rows of steel reflector assemblies and one row of B_4C shield assemblies. The principal design parameters of the proposed design are summarised in Table 2.15.

The main performance parameters for the selected point design are summarized in Table 2.16. The average discharge burn-up of 275 MWd/kg (29.5 at.%) is achieved with a 3.5 to 4-year fuel residence time. The burn-up reactivity loss is ~5% with the adopted half-year cycle duration. The volume fraction of fuel particles in the matrix required to achieve the targeted subcriticality level at BOEC is 20% in the inner zone and 26% in the outer zone, which is significantly lower than the dispersion fuel limit. The peak fast fluence value of 4.06×10^{23}n/cm^2 in the inner zone assemblies is close to the assumed fluence limit.

A remarkable feature is the TRU annual consumption rate comparison: results shown in Tables 2.14 and 2.16 indicate a substantial equivalence of the two systems, despite the difference in fuel and coolant types.

Figure 2.22. Core configuration selected for sodium-cooled ADS

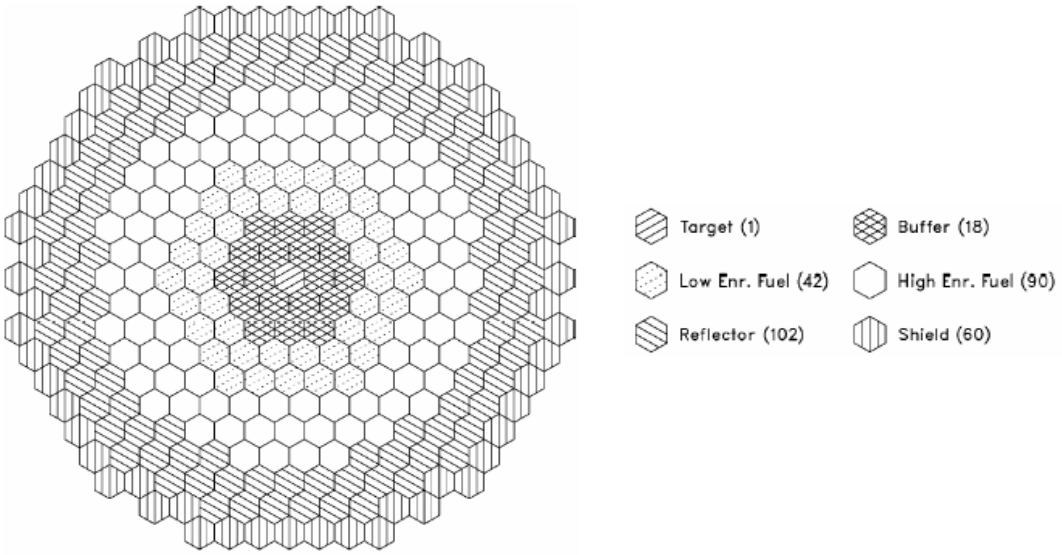

Table 2.15. Design parameters of selected ADS sodium-cooled SCM design

Proton energy (GeV)			1.0
Target material			LBE
Fuel material			(TRU-10Zr)-Zr
Pin diameter (cm)			0.744
Cladding thickness (cm)			0.056
Pitch-to-diameter ratio			1.197
Number of pins per assembly			271
Fuel smear density (%)			85
Volume fractions (as fabricated)	Fuel (smeared)		0.377
	Structure		0.257
	Coolant		0.366
Hexagonal assembly pitch (cm)			16.14
Number of assemblies	LBE target/buffer		19
	Fuel	Inner zone	42
		Outer zone	90
		Total	132
	Reflector		102
	Shield		60
TRU fraction split factor (outer zone/inner zone)			1.3
Active fuel height (cm)			107
Equivalent fuel region diameter (cm)			208
Maximum blanket diameter (cm)			300
Number of fuel batches	Inner zone		7
	Outer zone		8
Cycle irradiation time (days)			135

Table 2.16. Performance characteristics of selected ADS sodium-cooled SCM design

Fuel particle fraction (volume % in matrix)	Inner zone	19.9
	Outer zone	26.2
Multiplication factor	BOEC	0.970
	EOEC	0.920
Burn-up reactivity loss (%Δk)		4.94
Core average power density (kW/litre)		241
Power peaking factor	BOEC	1.501
	EOEC	1.508
Peak linear power (W/cm)	Inner zone	393 (at EOEC)
	Outer zone	397 (at BOEC)
Discharge burn-up (MWd/kg)	Average	275
	Peak	411
Peak fast fluence (10^{23} n/cm^2)	Inner zone	4.06
	Outer zone	3.97
Net TRU consumption rate (kg/year)		236
Equilibrium loading (kg/year)	LWR TRU	236
	Recycled TRU	565
	Total TRU	801
Heavy metal inventory (kg)	BOEC	2 620
	EOEC	2 504

2.3.4 ADS deployment scenarios

As far as the ADS deployment scenarios, two examples can help to quantify needs:

- The case of a Country A, which considers the phase-out of nuclear energy, but looks for a minimisation of wastes to be sent to a final repository. In the case considered, the amount of Pu and MA built-up at a hypothetical phase-out date ~2025 are respectively: $M_{Pu} \simeq 120$ t and $M_{MA} \simeq 20$ t.

- The case of a Country B with a LWR fleet producing ~60 GWe. MOX fuel is multi-recycled in the LWR with a specifically optimised core fuel assembly. MA are separated and sent, together with some Pu, to the dedicated transmuters of the second stratum in a "double-strata" strategy.

These examples have been treated recently in detail [13] with the code NFCSim, described in Section 2.2, and the major results are summarised in Figures 2.23 and 2.24. The ADScore is the ANL core described in Section 2.3.3.2.

In the case of Country A, since plutonium constitutes ~85% of the TRU contained in the spent nuclear fuel, SNF, the ADS used to transmute that TRU must necessarily employ relatively short cycles. In fact, the burn-up reactivity gradient resulting from use of the Country A TRU inventory limited the ADS cycle burn-up to 40 MWd/kg (with a reactivity swing $\Delta k_{eff} = 0.03$) and cycle time to slightly less than half of a year.

Figure 2.23. ADS: Design parameters and deployment strategy in Country A

The ADS is a Na-cooled, metal-fuelled facility with an LBE.
Eight 840 MWth facilities are deployed in the first generation and three in the second.

Top-level ADS parameters

Target k_{eff}	0.97 (BOC) 0.94 (EOC)
Core inventory	3 000 kgIHM
Thermal power	840 MWt
Discharge burn-up	200 MWd/kg
Fuel mgt.	5 batches/core
Cycle time	168 days

Facilities deployed

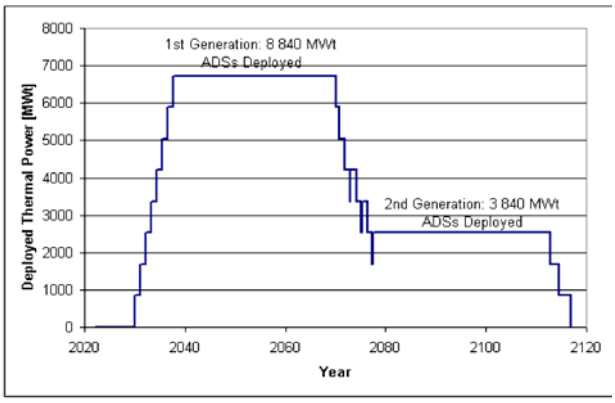

Figure 2.24. Deployment strategy in Country B (double strata)

Accelerator driven systems are deployed beginning in 2030. To maintain comparability between this scenario and that implemented for Country A, the top-level ADS design parameters were held constant. The more favourable feed stream, however, allows the fuel management to be changed to 210 MWd/kg discharge burn-up with a two-batch/core reloading scheme with the charge and discharge k_{eff} values being held at 0.97 and 0.94, respectively.

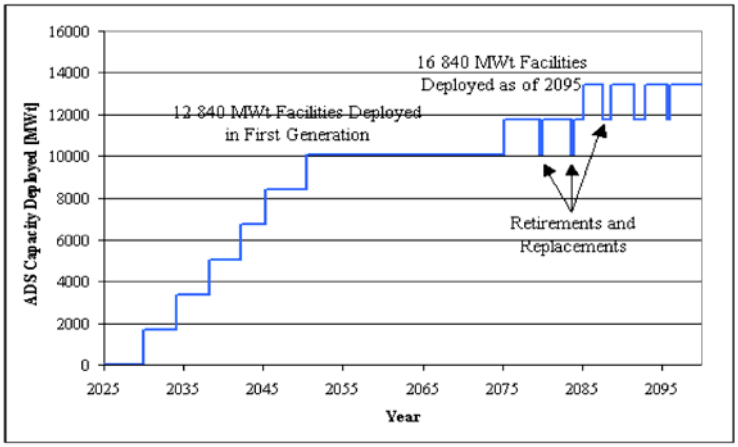

The scenario objective is to incorporate all spent nuclear fuel into the transmuting fuel cycle within one facility lifetime. With 40-year facility lifetimes assumed, it was found that eight transmuters are needed. The second and subsequent generations of transmuters take the final discharges of the previous generation as their feed. Since just over half of the transuranic content of Country A's SNF was transmuted by the first generation of eight facilities, the remaining TRU support another generation of three transmuters. All Country A SNF is reprocessed during the lifetimes of the first generation of eight ADS. The second generation of ADS obtains its feed exclusively from the final discharges of the first ADS generation.

The main result of the study is the TRU mass reduction by a factor of five over two generations of ADS operation.

For Country B, as opposed to the transmutation of a fixed-size SNF legacy, a continuously produced time-varying stream of transuranics constitutes the ADS feed stream. Therefore, the transmuting fleet must be sized and deployed with the aim of accepting this feed at the rate at which it is generated.

The net electric power delivered by the Country B LWR fleet is ~60 GWe, with 2/3 UOX-PWRs and 1/3 MOX-PWRs. This fleet would generate, by 2100, ~300 t of separated MA, if only Pu is used.

Accelerator-driven systems are deployed beginning in 2030. To maintain comparability between this scenario and the scenario of transmutation of SNF produced by the Country A fleet, the ADS design parameters are held constant. The more favorable feed stream, however, allows certain of the fuel cycle parameters to be improved. The discharge burn-up target is changed to 210 MWd/kg with a two-batch/core reloading scheme. Charge and discharge k_{eff} values are held constant at 0.97 and 0.94, respectively.

The ADS deployment then represents additional capacity over and above the 60 GWe. Twelve cores are deployed in the first generation; deployment is staggered with pairs of cores coming online every four years. Deployment is more gradual than was the case for Country A transmutation, as the material to be transmuted by Country B becomes available only gradually. Hence, it is necessary to delay the deployment of new ADS until sufficient MOX SNF and separated MA become available to provide feed for the start-up cores. Note that the second generation consists of a greater number of facilities: 16 transmuters. A larger number of facilities is required in the latter part of the century because the growing number of MOX-using reactors discharges an increasing quantity of minor actinides.

2.3.5 Conclusion

The elementary loss rate at reprocessing being fixed, all equilibrium scenarios show similar waste stream reductions with respect to the open cycle. For double-strata scenarios, the individual variations are dampened by the first stratum waste output, specially the output from the Pu burners. For double-component scenarios, the burn-up achieved impacts directly on the waste stream and inventory amounts.

The fraction of the reactor fleet electrical output due to MA burners ranges between 3 and 5% for the double-strata scenarios, and between 16 and 18% for the double-component scenarios.

Variations with the coolant used are insignificant, provided that a sufficient level of subcriticality can be ensured (reactivity coefficients). The double-strata MA burners exhibit better fuel reactivity regeneration properties than the double-component Pu + MA burners, and so require smaller proton beam intensities for similar reactor powers.

The results quoted in Section 2.3.2 are only prospective ones, because thorough fuel element design studies may change the geometry and composition of the fuel elements. In any case, the fundamental trends have been put in evidence.

The results of the time-dependent studies of Section 2.3.4 allow for quantifying the number and pace of ADS deployment in two contrasting situations. The relatively large number of facilities required to implement the respective strategies of Country A and Country B suggests the viability of a regional approach to an ADS-based transmutation strategy [14] as a means of optimising resources.

REFERENCES

[1] *Accelerator-driven Systems (ADS) and Fast Reactors (FR) in Advanced Nuclear Fuel Cycles*, OECD/NEA, Paris (2002).

[2] Ahn, J., P.L. Chambre, E. Greenspan, W.E. Kastenberg, M.D. LowenthaL, B. Park, J. Vujic, *Impacts of Waste Transmutation on Repository Performance*, Report UCBNE-4225, Prepared for Los Alamos National Laboratory, Department of Nuclear Engineering, University of California Berkeley, USA (1999).

[3] Robbins, C., D.R. Parker, C.H. Zimmerman, "Limits, Timescales and Optimisation of Fast Neutron Reactor P&T Schemes", *GLOBAL'03*, New Orleans, 16-20 November 2003.

[4] *Dose Coefficients for Intakes of Radionuclides by Workers*, ICRP Publication 68, Annals of the ICRP, 24, No. 4 (1994).

[5] Robbins, C., C. Hoggett-Jones, "Modular Simulation Software for Modelling the Impacts of Alternative Spent Fuel Management Practices in the Nuclear Power Industry", *Simulation Modelling Practice and Theory*, 10, 153 (2002).

[6] Hoggett-Jones, C., C. Robbins, G. Gettinby, S. Blythe, "Modelling the Inventory and Impact Assessment of Partition and Transmutation Approaches to Spent Nuclear Fuel", *Annals of Nuclear Energy*, 29, 491-508 (2002).

[7] Van Den Durpel, L., A. Yacout, D. Wade, H. Khalil, "DANESS – Dynamic Analysis of Nuclear Energy System Strategies", *GLOBAL'03*, New Orleans, 16-20 November 2003.

[8] Schneider, E., *et al*., "NFCSim: A Dynamic Fuel Burn-up and Fuel Cycle Simulation Tool", *Nucl. Tech*., Vol. 151, p. 35, July 2005.

[9] Grouiller, J.P., *et al*., "COSI: A Simulation Software for a Pool of Reactors and Fuel Cycle Plants", *Proc. Int. Conf*., Kyoto, 27 October-1 November 1991.

[10] Doriath, J.Y., C.W. McCallien, E. Kiefhaber, U. Wehmann, J.M. Rieunier, "ERANOS-1: The Advanced European System of Codes for Reactor Physics Calculations", *Conference on Mathematical Methods and Supercomputing in Nuclear Applications*, Karlsruhe, Germany, 19-23 April 1993.

[11] Tucek, K., *Neutronics and Burn-up Studies of an Accelerator-driven Transuranium Burner in a Start-up Mode*, Doctoral thesis, Royal Institute of Technology, Stockholm (2004).

[12] Herceg, J.C., *et al*., *Final Report on the Pre-conceptual Design of a Reference ADS for Transmutation of Spent Nuclear Fuel*, ANL-AAA-056 (2002).

[13] Schneider, E., *et al*., *Scenario Studies of German and European Reactor Fleets*, LANL LA-UR-04-4911 (2004).

[14] Salvatores, M., *et al*., "P&T Potential for Waste Minimisation in a Regional Context", *8th Int. Exchange Meeting on P&T*, Las Vegas, November 2004.

Appendix 2.1

The main text we assume that fuel in a reactor achieves a burn-up of *b*% per year. Under the further assumption that, to first order, a linear correlation may be made between the k-effective of the fuel, k_{eff}, and the burn-up allows the k_{eff} of a batch of fuel after *i* years of irradiation to be written as:

$$k_{eff}^{(i)} = k_{eff}^{(0)} - \beta i b \tag{A1}$$

for some reactor parameter, β, and fresh fuel k_{eff}, $k_{eff}^{(0)}$. For N_B batches, the overall k_{eff} of the reactor at cycle shutdown is the k_{eff} averaged over all the batches:

$$\begin{aligned} k_{eff}^{EOC} &= \frac{1}{N_B}\sum_{1}^{N_B} k_{eff}^{(i)} \\ &= \frac{1}{N_B}\sum_{1}^{N_B}\left(k_{eff}^{(0)} - \beta i b\right) \\ &= \frac{1}{N_B}\sum_{1}^{N_B}\left(k_{eff}^{(0)} - \beta \frac{iB}{N_B}\right) \end{aligned} \tag{A2}$$

where *B* is the overall discharge burn-up. Assuming k_{eff}^{EOC} is fixed for a given design by operational constraints allows Eq. (A2) to be simplified and re-written in terms of discharge burn-up to give:

$$B = \frac{2N_B}{\left(N_B + 1\right)} B_1 \tag{A3}$$

where B_1 is the burn-up for a one-batch scheme and is given by:

$$B_1 = \frac{\left(k_{eff}^{(0)} - k_{eff}^{EOC}\right)}{\beta} \tag{A4}$$

Using a one-batch burn-up value of 10% gives the variation in burn-up with the number of batches as shown in Figure A.1. Note, the range of burn-up values given under this assumption provides a range of 15% on either side of the average burn-up value given in [1].

Figure A.1. Variation of discharge burn-up with number of batches used for a reactor with fixed operating end of cycle k_{eff} constraints

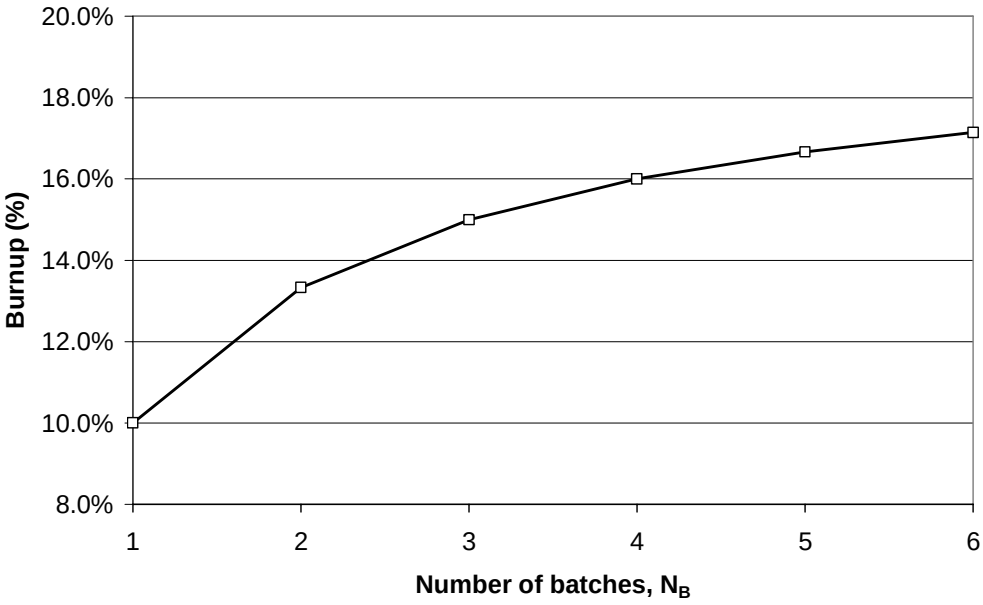

Appendix 2.2

The following symbols are used in this text.

Symbol	Definition
B	Total burn-up achieved for full-dwell fuel in a P&T reactor.
b	Annual incremental burn-up achieved by fuel in a P&T reactor.
D	Notation simplifying symbol, $D = T_A(\Lambda - \varepsilon_m B) + (N_B - 1)(1 - \varepsilon_m \varepsilon_r)$.
f	Annual reload mass for a P&T reactor.
k_{eff}	Effective neutron multiplication factor.
M_0	Initial inventory.
M_E	Residual inventory in the core and cooling after T_F years of operation.
M_{Ext}	Total LWR inventory that feeds the P&T reactor in a mixed LWR/P&T case.
M_{Lm}	Total irrecoverable inventory loss from manufacturing.
M_{Lr}	Total irrecoverable inventory loss from reprocessing.
M_{LWR}	Annual reload inventory for a mixed LWR/P&T case.
M_R	Inventory returned to the fuel store after T_F years of operation.
M_S	Instantaneous inventory in a store.
M_u	Total residual inventory after all P&T reactor operations.
N	Number of generations of P&T reactors for the case where an optimised reduction in size is implemented.
N_B	Number of batches in the P&T reactor. The fraction of the total inventory refuelled is $1/N_B$, so that the total inventory of the P&T reactor core is given by fN_B.
$N_{B,LWR}$	Number of LWR batches for a mixed LWR/P&T case.
$N_{B,P\&T}$	Number of batches in the P&T reactor for a mixed LWR/P&T case.
P_{LWR}	Total power produced by a LWR.
$P_{P\&T}$	Total power produced by a P&T reactor.
t_c	Time taken for cooling and reprocessing.
t_d	Full dwell time in the P&T reactor.
T_F	Years of operation of a P&T reactor.
t_m	Time taken for fuel manufacture.
T_R	Time taken for fuel to make a complete loop through the closed P&T fuel cycle.

Symbol	Definition
Δ	Notation simplifying symbol, $\Delta = T_R \varepsilon_r (1-B) + \varepsilon_r (N_B - 1)\frac{B}{2}$.
Γ	Notation simplifying symbol, $\Gamma = (N_B - 1)\left[1 - \varepsilon_m \varepsilon_r \left(1 - \frac{B}{2}\right)\right] + (1-B) T_R \varepsilon_m \varepsilon_r$.
Λ	Notation simplifying symbol, $\Lambda = 1 - (1-B)\varepsilon_m \varepsilon_r$.
α	Inventory reduction factor, $\alpha = M_0/M_u$.
α_{max}	Maximum reduction factor for a given set of fuel-cycle parameters.
β	Change in k_{eff} per unit burn-up in a P&T reactor.
ε_m	Manufacturing efficiency. This is the fraction of the material entering a manufacturing plant that emerges as useable fuel.
$\varepsilon_{P\&T}$	Fraction of P&T reactor power that is available to the electricity grid (not used for beam production, for example).
ε_r	Reprocessing efficiency. This is the fraction of the material entering a reprocessing plant that emerges as reusable material.
ϕ	Fraction of LWR fuel that feeds the P&T reactor in a mixed LWR/P&T case.
ρ_{LWR}	LWR specific power density (MW/t).
$\rho_{P\&T}$	P&T reactor specific power density (MW/t).

Appendix 2.3

Common hypothesis for the equilibrium scenarios of Section 2.3.2

Fleet's electrical power	60 GWe producing 400 TWhe
Reload average burn-up	60 GWd/t for PWR, 140 GWd/t for FNR fuels
Fuel cooling time/aging time	5 years/2 years
Reprocessing	U and Pu loss rates – 0.1%, MA loss rates – 0.1%

List of heavy nuclide in kg/TWhe for double-strata scenarios with ADS at equilibrium

Core type	**"Twin" ADS**			**ADS**		
Coolant	**Na**	**Pb**	**He**	**Na**	**Pb**	**He**
Fuel design	**Pin**	**Pin**	**Particle**	**Pin**	**Pin**	**Particle**
Fuel matrix	**Oxide**	**Oxide**	**Nitride**	**Oxide**	**Oxide**	**Nitride**
^{234}U	6.72	4.42	2.87	8.78	23.79	24.61
^{235}U	1.93	1.32	0.81	2.44	7.12	7.10
^{236}U	1.76	1.13	0.71	2.17	5.62	5.56
^{238}U	0.00	0.00	0.00	0.00	0.01	0.01
^{237}Np	1.33	0.93	0.58	1.74	5.41	5.62
^{239}Np	0.00	0.00	0.00	0.00	0.00	0.00
^{238}Pu	46.98	34.10	25.60	54.06	79.40	82.99
^{239}Pu	12.16	8.16	6.51	11.79	22.66	15.83
^{240}Pu	52.62	32.48	23.66	57.02	117.29	106.96
^{241}Pu	6.87	4.42	3.34	6.69	11.68	9.92
^{242}Pu	27.61	18.52	14.33	28.72	49.62	44.94
^{241}Am	34.08	23.16	15.73	43.30	88.96	94.60
^{242f}Am	0.00	0.00	0.00	0.00	0.00	0.00
^{242m}Am	3.99	2.70	1.93	4.94	8.49	9.16
^{243}Am	25.48	17.90	13.04	31.33	57.87	62.47
^{242}Cm	0.01	0.01	0.01	0.02	0.02	0.03
^{243}Cm	1.64	0.87	0.74	1.65	0.95	0.98
^{244}Cm	45.06	32.13	26.76	49.18	49.51	54.29
^{245}Cm	10.56	8.37	6.98	11.09	12.27	12.99
^{246}Cm	7.29	5.52	4.72	7.08	6.50	6.89
^{247}Cm	1.36	0.98	0.83	1.18	0.95	0.95
^{248}Cm	0.54	0.36	0.31	0.45	0.28	0.54

List of heavy nuclide in kg/TWhe for the double-component scenarios with ADS at equilibrium

Core type	ADS	
Coolant	He	He
Fuel matrix	Oxide	Nitride
Fuel design	Pin	Particle
^{235}U	2.55	0.41
^{236}U	2.82	0.56
^{238}U	0.01	0.00
^{237}Np	16.61	1.78
^{239}Np	0.00	0.00
^{238}Pu	35.76	14.01
^{239}Pu	83.57	18.35
^{240}Pu	170.30	75.32
^{241}Pu	20.44	13.77
^{242}Pu	7.15	37.67
^{241}Am	30.52	6.56
^{242f}Am	0.00	0.00
^{242m}Am	1.96	0.35
^{243}Am	18.44	9.10
^{242}Cm	0.01	0.00
^{243}Cm	0.20	0.39
^{244}Cm	10.43	14.85
^{245}Cm	1.98	4.19
^{246}Cm	0.87	4.24
^{247}Cm	0.01	1.14
^{248}Cm	0.02	0.54

Chapter 3

SPECIFIC ISSUES

As indicated in the general introduction of this state-of-the-art report, most aspects of the ADS physics have been treated in detail in previous reports. In the present report we have focused on three relevant, specific issues, namely a) ADS dynamics and safety; b) transmutation of long-lived fission products and c) nuclear data uncertainty impact, all of which have been less treated in recent summary reports.

3.1 ADS dynamics and safety

3.1.1 Different behaviour of transients induced by reactivity insertions and/or thermal-hydraulic conditions

The neutron kinetic and reactor dynamic behaviour of accelerator-driven subcritical systems (ADS) is known to be considerably different from that of currently operating conventional, critical power reactor systems. It is thus of interest to examine the intrinsic differences of the kinetic and dynamic behaviour of accelerator-driven systems to typical plant transient initiators in comparison to the known kinetic and dynamic behaviour of critical, thermal or fast systems.

The major issues in reactor dynamics of subcritical systems requiring special attention can be summarised as follows: 1) the dynamic response of the subcritical system to changes either in accelerator beam strength or sudden inadvertent reactivity insertions, 2) the shutdown characteristic of an ADS without control rods from the nominal power state to the cold condition, and 3) the response of the system to typical plant transient initiators that may have to be encountered during the normal operation of the ADS (such as inadvertent trip of the accelerator beam, loss of flow due to coolant pump failure, loss of primary system heat sink, etc.). The latter type of transients are usually categorised into two types of transients, namely those transients in which the accelerator shutdown system is assumed to function as designed (these transient are then classified as “protected” transients), and those transients in which the accelerator beam is postulated not to shut off on demand. The latter transients are usually denoted as “unprotected” transients. This category of unprotected transients requires special attention, because the dynamic response of the subcritical system is significantly different when compared to the response of critical reactor systems.

For protected transients in which the accelerator beam is presumed to shut off, or the control rod system shuts down the reactor (in the case of the critical systems), the dynamic response of both systems is essentially similar in that the neutron flux level decreases below the decay heat level some time after shutdown. These types of transients will thus not be emphasised aside from the special case wherein the “protected” transient should lead to a significant under-cooling of the core configuration (in which case one must assure that the subcritical core always remains subcritical). The latter issue will be discussed further on, within the topic of shutdown characteristics of an ADS without active control rod systems when taking the plant from the hot to the cold shutdown state.

In order to demonstrate the intrinsic characteristics of subcritical systems, the influence of temperature-dependent reactivity feedbacks that are specific to a particular reactor concept will be neglected for the time being. This then allows for the investigation of the basic, or intrinsic, kinetic transient characteristics of subcritical systems, corresponding to the kinetic characteristics as observed under zero power conditions. In addition, intrinsic characteristics of subcritical systems can be best visualised by employing simplified methods such as the point kinetic model and thermohydraulic channel averaged reactivity feedback assessments. In reality, more complicated calculation procedures are required, and in principal are available, when assessing the spatial neutron flux and thermohydraulic conditions within such systems.

Figure 3.1 displays the kinetic response of a subcritical system to a change in source strength of the accelerator and Figure 3.2 displays the kinetic response to different step reactivity insertions at different levels of subcriticality. Figure 3.3 displays the power response of a subcritical and critical system to a specific reactivity insertion of 270 pcm, assuming a thermal, LWR-like system, chosen for display purposes. The same kinetic response will be observed for a fast system, the only difference will be a shorter time scale of the x-axis. As can be observed in Figure 3.1, the response of the ADS to a source strength change (source strength is doubled) is essentially described by the prompt jump characteristics of the system. For relatively low k_{eff} values (i.e. k_{eff} ~0.95), the prompt jump amplitude is much closer to the final, asymptotic value than for high levels of subcriticality, namely k_{eff} ~0.995, where the prompt jump power level is only about 50-60% of the final value. In the latter case, the time characteristics of the delayed neutrons regain some importance since they determine the dynamics of the transition phase between the prompt jump and the final asymptotic value. For low levels of k_{eff} (~0.95) the delayed neutrons essentially loose their importance in subcritical systems.

The importance of a reactivity insertion into the subcritical system is displayed in Figure 3.2. For the critical system, we observe the exponential power increase after the initial prompt jump. In the subcritical system case, all transients eventually approach an asymptotic power level as long as the sum of the level of subcriticality, as expressed in k_{eff}, and the inserted reactivity ρ is less than unity, i.e. (k_{eff} + ρ) < 1.0. Should the sum of (k_{eff} + ρ) = 1.00, then the power level continues to increase linearly after the prompt jump. When the sum of (k_{eff} + ρ) > 1.0, then the power response of the subcritical system after the prompt jump will increase exponentially, corresponding to the power response of a critical system.

Figure 3.1. Kinetic response of ADS to doubling the beam strength as a function of different levels of subcriticality

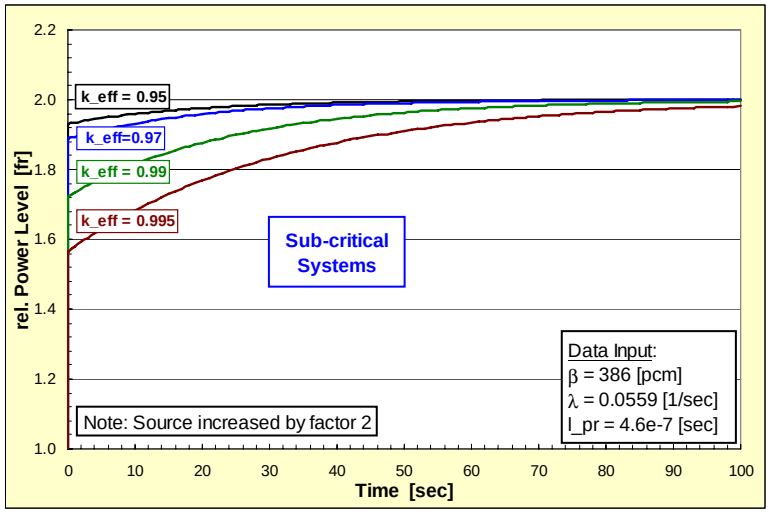

Figure 3.2. Kinetic response of ADS and critical system to a positive reactivity insertion at different levels of subcriticality

Reactivity inserted was selected to result in similar prompt jump behaviour

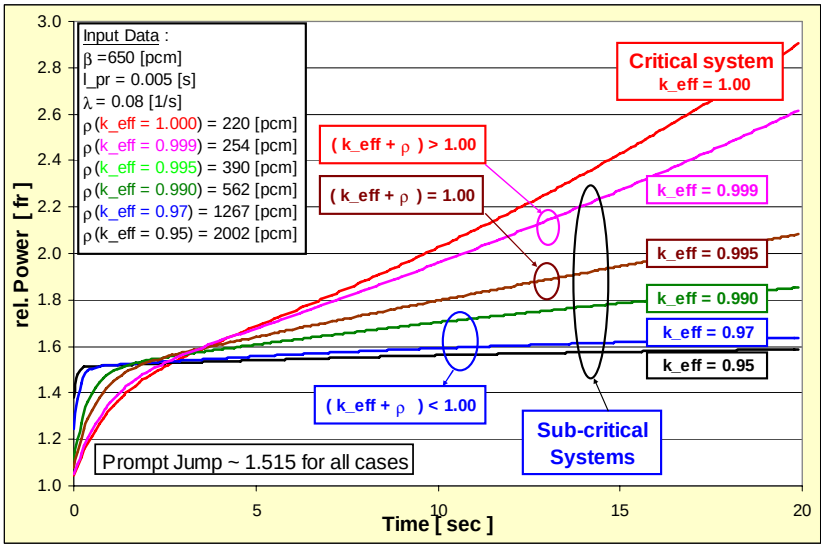

Figure 3.3 Transient response of a subcritical and critical system to a reactivity insertion of 270 pcm (thermal system)

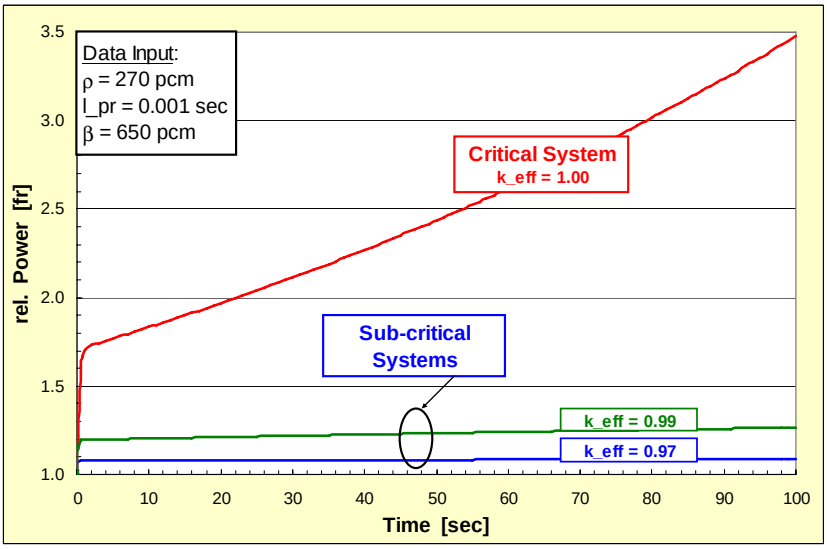

Figure 3.3 summarises the response of subcritical systems and a critical system to a specific reactivity insertion of ρ = 270 pcm in thermal, LWR-like systems. As can be observed, the power level in the critical system increases exponentially after the prompt jump, whereas the power of the subcritical systems approaches its asymptotic value shortly after transient initiation.

The second major difference of subcritical systems is their characteristics when shutting off the accelerator. For ADS systems without control rods, special attention must be placed on the reactivity feedback coefficients, which usually add reactivity into the system when the core materials are cooling down in temperature. Figures 3.4 and 3.5 display the dynamic response of a subcritical system when

Figure 3.4. Kinetic power response of subcritical and critical systems to source shut-off or control rod insertion assuming no temperature reactivity feedbacks

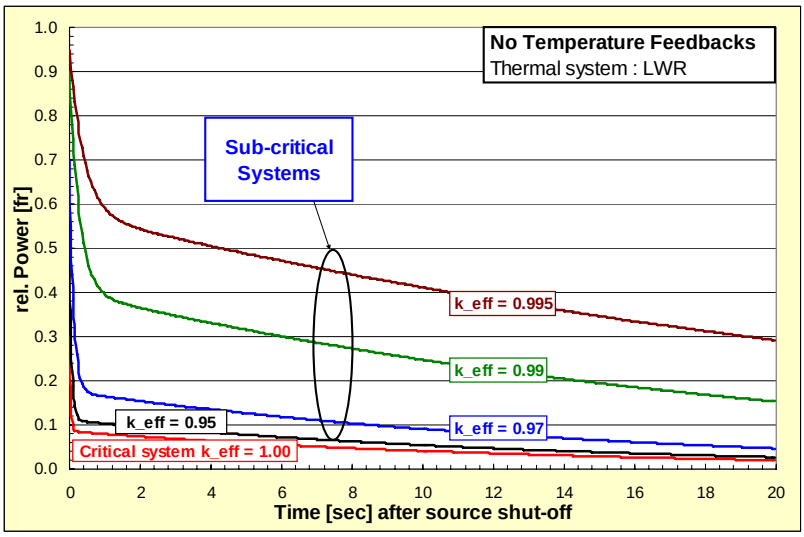

Figure 3.5. Kinetic power response of subcritical and critical systems to source shut-off or control rod insertion assuming no temperature reactivity feedbacks

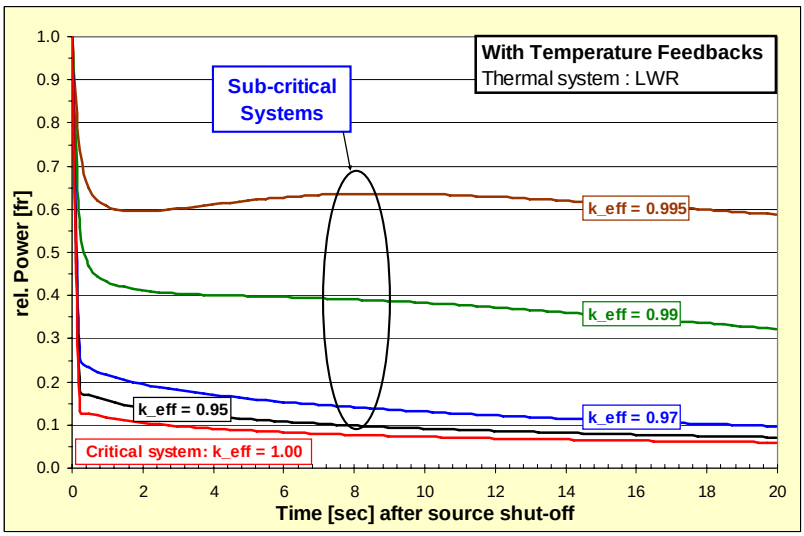

shutting the accelerator beam off. In Figure 3.4, no temperature reactivity feedbacks are assumed, thus displaying the intrinsic kinetic response of such a system. In critical systems, control rods are assumed to shut down the reactor. The reactivity inserted by these control rods is usually chosen in such a manner that the power level after control rod insertion drops to below the decay heat level, thus about \$10-\$12 of reactivity are inserted in a thermal reactor to assure that the power level drops below 6% after rod insertion. In the case of the subcritical system, shutting off the neutron source does not automatically imply that the power level drops to below 10%. As can be observed in Figure 3.4, for a subcritical system with a low level of k_{eff} (i.e. k_{eff} ~ 0.95) the power level does drop relatively quickly (<1 sec) to ~10% power after source shut-off, a response quite similar to that of the critical system (the decay of the neutron flux after the prompt jump is governed by the decay of the delayed neutron precursors; both subcritical and critical systems exhibit similar characteristics in this phase of the

transient). Should however our ADS have a relatively high level of subcriticality (i.e. k_{eff} ~0.99) we can observe from Figure 3.4 that the power level drops to only about 40% after source shut-off (prompt jump). Thereafter, the power remains at a relatively high power level in comparison to subcritical systems with k_{eff} ~0.95, or to the critical system. Here the question can arise if this "slow" behaviour in the decrease in power level after source shut-off of a subcritical system with k_{eff} larger than 0.98 is consistent with the thermohydraulic design of the system, especially under transient conditions in which the heat removal system is assumed impaired (as under loss of flow transients due to pump failure). For the LBE-cooled XADS design by ANSLADO, the natural convection capabilities in conjunction with the large LBE-coolant specific thermal inertia and heat sink characteristics of the system (pool-type design) assure that this "slow" decay in power does not lead to excessive core temperatures. In the He-cooled XADS design with its much lower He-coolant specific thermal inertia, this "slow" power response could lead to higher core temperatures (i.e. cladding temperatures) after failure of the coolant pump for a short time interval after beam shutdown. However, appropriate design measures on the system level can considerably mitigate this effect.

Figure 3.5 addresses the same issue as Figure 3.4, namely the power response of subcritical systems to source shut-off, but the influence of temperature reactivity feedback effects are now taken into consideration. After shutting down the source, the decreasing temperatures of the reactor materials (i.e. fuel, coolant) insert a net positive reactivity into the core since the temperature coefficients of these materials are usually negative. This positive reactivity insertion counteracts the decreasing neutron flux. Should the level of subcriticality be relatively high (i.e. k_{eff} ~0.99), only 1 000 pcm in reactivity needs to be inserted into the subcritical system before our system actually becomes critical [i.e. (k_{eff} + ρ) ~ 1.00]. In this case, the power level is shown in Figure 3.5 to level off at about 40% within a few seconds after the prompt jump; no significant decrease in the power level can be expected thereafter unless other means of inserting negative reactivity into the core are provided by design. Thus the chosen operating level of subcriticality and the reactivities added into the system subsequent to beam shutdown [going from hot full power (HFP) to hot zero power (HZP)] must be consistent to ascertain that the subcritical system actually always shuts down to decay heat levels fairly quickly.

A similar behaviour to that depicted in Figure 3.5 must be expected when taking subcritical configurations without active control rods systems from the normal operational (hot) state to cold shutdown, i.e. cold zero power (CZP). Positive reactivity will be inserted during this procedure into the subcritical core, the only difference being the time scale. It is absolutely mandatory to ascertain that the level of subcriticality at the hot state is always consistent with the positive reactivities that will be added into the core while taking the system from hot (HFP) to cold shutdown (CZP). It must be absolutely assured that (k_{eff} + $\rho_{feedbacks}$) will always remain less than 1.0. Thus particular attention must be placed on the assured knowledge of all the various temperature reactivity feedback components which impact subcritical systems, especially when operating at relatively high levels of subcriticality, i.e. k_{eff} > 0.98. In this case, less than 2 000 pcm in reactivity margin is available when the system is taken to CZP. Under realistic conditions, at least 1 500 pcm of reactivity must be expected to be released into the subcritical system during this procedure (both LBE-cooled and He-cooled 80 MWth PDS_XADS designs release about 1 400 pcm). The reliable and ascertained predictability of all the different temperature feedback mechanisms thus becomes an essential requirement when operating a subcritical system without active control rod systems.

The third major issue associated with subcritical systems is their response to so-called "unprotected" transients in which it is arbitrarily postulated that the accelerator beam does not shut off upon demand. For this category of transient, two different classes of transients must be considered: 1) those transients during which *positive* reactivity is inserted into the core (i.e. due to a geometric rearrangement of core configuration, etc.), 2) those transients, during which *negative* reactivity is inserted into the core.

Figure 3.6 displays the kinetic response of subcritical and critical systems to a positive reactivity insertion without temperature feedbacks. It is well known that the addition of +$1 in reactivity in critical systems leads to a prompt critical configuration in the zero power state, implying a power excursion. For subcritical systems, substantially larger positive reactivities need to be inserted into the system before the power level rises significantly. For example, in case the level of subcriticality should be k_{eff} ~0.95, about +$7 of reactivity needs to be inserted into the subcritical system before the power level doubles. This benign behaviour of subcritical systems to unprotected positive reactivity insertions is clearly the major advantage of subcritical systems. Thus for unprotected transients with a positive reactivity insertion, subcritical systems show a clear advantage compared to critical systems because significantly larger amounts of reactivity can be inserted before the power level rises significantly. In addition, the delay in time before the power rises translates into an increased "grace period" that is available for manual operator intervention to shut off the source. Under realistic conditions, these types of transients are, however, considered to have a very low probability of occurrence because of the inherent system design features protecting against these types of events. These transients are therefore classified as so-called "hypothetical" transients.

Figure 3.6. Kinetic response of subcritical and critical systems to *positive* reactivity insertions without temperature feedbacks

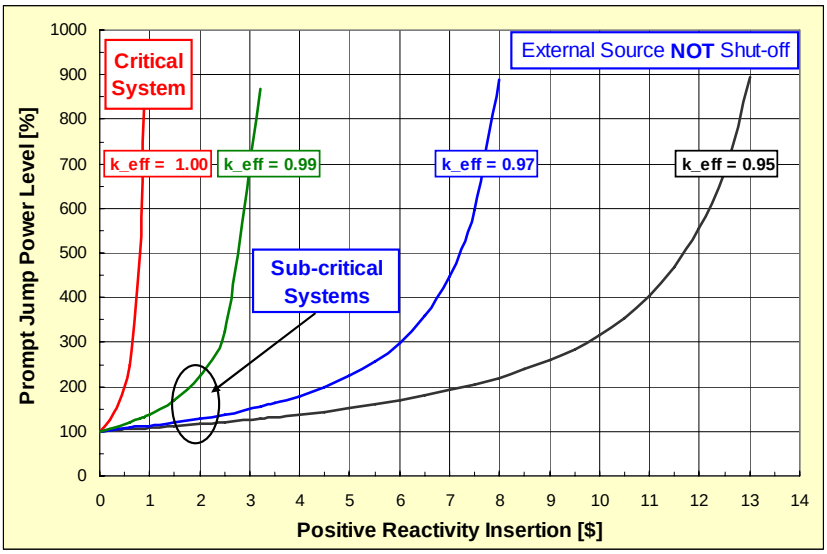

During the course of an unprotected transient in either subcritical or critical systems, a net negative reactivity is normally expected to be inserted into the core due to increasing core temperatures. For example, during an unprotected loss of flow transient (failure of the coolant pump), core temperatures (fuel, coolant) will increase because cooling is impaired. Increasing core temperatures will lead to a negative reactivity insertion due to the temperature coefficients being negative (i.e. Doppler coefficient). Figure 3.7 displays the kinetic response of subcritical systems and critical systems without temperature feedbacks to such transients. For the critical system it is known that adding $1 of negative reactivity into the system will decrease the power level to 50%, while inserting -$5 will decrease the power level to below 20%. As observed in Figure 3.7, the power level will however remain at relatively high levels for subcritical systems. Inserting $10 of negative reactivity in a subcritical system of k_{eff} ~0.95 decreases the power level to only 60%, while if the system were critical, the corresponding power level would drop to below 10%. Thus in order to decrease the power level of a subcritical system during unprotected transient conditions to below 10%, excessively large reservoirs of negative reactivities (~ -$60) will be required. Thus for all unprotected transients with

Figure 3.7. Kinetic response of subcritical and critical systems to *negative* reactivity insertions without temperature feedbacks

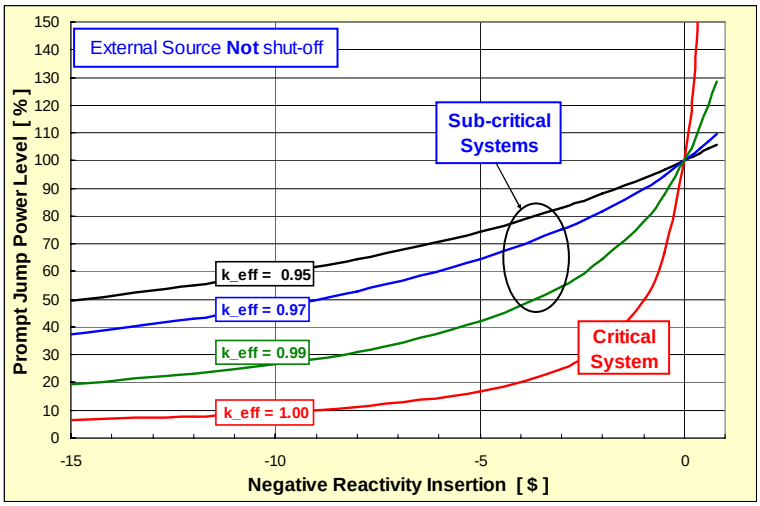

negative reactivity insertions (most unprotected transients will proceed in this direction), subcritical systems exhibit a clear disadvantage in comparison to critical systems because of the very large negative reactivities that must be inserted into the system before the nuclear power level drops significantly. For current ADS designs (i.e. PDS_XADS), the effect discussed above is clearly observed by the much higher power level and corresponding higher core temperatures in the case of the subcritical system compared to the critical system, as was demonstrated by the exhaustive transient analyses performed over the last two years within the PDS_XADS project when the two ADS designs (LBE-cooled, He-cooled) were exposed to postulated unprotected, negative reactivity transients.

The above discussion briefly summarised that the dynamic response of subcritical systems is significantly different from the dynamic response of critical systems. The level of subcriticality is a very important parameter that substantially determines the dynamic response of the subcritical system. The level of subcriticality k_{eff} requires careful, continuous monitoring during the entire operational power phase of subcritical systems. In addition, temperature reactivity coefficients play the most dominant role controlling the operational level of subcriticality, especially in those subcritical systems that are designed without active control rod systems. Reactivity coefficients alone determine the course and direction of transients (in systems without active control rods) since there are no other reactivity means available to influence the system. During the shutdown procedure of subcritical systems from hot to cold state, careful attention must be paid to all of the different reactivity effects that might add positive reactivity into the system, not only those relevant to the thermal feedback effects but also accidental (external) reactivity insertions occurring possibly before or after the ADS shutdown. Moreover, a high degree of confidence in the assured predictability of all the different reactivity coefficients is therefore absolutely mandatory before such a system can be operated safely.

From the phenomenological point of view, it is well known that reactivity insertions induce effects on the ADS [1,3] power much lower than those induced in critical systems [4]. Therefore, it appears evident that in principle the system subcriticality may compensate for the lower delayed neutron fraction due to the higher concentration of minor actinides in nuclear waste incinerators. For analogous reasons, thermal-hydraulic transients in ADS are less sensitive to the thermal feedback effects [5]. Practically, in highly subcritical ADS, neutron kinetics and thermal-hydraulics are much less coupled than in critical reactors. In general, this can be an important asset for ADS safety, as during transients the system is largely driven by the external source intensity [6]. In Ref. [7], Venneri

stressed these concepts as follows: "…sufficiently subcritical nuclear systems containing arbitrary mixtures of fissionable material will behave neutronically in the same way, independent of the internal fuel composition. Power control of subcritical systems is not linked to delayed neutrons, reactivity feedbacks or control rods, but solely to the externally operated accelerator beam". Actually, at least in principle, there is no problem to mitigate accidental transients in largely subcritical ADS by reducing the accelerator beam power. However, if the external operation of the accelerator beam would fail, the reduced feedback effects in ADS become a disadvantage. In particular, if source shutdown fails, the temperature rise during ADS unprotected transients can be much larger than in critical reactors [8-20] without scram (WS). Therefore, the ADS dynamics specificity can have a negative impact on the system safety in the case of unprotected accidents. Although the probability of this kind of accident is extremely low, they must be carefully considered as concerns highly subcritical ADS. The natural convection of the coolant may effectively mitigate such an accident, as well as the source jump (also called beam dumps) accidents, in well-designed, small-size liquid-metal-cooled ADS [13-15]. A low value of the fuel power density can further help the natural convection mitigation of unprotected accidents, as in the PDS-XADS experimental ADS [16,17].

Much more complex dynamics are relevant to less subcritical ADS [20]. In fact, in this case the field of open design parameters is increased for ADS systems compared with critical systems. Practically, the level of subcriticality becomes a very important parameter that determines the dynamic behaviour and the safety margins [20].

Thus, it is clear that the level of subcriticality is a key parameter that requires careful monitoring in ADS. In order to detect any unexpected reactivity variation and allow the continuous verification of the subcriticality margin during the operation, the level of subcriticality must be continuously monitored in ADS. With this goal in mind, experimental techniques have been proposed and investigated in the specific case of ADS [21-32]. Most of the experimental techniques are being tested in the MUSE [33-37] pulsed-ADS experimental campaign at the MASURCA facility at Cadarache. Optimised neutron detectors have also been proposed [38-39]. A functional definition of the core instrumentation and reactivity monitoring has already been formulated for the PDS-XADS experimental system [40-43]. However, it must be underlined that many of the experimental methods for monitoring the ADS subcriticality level would require further tests and validation which should be carried out at the TRADE [44-47] and in the MYRRHA [48] experimental ADS.

As concerns the methodological point of view, methods are being developed and tested to allow improved analyses of some particular systems or aspects of ADS dynamics [49-53].

3.1.2 Transients induced by variations of the external source term

Transients induced by variations of the external source term are specific of ADS because they do not occur in critical systems.

Concerning this ADS-specific type of transient, the source jumps (called also beam dumps) were briefly mentioned above. This transient must also be taken into consideration during the "start-up" phase of an ADS, in particular if the ADS system is designed without active control rods. It was previously mentioned that the coolant natural convection can mitigate these accidents in LBE-cooled systems, and that a low fuel power density (i.e. low fuel temperature) facilitates this mitigation [13-15].

A second kind of transient, induced by (fast) variations of the accelerator beam intensity, cannot always be classified as an accident in ADS systems. The problem of frequent accelerator beam trips that could induce thermal stresses in the case of ADS, in the fuel or in the regions above the core and

in the intermediate heat exchangers structures, was first pointed out during the NEA Workshop on the Utilisation and Reliability of High-power Proton Accelerators at MITO (Japan), 13-15 October 1998 [54-55]. Ever since this MITO meeting, the experts in the accelerator community have been working to improve the reliability of accelerators for ADS, to drastically reduce the frequency of unexpected beam trips, or to recover the beam in as short a time interval as possible thereby reducing the number of reactor trips.

During the same period, dynamic ADS investigations were carried out to evaluate the impact of the duration time of the beam trip in terms of fuel and coolant temperature variations [56,57].

More recently, a NEA/WPPT computational benchmark entitled "Beam Interruptions in a Lead-bismuth-cooled and MOX-fuelled Accelerator-driven System" was started in 2003 [58].

Table 3.1 summarises the list of the benchmark participants and the codes they used to calculate the beam interruption transients.

Table 3.1. Participation in the beam interruption transient benchmarks

1	Antonio D'Angelo	ENEA Casaccia (Italy)	TIESTE-MINOSSE
2	Gert Van den Eynde and Baudouin Arien	SCK•CEN Mol (Belgium)	SITHER-PKS
3	Kazafumi Tsujimoto	JAERI Tokai (Japan)	EXCURS-M
4	Marcus Eriksson	Royal Institute of Technology (Stockholm, Sweden)	SASSYS/SAS4A
5	Michael Schikorr	FZK Karlsruhe (Germany)	SIM-ADS
6	Paul Coddington and Konstantin Mikityuk_1	PSI (Switzerland)	TRAC-M/AAA
7	Paul Coddington and Konstantin Mikityuk_2	PSI (Switzerland)	LOOP2
8	Pieter Wakker and Jim Kuijper	NRG Petten (The Netherlands)	TRAC (Modif. lead)
9	Ron Dagan and Cornelis Broeders	FZK Karlsruhe (Germany)	SAS4ADS
10	Yonghee Kim	KAERI Daejon (Republic of Korea)	DESINUR

The first two phases of the computational benchmark were carried out in 2003 [59-61]. The first phase of calculations was devoted to the comparative assessment of the different computation tools and methods used to evaluate power and temperature transients induced by beam interruptions. In this aim, the first phase of the benchmark was successful, because the differences among the ten sets of results provided by the nine participants were practically negligible. The good agreement (within about 3%) among all the calculated temperatures considered relevant to the benchmark's first phase allowed the definition of a second phase with the gaol to investigate the impact of different and more complex calculation assumptions on fuel and coolant temperatures.

In particular, the beam interruption investigation was extended to cases characterised by larger fuel power densities. In particular, the assessment was no longer limited to the Ansaldo-XADS design but extended to include the MYRRHA experimental ADS design. The benchmark participants calculated four sets of beam interruption solutions, by assuming models and data as close as possible to those recommended in the benchmark specification:

- Ansaldo-XADS system-type average fuel pin (~80 W/cm).
- Ansaldo-XADS system-type hottest fuel pin (~115 W/cm).
- MYRRHA-XADS system-type average fuel pin (~220 W/cm).
- MYRRHA-XADS system-type hottest fuel pin (~320 W/cm).

Moreover, to evaluate the uncertainty on the calculation results, the benchmark was also extended to "sensitivity analyses" of the main results to assumptions (on models and data) different from those recommended in the benchmark specification. Practically, the participants also evaluated the impact on the benchmark main results of any assumption they thought to be a valid alternative or improvement upon the recommendations given in the benchmark specifications. The calculated steady-state and transient coolant temperature results as calculated by the various benchmark participants do not show significant dispersions for both low- and high-power density cases. From sensitivity analyses, all the investigated variations of calculation assumptions lead to negligible or relatively limited effects on the calculated coolant temperatures. The dispersion of the calculated fuel centreline temperatures increases going from low- to high-power density cases (roughly, by a factor 2). Fuel temperature variations depend on the fuel thermal conductivity, the fuel-to-clad heat transfer and the fuel specific heat. The sensitivity analysis confirms that the benchmark's main results (temperature variations induced by beam interruptions) are largely independent of feedback effects on neutron kinetics, mainly because of the large subcriticality level (8$). The report on the second phase of calculations was published in 2004.

Following the increased interest in beam trip issues in member countries, possible continuations of the benchmark were discussed. Several lines of research were suggested, including:

- Evaluation of fuel and internal structures response to the beam trips using the corresponding stress analyses.
- Refinement of calculation with spatial kinetic effects.
- Evaluation of trip response with irradiated MOX fuels.
- Response with transmutation dedicated fuels and evaluation of dynamic responses of ADS with different subcriticality levels.

3.2 Long-lived fission product (LLFP) transmutation

3.2.1 Introduction

The long-term risk of a geologic repository of nuclear waste is usually dominated by fission products such as ^{129}I, ^{135}Cs, ^{99}Tc, ^{126}Sn and ^{79}Se, which are generally more mobile than actinides. Those LLFPs also have a relatively high radiological toxicity. In most repository designs, the early dose contribution is mainly from those LLFPs and their order of importance is dependent on the characteristics of the repository. To reduce the long-term dose, it has been suggested that LLFPs should be transmuted into stable or short-lived isotopes, or that they should be specially conditioned for disposal [62-64].

R&D activities on LLFP transmutation are mainly tuned to the transmutation of ^{99}Tc and ^{129}I, since they can be rather efficiently transmuted in nuclear reactors. Other LLFPs are evaluated to be very difficult to transmute due to very small neutron absorption cross-sections, and some LLFPs such as ^{135}Cs require a costly isotope separation [64,65]. Nevertheless, it has been shown that ^{135}Cs could be incinerated without isotope separation in a special nuclear system with a very high neutron flux [66,67]. Table 3.2 shows some basic properties of major LLFPs.

Table 3.2. Properties of major LLFPs

Isotope	Decay type	Half-life, yr	Capture cross-section*, b		Remark
			Fast	Thermal	
^{79}Se	β^-	6.5×10^4	0.002	0.33	Non-transmutable
^{99}Tc	β^-	2.1×10^5	0.45	9.32	Transmutable
^{126}Sn	β^-	1.0×10^5	0.007	0.03	Non-transmutable
^{129}I	β^-	1.6×10^7	0.35	3.12	Transmutable
^{135}Cs	β^-	2.3×10^6	0.07	2.48	Transmutable

** ORIGEN2 library (standard PWR spectrum).*

A general description on the LLFP transmutation can be found in Refs. [62,63]. In this chapter, the status of R&D on the LLFP transmutation is reviewed once again. Technical developments and findings were assembled and described in the broad field of the topic.

3.2.2 Neutronic consideration of ^{99}Tc and ^{129}I transmutation

Figure 3.8 shows the transmutation process of ^{99}Tc and ^{129}I in a neutron field. A neutron capture of ^{99}Tc forms ^{100}Tc, which shortly decays to stable ^{100}Ru with a half-life of 15.8 s. ^{100}Ru is transmuted only to stable or short-lived nuclides by further neutron captures. The capture cross-sections of ^{99}Tc and ^{100}Ru are shown in Figure 3.8. ^{99}Tc has a large resonance at 5.6 eV and a series of smaller resonances at higher energies. The resonance integral is ~340 b. The relatively large resonance of ^{99}Tc, in conjunction with its high density, usually results in substantial self-shielding effects when a rod-type target is used. This indicates that ^{99}Tc might be effectively transmuted in the epithermal energy range. Since ^{100}Ru has a much smaller capture cross-section than ^{99}Tc, ^{99}Tc is mainly transmuted to ^{100}Ru with slow conversion ratios into ^{101}Ru and ^{102}Ru. It is worthwhile to note that an extremely small fraction of ^{99}Tc is converted to another long-lived isotope ^{98}Tc ($T_{1/2} = 4.2 \times 10^6$ yrs) via an (n,2n) reaction.

Elemental iodine in spent fuel consists of ^{127}I and ^{129}I, and their typical composition is 23% ^{127}I and 77% ^{129}I in the case of PWR. Since the half-lives of the unstable nuclides ^{128}I, ^{130}I, ^{131}I and ^{132}I are very short, ^{127}I and ^{129}I are primarily converted by a neutron capture to ^{128}Xe and ^{130}Xe, respectively. The conversion of ^{127}I to ^{129}I is very small, since ^{128}I quickly decays to ^{128}Xe. As a result, both ^{127}I and ^{129}I are transmuted into stable xenon isotopes through neutron capture reactions. In the thermal energy range, the capture cross-sections of ^{127}I and ^{129}I, and ^{130}Xe are inversely proportional to the neutron velocity, and ^{129}I has a much larger capture cross-section than the other two isotopes (see Figure 3.9). ^{129}I has a series of resonance, and the resonance integral is ~36 b, much smaller than that of ^{99}Tc. In an iodine target, the self-shielding effects are generally small.

Figure 3.8. Transmutation process of ^{99}Tc and ^{129}I

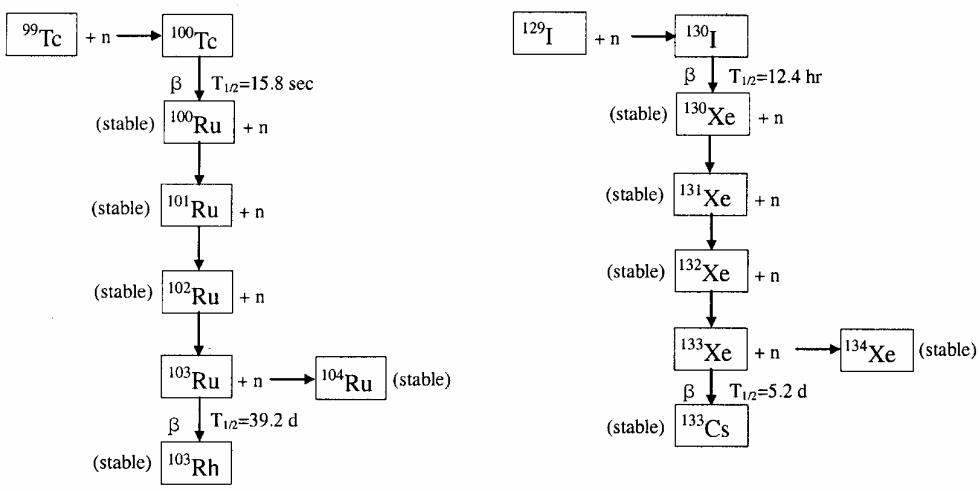

Figure 3.9. Neutron capture cross-sections of ^{99}Tc and ^{129}I (ENDF-B/VI)

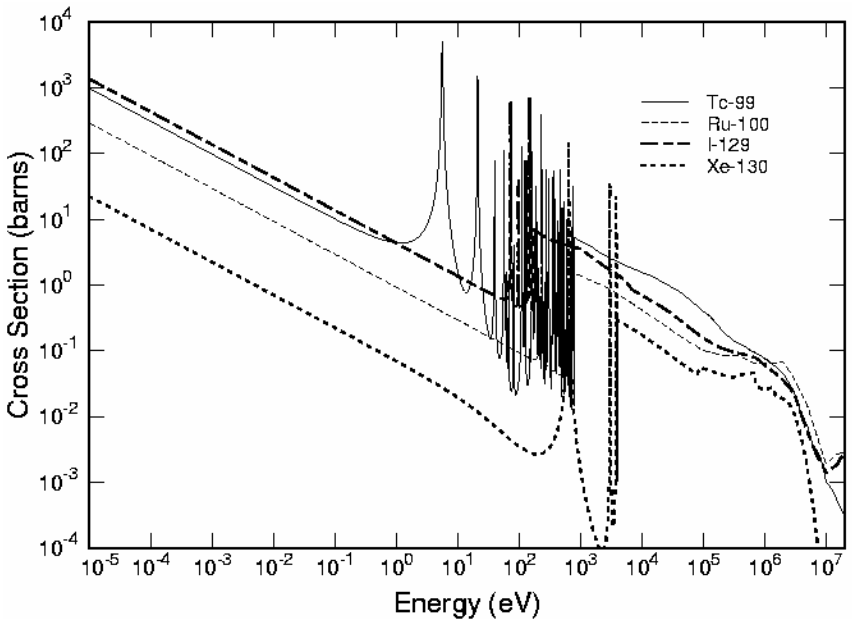

3.2.3 Selection of target materials for ^{99}Tc and ^{129}I

3.2.3.1 Fundamental properties

It is very important to select an appropriate LLFP target material from the viewpoints of material properties such as melting temperature, compatibility with cladding material and irradiation behaviour. Additionally, the target should fulfil the requirements of fabrication, recycling and re-fabrication.

Normal densities of Tc and Ru are 11.5 g/cm^3 and 12.4 g/cm^3 at room temperature, respectively. Important material properties of Tc and Tc-Ru alloy have been revealed by some researchers [68,69]. Both Tc and Ru have very high melting temperatures, 2 157°C and 2 334°C, respectively. The two

elements form a complete solid solution. Thermal expansion of Tc and Tc-Ru alloy are much smaller than that of stainless steels and Tc has slightly larger thermal expansion than Ru. Thermal conductivity of Tc is quite good, ~50 W/mK with a weak temperature dependency and the Ru metal has a much higher thermal conductivity than the Tc metal. A Tc-rich Tc-Ru alloy has a thermal conductivity comparable to that of Tc. The effective neutron capture cross-section of ^{100}Ru is about a quarter of that of ^{99}Tc. The beta decay energy of ^{100}Tc is about 3.2 MeV; consequently, a considerable heat may be generated in the Tc target. Based on the known material properties and some irradiation results, it is expected that a metallic Tc would be a good target material, and no serious showstoppers regarding the target behaviour are envisioned for a high Tc burn-up, even in a high-temperature reactor.

A repeated recycling of Tc is required since a complete transmutation of a Tc target is almost impossible. Thus, separation of Tc from the irradiated target is essential. The irradiated target is primarily composed of Tc and Ru and some impurities. Recalling the Tc separation from the spent fuel, it is expected that the Tc recovery from the irradiated target would be feasible. The recovery rate should be as high as possible in order to minimise Tc loss into waste.

Unlike Tc, there is no general consensus concerning an iodine target material. Iodine is highly volatile (melting point of 386.8 K and boiling point of 457.7 K) and the iodine nuclides are transmuted into Xe gas, which may lead to a target with high internal pressure. Additionally, iodine is very corrosive. Table 3.3 shows the properties of some potential candidates for the iodine target [68,70,71].

Table 3.3 Properties of iodine compounds

Compound	Melting point (°C)	I density (10^{22}/cm^3)	Production of long-lived nuclide	Chemical stability
NaI	660 (98)*	1.47	No	Deliquescent
MgI_2	634 (649)	1.84	No	Deliquescent
CaI_2	779 (839)	1.62	^{41}Ca	Deliquescent, light sensitive
CeI_3	760 (798)	1.97	^{137}La	Deliquescent, light sensitive
CuI	595 (1 085)	1.78	^{65}Zn, ^{63}Ni	Stable in the air
CrI_2	793 (1 857)	2.05	No	Hygroscopic

** Melting point of metal.*

As in the Tc target, an iodine transmutation generates a considerable amount of energy since the beta decay energies of ^{128}I and ^{130}I are high. In general, the thermal conductivity of metal iodides is known to be rather small and shows roughly a $1/T$ behaviour. For NaI, thermal conductivity decreases from 3.9 W/mk at 120 K to 0.9 W/mK at 400 K, and it is 1.7 W/mK at 290 K [72]. It is expected that thermal conductivities of other iodides would not be much different from those of NaI and CuI. Adequate cooling must be provided when a high iodine transmutation rate is expected, as most iodine targets under consideration have a relatively low fusing temperature. The cooling requirement may be important in a high-temperature reactor.

As shown in Table 3.3, most iodine targets under consideration are chemically unstable in the air. On the other hand, CuI is stable in the air, which is very favourable from the viewpoint of fabrication and handling of the target. However, the CuI target was found to be quite corrosive and has a relatively high vapour pressure [70,72]. To mitigate the corrosion behaviour of CuI, a Cu metal liner, which is compatible with CuI, was proposed [70]. In this approach, some crucial issues need to be addressed: substantial dissociation of CuI at high temperature, deleterious impact of Cu on neutron economy.

Some iodine targets like CaI_2 produce long-lived radionuclides. However, it is recognised that the net reduction of radiotoxicity is still significant and the by-product radionuclide would not be problematic in a repository [68,73]. The resulting radionuclides could be reutilised as the target repeatedly, thus this seems not to be a serious disadvantage.

When a large fraction of iodine is transmuted in a metal iodide target, a metal phase would be formed. In a target such as NaI, the liberated metallic Na would melt in most reactor environments, and may cause some concern about the target integrity if the iodine burn-up is high.

3.2.3.2 Irradiation studies

In 1989, an irradiation study on ^{99}Tc and ^{129}I was performed in the reflector region of the Fast Flux Test Facility (FFTF) with an aim to validate computational methods and nuclear data [74]. A metallic Tc target and a NaI iodine target were used and the transmutation rates were fairly low. The experiments showed that the self-shielding effect was significant in the case of ^{99}Tc, while the ^{129}I target had a negligible self-shielding effect. The calculation to experiment (C/E) reaction rate ratios were reasonably good, 0.7~0.9.

Within the framework of the EFTTRA (Experimental Feasibility of Targets for Transmutation) collaboration between European countries, extensive experimental works have been performed for the transmutation of ^{99}Tc and ^{129}I in the thermal high flux reactor (HFR) at Petten in the Netherlands [71,75-78].

In the EFTTRA-T1, metallic Tc rods were encapsulated in a 15.15 Ti stainless steel capsule and were irradiated for eight reactor cycles (192.95 full power days). The Tc burn-up was ~6 a/o. The flux level was about 1×10^{15} n/cm^{2}sec. The EFTTRA-T1 experiments revealed that there are virtually no problems with the metallic Tc targets. After the successful EFTTRA-T1, EFTTRA-T2 experiments were continued, in which a much higher Tc transmutation was targeted. In the EFTTRA-T2, two of the six samples from EFTTRA-T1 were re-encapsulated in the same 15.15 Ti stainless steel capsule and they were irradiated in HFR for 579.3 full power days. Total neutron fluence was 5.4×10^{22} n/cm^2. From the post-irradiation examination, it was found that the Tc burn-up was 15~18 a/o and there were no noticeable changes in the microstructure compared to the un-irradiated samples. The volumetric changes were observed to be very small, as shown in Table 3.4. The temperature in the vicinity of the sample was measured to be around 700 K and the central temperature of the Tc metal was calculated to be about 1 100 K. Based on these irradiation studies, it is expected that there is no technical limit to the use of a metallic Tc target even for a much higher Tc burn-up. In France, metallic Tc targets were irradiated in a local moderated zone of the Phénix reactor (ANTICORP-1 experiment) [79]. It was reported that a high Tc burn-up of ~25% was achieved in ANTICORP-1. Unfortunately, detailed results of the experiment are not available at the time of publication.

Table 3.4. Dimensional changes of the Tc rods in EFTTRA-T1, -T2 experiments

Dimension	Sample	Pre-test	EFTTRA-T1	EFTTRA-T2
Diameter, mm	A	4.80 ± 0.01	4.83 ± 0.01	4.83 ± 0.01
	B	4.81 ± 0.01	4.84 ± 0.01	4.83 ± 0.01
Length, mm	A	25.05	25.09	25.14
	B	25.05	25.12	25.16

In the EFTTRA-T1, iodine targets were also irradiated in HFR. Three metal iodides, NaI, CeI_3 and PbI_2 were fabricated and encapsulated in a 15.15 Ti stainless steel capsule with a He filling gas. In the experiment, ^{127}I was used, as its transmutation is similar to the transmutation process of ^{129}I. The samples were irradiated up to an iodine burn-up of 5~5.9 a/o. From the EFTTRA-T1 experiments, NaI was recommended as the best target and PbI_2 was identified as unsuitable due to its corrosive behaviour, although NaI does not meet *all* the requirements satisfactorily.

After EFTTRA-T1, Schram, *et al*. [72], in the Project I irradiation, also performed irradiation tests for NaI, MgI_2, CaI_2 and CuI in HFR. The calculated iodine transmutation rates were in the range 6.6-7.3 a/o. In the study, it was pointed out that NaI and CaI_2 show a good material compatibility with 316 steel, while CuI has a serious corrosion concern. The Project I tests also showed that volumetric expansion was quite significant in the four targets primarily due to the production of Xe, and all the targets except for CaI_2 showed a less-dense central region.

One of the concerns in an iodine target is build-up of the Xe pressure. The Xe release rate is dependent on the target material and irradiation conditions. A powder-type target has a much higher Xe release compared to a pellet-type one [82]. Even with a pellet-type target, irradiation study showed that the xenon release rate would be high at a high-temperature condition. Consequently, a large gas plenum should be provided for the transmutation of iodine [71,82].

Based on the experimental studies, it may be said that none of the candidates (NaI, MgI_2, CaI_2, and CuI) can be disqualified, although some design measures would be required to prevent corrosion in the case of CuI. Making a choice between the metal iodides will strongly depend on the transmutation scenario. Studies for a better target material should be performed with a much higher iodine burn-up condition.

3.2.4 LLFP transmutation in fission reactors

3.2.4.1 Overview

LLFPs are basically neutron absorbers, and a reactor system needs to have a high neutron surplus as much as possible for efficient LLFP transmutation. As shown in Figure 3.9, both ^{99}Tc and ^{129}I have relatively high absorption cross-sections in the thermal and epithermal energy ranges. Thus a high flux thermal reactor has a good transmutation potential for the two nuclides. Nevertheless, it is recognised that the LLFP transmutation in existing thermal reactors (PWR and CANDU) is quite limited due to the relatively poor neutron economy. It is generally known that a fast neutron system is more favourable, either critical or ADS (accelerator-driven system), from the viewpoint of the LLFP transmutation potential due to a better neutron economy. It is also known that a critical reactor and ADS have a similar LLFP transmutation capability. Table 3.5 compares the Tc transmutation capability of a fast reactor, a PWR and a HWR [62-64,83,84].

Table 3.5. Ranking of reactors with respect to ^{99}Tc transmutation capability

Reactor	Configuration	Inventory (kg)	Transmutation (kg/yr)	Half-life (yr)
Fast	Moderated assembly in inner core	2 741	122	15
Fast	Non-moderated assembly in inner core	2 662	101	18
PWR	Pin in guide tube (UO_2 fuel)	3 633	64	39
PWR	Pin in guide tube (MOX fuel)	1 907	17	77
HWR	Target pins in moderator	4 100	115	25

In general, LLFPs are co-transmuted in a transuranic element (TRU) or minor actinide (MA) burner. In the TRU burner case, ^{99}Tc and ^{129}I can be transmuted with the same supplier-to-burner reactor support ratio. However, when the support ratio is maximised with the MA fuel, both ^{99}Tc and ^{129}I cannot be transmuted with a sufficient support ratio due to the limited neutronic potential [64,73].

3.2.4.2 Thermal reactors

Kloosterman and Li [83,84] performed a feasibility study on the ^{99}Tc transmutation in both heavy water reactors (HWR) and light water reactors (LWR). Their analyses were based on fuel assembly (element) calculations. In the HWR (935 MWe) case, they considered several Tc loading options, including target pin (or pins) inside fuel bundle, Tc pins in the moderator region, and homogeneous dissolution in the moderator. They concluded that the Tc loading in the moderator is the most promising option, providing a 115 kg/yr transmutation rate for a 4.1 tonne loading and a transmutation half-life of ~25 years. The Tc transmutation in a HWR requires a substantial increase in the uranium enrichment. Also, the coolant void reactivity is strongly affected by the Tc loading. Apart from the uranium enrichment and core design issues, they concluded that a HWR reactor has a higher Tc transmutation potential in terms of the transmutation rate.

In the study by Kloosterman and Li, a pin-type Tc target was uniformly loaded into the guide tube locations of a Westinghouse-type PWR with a power of 900 MWe. The Tc transmutation performance was evaluated as a function of Tc density for both a full UO_2 core and a 1/4 MOX core. The study shows that the resonance and special self-shielding effect is significant and a low-density Tc target would be beneficial. The UO_2 core shows a better transmutation capability than the MOX core due to the harder neutron spectrum in the MOX-loaded core. When the Tc loading was 1 453 kg in the UO_2 core, the transmutation half-life was evaluated to be ~26.8 years (37.2 kg/yr), while the transmutation half-life was ~39.2 years (63.8 kg/yr) for a 3 633 kg Tc loading. It is shown that significantly higher uranium enrichment is needed for the transmutation of ^{99}Tc – 5.1% for 726.5 kg, 6.5% for 3 633 kg.

Golfier, *et al*. [81] performed a similar parametrical analysis of ^{99}Tc and ^{129}I transmutation in the 1 450 MWe European Pressurised Water Reactor (EPR). They explored two LLFP loading schemes: 1) replacing fuel pins by target pins and 2) mixing Tc with the fuel. In this study, a CeI_3 iodine target was assumed. The results showed that EPR has a very promising LLFP transmutation potential. When the fuel was mixed with 1% ^{99}Tc and four pins were replaced by iodine targets (1 620 kg of ^{99}Tc and 668 kg of ^{129}I), the transmutation rates of ^{99}Tc and ^{129}I were calculated to be 178.2 kg/yr and 49.4 kg/yr, respectively (11%/yr for ^{99}Tc and 7.4%/yr for ^{129}I), with a ^{235}U enrichment of 4.57%. Comparing the results with those from Ref. [83], transmutation performance is much better in this work.

Recently, Yang, *et al*. [82] revisited LLFP transmutation in PWR. The analyses were performed for a typical Westinghouse-type PWR assembly. They compared various LLFP loading options: 1) mixing ^{99}Tc with fuel, 2) ^{99}Tc coating on the fuel pellet, annular target in the guide tube, 3) with and 4) without ZrH_2 moderator, and 5) LLFP mixed with ZrH_2 in the guide tube. Also, they assessed the impacts of LLFP loading on the major safety parameters of PWR. It is indicated that options 1) and 2) provide a better ^{99}Tc transmutation performance than the others due to the reduced self-shielding effect. For the iodine transmutation, the annular target, option 3), is best in terms of transmutation rate. However, accounting for the Xe pressure build-up, they recommended an annular iodine target with an inner void as the practical approach. The study shows that both ^{99}Tc and ^{129}I can be stabilised (zero net LLFP production) at the cost of higher fuel enrichment, but still less than the practical limit of 5.0%. Typical discharge burn-up of ^{99}Tc and ^{129}I were evaluated to be ~20% and ~12% in a UO_2 core with an 18-month cycle length. The study shows that impacts of LLFP transmutation in PWR are marginal from the safety point of view, if the LLFP loading is limited by the maximum ^{235}U enrichment of 5.0%.

As already described, ^{99}Tc has a relatively large resonance cross-section. Thus, the resonance shielding effect could be significant when ^{99}Tc is transmuted in a thermal neutron spectrum. In Figure 3.10, the radial Ru concentration is plotted for an irradiated sample from the EFTTRA-T2 experiment in HFR [77]. The resonance shielding effect is clearly observed in the figure: the Tc transmutation is about 16 a/o in the central region while the Ru concentration is 30~40 a/o near the rim (~0.15 mm thickness) of the pellet. Thermal neutrons are mainly absorbed in the vicinity of the target surface. The results experimentally confirm that a thick rod-type metallic Tc is not a good target form in a thermal reactor. Instead, the Tc target should be very thin or needs to be diluted in order to increase the effective capture cross-section of the target, as is already indicated in Refs. [82,83].

Figure 3.10. Two EPMA profiles of the Ru concentration in a Tc rod of EFTTRA-T2

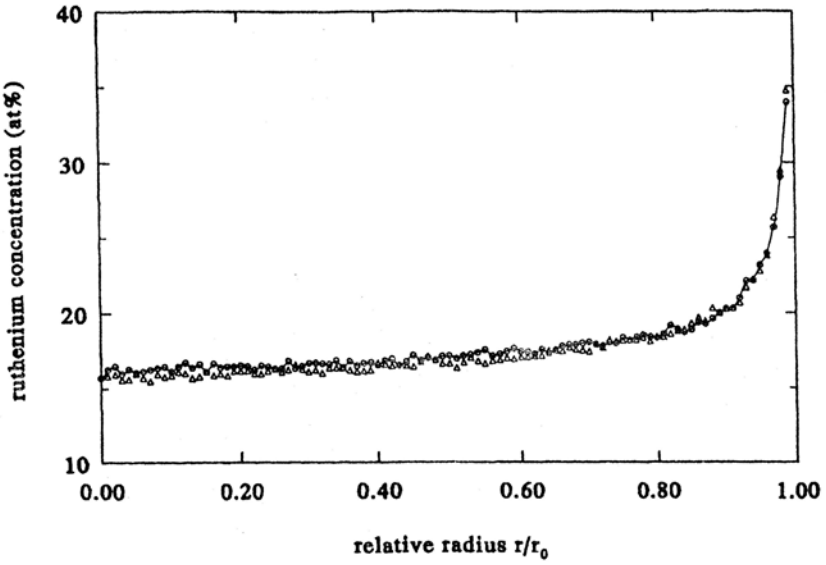

3.2.4.3 Fast reactors

Fast reactors are known to have a higher LLFP transmutation potential due to their greater number of surplus neutrons and the high neutron flux. Various avenues have been explored for the transmutation of LLFPs in fast spectrum, including a moderated subassembly loaded either at the core periphery or in the inner core. For ^{99}Tc, a direct transmutation in a fast spectrum without moderator was also studied due to the high flux and the relatively large resonance in the epithermal range. One of the advantages of the transmutation in a fast spectrum is that there is no concern about local power peaking, which is an issue in the moderated subassembly case. In general, moderated LLFP assembly in the core periphery provides a better neutron economy relative to the other two schemes, since the transmutation is based on the neutron leakage. Thus, it is often called the leakage slowing down (LSD) concept.

As an example of the LSD approach, the adiabatic resonance crossing (ARC) method was studied to enhance the LLFP transmutation in a high Z medium such as lead [85]. The idea is based on the small lethargic steps of neutrons slowing down in lead and the resonance width of ^{99}Tc is usually larger than the lethargic step, thereby enhance the probability of being captured. The principle was demonstrated in the TARC (Transmutation by ARC) experiment [85].

3.2.4.3.1 Spectral optimisation of moderated LLFP target

Among the various transmutation options, the moderated subassembly method is found to be best in terms of the transmutation performance. The moderated subassembly method can be classified into two categories, heterogeneous [86-88] and homogeneous [81,82,88,89]. In the heterogeneous concept, moderator pins are distinguished from the LLFP target pins, while both moderator and target are loaded into a single pin in the homogeneous concept. Based on the related works, the homogeneous approaches are better in terms of the transmutation performance than the heterogeneous one [88].

Regarding the homogeneous concept, there are two approaches depending on the configuration of moderator and target, as shown in Figure 3.11. The duplex concept was studied in Ref. [88] and the annular target was introduced by Kim [89]. The double-annular LLFP target was also proposed by Kim, *et al*. [90] for a simultaneous transmutation of ^{99}Tc and ^{129}I in a single target pin. For a simple duplex-like configuration, Golfier, *et al*. [91] undertook a parametric study to optimise the transmutation rate. In Refs. [81,88], various moderator materials were evaluated and compared. The works showed that metal hydrides such as ZrH_2 and CaH_2 provide a better environment for higher LLFP transmutation rates. For the annular target configuration, similar analyses were performed in more detail in Refs. [82,89] for an LLFP assembly placed in a reflector zone of a sodium-cooled fast reactor. Figures 3.12 and 3.13 show the transmutation performances of ^{99}Tc and ^{129}I as a function of the moderator (ZrH_2) volume fraction inside a steel cladding [82,89].

Figure 3.11. Configurations of the duplex and annular LLFP targets

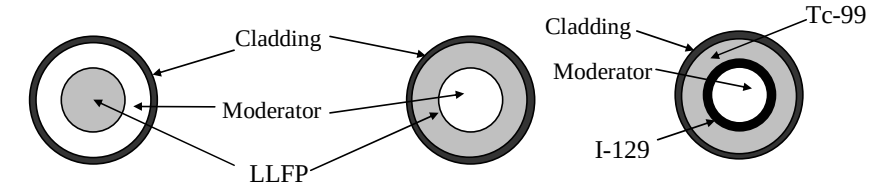

a) Duplex target b) Annular c) Double-annular target

Figure 3.12. ^{99}Tc transmutation rates versus moderator volume fraction

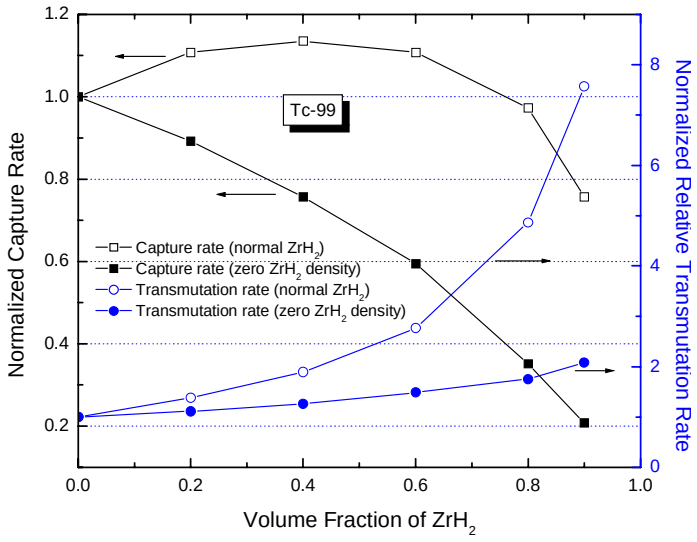

Figure 3.13. ^{129}I transmutation rates versus moderator volume fraction

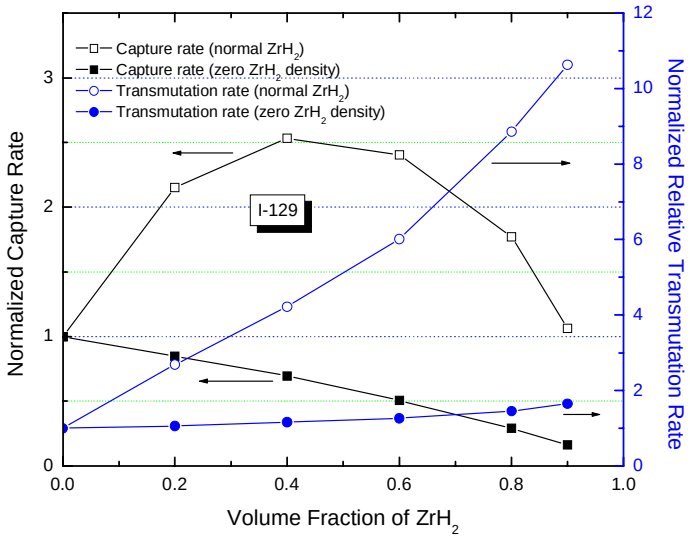

One can note that both ^{99}Tc and ^{129}I have an optimal moderator volume fraction (0.4~0.5) for the absolute transmutation rate (kg/time) and a desired absolute transmutation rate can be achieved with a much smaller LLFP loading by employing a moderator. It is noteworthy that the moderator gain is much larger for ^{129}I, ~150% than in ^{99}Tc, ~15%. In the meantime, the relative transmutation rate (%/time) increases monotonically with the moderator volume. It was also shown that the local power peaking in a neighbouring fuel assembly increases with the moderator volume. The analysis by Golfier, *et al*. [81] provides quite similar results. However, in the so-called duplex configuration, the power peaking might be substantially larger than that in the annular and the double-annular concepts.

The annular LLFP target seems to have several advantages over the duplex one: 1) the effective capture cross-sections are slightly larger due to more reduced self-shielding effects, 2) local power peaking is substantially reduced due to filtering of thermal neutrons by the annular target (especially for ^{99}Tc), 3) heat is easily removed from the target. In the duplex target, heat generated in the target might not be efficiently removed, as the envisioned moderators generally have low thermal conductivity. However, fabrication of an annular LLFP target would be more difficult than in the case of the duplex type. Material compatibility should be verified in both duplex and annular concepts. Basically, the double-annular concept shares the above advantages/issues of the annular target. An additional feature of the double-annular concept is that the outer Tc ring plays the role of thermal neutron filter for all the LLFP target pins. Filtering of thermal neutrons should be done such that the deleterious impact on LLFP transmutation performance should be minimised. Using ^{99}Tc as a filter is advantageous in that the filter is a LLFP to be transmuted. Dobbin, *et al*. [91] showed that placing a thick filter between fuel and LLFP assemblies results in a significant reduction in transmutation performance.

3.2.4.3.2 Performance of LLFP transmutation

Based on the duplex LLFP assembly placed in the reflector zone, the transmutation performance of ^{99}Tc and/or ^{129}I in fast reactors was studied [81,88]. It was shown that fast reactors have an excellent potential for transmuting ^{99}Tc and ^{129}I. It was further demonstrated that a fast reactor supports several PWRs in terms of ^{99}Tc and/or ^{129}I incineration, depending on the LLFP loading. It is revealed that the LLFP transmutation rate is highly dependent on the LLFP loading amount.

In Refs. [82,89], the annular target concept was applied to the transmutation of ^{99}Tc and ^{129}I in a sodium-cooled ADS loaded with a TRU fuel. Among various loading options, the loading in the reflector regions was found to be the best option from the neutron economy and safety points of view. It was shown that a balanced transmutation of TRU and LLFP could be achieved with a support ratio of ~3 at the cost of increased fuel inventory by about 10%. Transmutation rates of ^{99}Tc and ^{129}I were approximately 5.7%/yr and 7.2%/yr, respectively, for a loading of 530 kg ^{99}Tc and 92 kg ^{129}I. Discharge burn-ups of 29% and 37% are attained for ^{99}Tc and ^{129}I, respectively, with a five-year irradiation period. It was pointed out that, in the case of a ^{129}I target, a rather strong thermal neutron filter should be placed along the interface between a moderated LLFP assembly and the fuel assembly, since the iodine ring is not a good thermal neutron filter, relative to the ^{99}Tc ring.

LLFP transmutation based on the double-annular concept was explored in an LBE-cooled ADS [90] and a lead-cooled critical reactor [92]. It is observed that the new concept works quite well. The transmutation rates were 6~7% on the average for ^{99}Tc and ^{129}I, and relatively high discharge burn-ups were achieved, comparable to those of the simple annular concept. The studies show that with the double-annular configuration the thermal neutron filter requirement is largely alleviated compared with the single annular target, leading to more effective incineration of LLFPs.

In the LSD concept, the radial reflector zone is usually utilised for the transmutation of LLFPs. In the mean time, if a large amount of LLFPs is to be transmuted in a reactor, both radial and axial reflector could be used simultaneously, as in a MA burner. An advantage of the axial zone case is that the flux level is usually higher. Nishihara, *et al*. [93] studied the transmutation of ^{99}Tc and ^{129}I in a MA-loaded ADS. The LLFP transmutation requirement is huge in this case, approximately 56 kg/yr of ^{129}I and 200 kg/yr of ^{99}Tc for a balanced transmutation. In the study, LLFPs were loaded in the two reflector zones moderated with independent metal hydride pins. The results show that ^{129}I can be transmuted with the MA support ratio while a balanced Tc transmutation is hardly achievable. It was indicated that transmutation in the axial reflector is limited due to the limited irradiation time. The xenon pressure in particular is a very limiting factor for the iodine target. With respect to the moderated LLFP assembly in the axial reflector, careful evaluation of the possible power peaking needs to be done since the thermal neutron filtering would be difficult in the zone.

Most LLFP transmutation studies are mainly focused on the evaluation or assessment of the transmutation potential of a system of interest. The impacts of LLFP loading on the core characteristics have not been intensively evaluated. Some of the studies on LLFP transmutation reveal an interesting effect of the LLFP loading on the core characteristics. Park, *et al*. [86] showed that the coolant void reactivity becomes more negative when moderated LLFP assemblies are loaded in the inner core of an ADS loaded with a TRU fuel. Also, Kim *et al*. [92,93] showed that LLFP transmutation in the reflector zone makes the coolant void reactivity substantially more negative, relative to a no-LLFP case, both in an LBE-cooled ADS and a lead-cooled critical TRU transmuter. For example, in the ADS case of Ref. [32], the active core void reactivity was reduced from 3 337 pcm without LLFP to only 405 pcm with LLFP loading. It seems that LLFP transmutation in the core periphery would be most effective in reducing the void reactivity. The LLFP transmutation could be a design measure to reduce the void reactivity in fast reactors.

3.2.5 Other approaches

Transmutation of ^{135}Cs in the blanket of a fusion nuclear system was proposed by Saito, *et al*. [67]. In the study, caesium was loaded in an elemental form, i.e. no isotopic separation and Pb-15Cs was used as a caesium carrier. The neutronic study reveals the advantage of the blanket configuration with a large Be fraction that provides a neutron spectrum softer than in a thermal reactor. In the FNS, the

neutron flux is largely dependent on the first wall neutron loading. It was shown that the lifetime of ^{135}Cs could be reduced to 7.3 years for 2.5 MW/m^2 first wall loading and 23.5 years for a 1 MW/m^2 neutron loading. These lifetimes of ^{135}Cs are much shorter than those available at conventional fission reactors or ADS. The 2.5 MW/m^2 first wall neutron loading is considered in future demonstrative fusion reactors.

Recently, a high-power laser has been also applied to the transmutation of ^{129}I and ^{99}Tc. Ledingham, *et al*. [94] used the VULCAN petawatt laser to drive the photo-transmutation of ^{129}I through the (γ,n) reaction. A 360 J laser pulse, of wavelength $\lambda \sim 1\mu m$ and duration 0.7 ps, was focused on a gold target with dimension $5 \times 5 \times 4$ mm, resulting in an intensity of about 5×10^{20} W/cm^2. The resulting bremsstrahlung gamma radiation was used in the photo-transmutation of ^{129}I. It was reported that the single 360 J laser shot produced about 2.9×10^6 nuclei of ^{128}I from the initial 1.8×10^{23} nuclei of ^{129}I. A similar study on the photo-transmutation of ^{99}Tc was performed with the VULCAN laser [95]. In this study, transmutation of ^{99}Tc to ^{96}Tc via the (γ,3n) reaction was explored. However, no evidence of the ^{99}Tc transmutation was observed.

As another application of the high-power laser, Ledingham, *et al*. [96] indicated that a much higher-power laser, with an intensity of the order of 10^{28} W/cm^2, can directly excite the nucleus. Consequently, nuclear energy levels and hence decay lifetimes could be directly altered.

3.2.6 R&D issues

Nuclear data on fission products are known to have relatively large uncertainties [97]. For an accurate evaluation of the LLFP transmutation, the nuclear data libraries need to be re-evaluated.

It is clear that more researches are required to decide the appropriate chemical forms of iodine. For the selection of the iodine target, material compatibility issues should be fully addressed under a much higher iodine burn-up condition.

Material compatibility could be an issue in some special configurations of the LLFP targets such as the duplex and annular concepts. Compatibility between the target components should be verified.

In the conventional PUREX process, it seems that a satisfactory means can be developed for recovery of ^{99}Tc and ^{129}I contained in the LWR spent fuel. However, for recovery of those LLFPs in the less well-defined pyro-processing, more experimental studies are required [98].

A multiple recycling of LLFPs is inevitable in the LLFP transmutation. Reprocessing of the irradiated LLFP targets should be studied with an aim to minimise the loss to the environment. It is expected that recovery of remaining iodine would be rather complex due to the possibility of dissociation of the target and interaction between iodine and structural material. Re-fabrication of the LLFP target is an important unresolved issue, as well. In order to minimise the LLFP loss during the reprocessing, different means of maximising the LLFP discharge burn-up need to be explored.

Most studies on the LLFP transmutation are focused on the assessment of the transmutation rate of a specific target in a reactor system. A loading of a significant amount of LLFPs into a reactor system may have noticeable impacts on the characteristics of the reactor core such as safety parameters. Those impacts must be addressed in more detail.

3.2.7 Concluding remarks

Taking into account transmutability and impacts on the repository, ^{99}Tc and ^{129}I are the only LLFPs which can be transmuted in reactor systems. A metallic Tc can be used as a target material. However, there is no general consensus on the chemical form of the iodine target. The possible candidates are NaI, CaI_2 and MgI_2. Further studies are necessary for the appropriate selection of the iodine chemical compound in a more practical condition.

In terms of the LLFP transmutation performance, fast reactors or ADS have the highest potential due to their greater surplus neutrons. In thermal reactors, HWRs have better LLFP transmutation capabilities than PWRs. However, HWRs loaded with LLFPs cannot be operated with the natural uranium; significantly enriched uranium is required, which could be a crucial issue. Furthermore, the HWR core characteristics would be affected by the LLFP loading. Although PWRs have a relatively low LLFP transmutation potential, they can be used as an LLFP stabiliser, i.e. zero net production, without causing any serious concern about the core safety.

For an efficient LLFP transmutation in a fast reactor, a moderated LLFP assembly needs to be employed. Metal hydrides such as ZrH_2 and CaH_2 would be good moderators. The LLFP transmutation rate could be significantly enhanced by using an annular target or a duplex configuration. It seems that the annular LLFP target enclosing a moderator might have some advantages over the duplex one from the neutronic point of view. LLFP transmutation in the reflector would be beneficial in terms of the neutron economy and core safety. A radial reflector would be preferable to the axial one since the fuel and target management would be more complex in the case of the axial reflector. Also, the irradiation period might be limited by the fuel management scheme for LLFPs in the axial reflector.

Moderated LLFP assemblies in the inner core slightly reduce the coolant void reactivity. LLFP assemblies loaded in the reflector zone might substantially reduce the coolant void reactivity. This feature could be employed to improve the safety feature of a fast transmuter.

Currently, the motivation for LLFP transmutation is not so strong, as it is only a marginal improvement from the viewpoint of reducing radiotoxicity. However, reduction of the LLFP inventory of a repository could allow some relaxation of the stringent waste form and the container performance criteria, with associated economic benefits. Therefore, some development of the LLFP transmutation is prudent, especially when a sustained fission power production (with accumulating FP inventory) is envisioned for future application. Also, LLFP transmutation is generally in accordance with the concept of clean nuclear energy.

3.3 Nuclear data uncertainty impact on ADS design parameters

A specific issue of relevance in the assessment of ADS feasibility is the investigation of the impact of nuclear data uncertainties on ADS design parameters. The following paragraphs will describe a specific application, in order to quantify potential effects.

3.3.1 Sensitivity and uncertainty analysis for a specific ADS transmuter core

The following parameters are of a particular relevance for a transmuter core:

- Criticality (multiplication factor).
- Doppler reactivity coefficient.

- Coolant void reactivity coefficient.
- Effective delayed neutron fraction.
- Reactivity loss during irradiation.
- Transmutation potential.
- Peak power value.
- φ* parameter (for subcritical ADS systems).
- Max dpa, max He and H production, max (He production)/dpa.
- Decay heat.

A representative transmuter core has been designated so as to quantify the impact of uncertainties.

The transmuter which has been examined is an intermediate size (~800 MWth) ADS with Pu/MA nitride fuel (MA/Pu ratio equal to 2), lead-bismuth cooled. This transmuter is representative of most current proposals, as indicated in different international programmes (see Section 2.3).

As far as nuclear data uncertainties, the variance data given in Tables 3.6 and 3.7 have been applied. The data for major actinides have been deduced from studies related to the JEF nuclear data file. The data for MA have been deduced from a different file intercomparison.

The following hypothesis on correlations has been used:

- No correlation (in energy, among reactions, etc.).
- Full energy correlation.
- Partial energy correlation (by energy "band").

The main calculated parameters are given in Tables 3.8 and 3.9. The calculations were based on the ENDF/B-VI file.

The resulting uncertainties, obtained with the sensitivity analysis outlined in Ref. [99], and using the nuclear data uncertainties of Tables 3.6 and 3.7, are given in Tables 3.10 and 3.11.

The values are shown for two hypotheses of energy data correlation (no correlation and partial energy correlation).

As an example, the breakdown of uncertainties by energy group and by isotope in the case of k_{eff} is given in Tables 3.12 and 3.13, and the breakdown by isotope of the uncertainties of nuclide density variations during the irradiation cycle is given in Table 3.14.

The standard ENDF/B file up to 20 MeV has been extended up to 150 MeV, based on the data of Ref. [100], for Pb, Bi and Fe. This extension makes possible to analyse the dependence of some relevant parameters to high-energy data (i.e. above 20 MeV). An example of energy and isotope breakdown for the case of the ratio max (He production)/dpa is given in Tables 3.15 and 3.16.

Table 3.6. Variance matrix (δσ/σ) for major actinides

		^{238}Pu and ^{240}Pu						^{239}Pu					
Gr	**[MeV][(a)]**	**ν**	**σ_f**	**σ_{inel}**	**σ_{el}**	**σ_{capt}**	**$\sigma_{n,2n}$**	**ν**	**σ_f**	**σ_{inel}**	**σ_{el}**	**σ_{capt}**	**$\sigma_{n,2n}$**
1	**19.6**	0.12	0.05	0.15		0.3	0.16	0.008	0.03	0.1		0.1	0.13
2	**6.07**	0.14	0.05	0.15		0.3		0.0075	0.037	0.1		0.085	0.25
3	**2.23**	0.18	0.1	0.15		0.3		0.007	0.037	0.1		0.095	
4	**1.35**	0.02	0.1	0.15	↑	0.3		0.0065	0.065	0.15		0.13	
5	**4.98e-1**	0.028		0.2		0.25		0.0055	0.04	0.15	↑	0.13	
6	**1.83e-1**	0.03		0.2		0.15		0.008	0.028	0.15		0.078	
7	**6.74e-1**	0.0312	↑	0.2	0.1	0.1		0.015	0.03	0.2		0.039	
8	**2.48e-2**	0.0311				0.1		0.008	0.045	0.25	0.05	0.056	
9	**9.12e-3**	0.031	0.2		↓	0.1		0.008	0.063	0.25	↓	0.056	
10	**2.04e-3**	0.03	↓			0.1		0.0051	0.02			0.065	
11	**4.54e-4**	0.029				0.1		0.005	0.025			0.065	
12	**2.26e-5**	0.028				0.08		0.003	0.025			0.065	
13	**4.00e-6**	0.027				0.03		0.0024	0.025			0.039	
14	**5.40e-7**	0.026	0.5		0.5	0.005		0.0022	0.0025			0.008	
15	**1.00e-7**	0.019	0.5		0.5	0.005		0.002	0.0025			0.008	

		^{241}Pu						^{242}Pu					
Gr	**[MeV][(a)]**	**ν**	**σ_f**	**σ_{inel}**	**σ_{el}**	**σ_{capt}**	**$\sigma_{n,2n}$**	**ν**	**σ_f**	**σ_{inel}**	**σ_{el}**	**σ_{capt}**	**$\sigma_{n,2n}$**
1	**19.6**	0.01	0.125	0.15		0.5	0.18	0.12	0.05	0.15		0.3	0.25
2	**6.07**	0.0095	0.2	0.15		0.5	0.2	0.15	0.05	0.15		0.3	
3	**2.23**	0.009	0.05	0.15		0.4		0.19	0.1	0.15		0.3	
4	**1.35**	0.0085	0.05	0.15		0.3		0.02	0.1	0.15		0.3	
5	**4.98e-1**	0.008	0.06	0.2		0.2		0.03		0.2	↑	0.25	
6	**1.83e-1**	0.007	0.1	0.2	↑	0.2		0.0317		0.2		0.15	
7	**6.74e-1**	0.0065	0.1	0.2		0.15		0.0316	↑	0.2	0.1	0.1	
8	**2.48e-2**	0.006	0.08		0.1	0.15		0.0315				0.1	
9	**9.12e-3**	0.0055	0.08		↓	0.1		0.031	0.2		↓	0.1	
10	**2.04e-3**	0.005	0.03			0.1		0.03	↓			0.1	
11	**4.54e-4**	0.0045	0.03			0.1		0.029				0.09	
12	**2.26e-5**	0.004	0.03			0.1		0.028				0.08	
13	**4.00e-6**	0.0035	0.03			0.1		0.027				0.08	
14	**5.40e-7**	0.003	0.006			0.014		0.025	0.5		0.07	0.01	
15	**1.00e-7**	0.0024	0.006			0.014		0.02	0.5		0.07	0.01	

[(a)] *Upper energy boundary.*

Table 3.7. Variance matrix (δσ/σ) for minor actinides

	^{237}Np					^{241}Am and ^{243}Am					^{242m}Am				
Group [(a)]	**ν**	**σ_f**	**σ_{inel}**	**σ_{el}**	**σ_{capt}**	**ν**	**σ_f**	**σ_{inel}**	**σ_{el}**	**σ_{capt}**	**ν**	**σ_f**	**σ_{inel}**	**σ_{el}**	**σ_{capt}**
1-2	0.05	0.25	0.5	0.05	0.4	0.05	0.2	0.5	0.05	0.4	0.05	0.2	0.5	0.05	0.4
3-6	0.05	0.25	0.5	0.05	0.15	0.05	0.2	0.5	0.05	0.4	0.05	0.2	0.5	0.05	0.4
7-15	0.05	0.25	0.5	0.05	0.15	0.05	0.2	0.5	0.05	0.2	0.05	0.2	0.5	0.05	0.04

	^{242}Cm, ^{243}Cm, ^{245}Cm, ^{246}Cm					^{244}Cm				
Group [(a)]	**ν**	**σ_f**	**σ_{inel}**	**σ_{el}**	**σ_{capt}**	**ν**	**σ_f**	**σ_{inel}**	**σ_{el}**	**σ_{capt}**
1-4	0.05	0.3	0.5	0.05	0.4	0.05	0.4	0.5	0.05	0.4
5-13	0.05	0.3	0.5	0.05	0.4	0.05	0.3	0.5	0.05	0.4
14-15	0.05	0.3	0.5	0.05	0.04	0.05	0.3	0.5	0.05	0.04

[(a)] *Same energy boundary as in Table 3.6.*

Table 3.8. Main parameters of the reference system

K_{eff}	$\hat{\beta}_{eff}$ [pcm]	$\Delta\rho^{Doppler}$ (a)	$\Delta\rho^{void}$	$\Delta\rho^{cycle}$		Decay heat (d)	Peak power
				1 year (b)	2 years (b)		
0.948164	185.4	-0.00026	+0.02906	-0.01196	-0.02158	25 MWth	2.9

$(\Delta n)^{cycle}$ (c) [10^{24} at./cm^3]						
^{238}Pu	^{241}Am	^{242m}Am	^{243}Am	^{242}Cm	^{244}Cm	^{245}Cm
5.19E-5	-8.64E-5	8.34E-6	-5.24E-5	2.68E-5	2.28E-5	1.50E-6

(a) *For $\Delta T = T - TRef = 1\,773\ K - 980\ K$.*
(b) *At full power.*
(c) *One-year irradiation.*
(d) *At discharge, nominal power of the core: 377 MWth.*

Table 3.9. Main parameters of the reference system

φ*	Max dpa [sec^{-1} × cm^{-3}]	Max He production [sec^{-1} × cm^{-3}]	Max H production [sec^{-1} × cm^{-3}]	Max (He production)/dpa
1.18	2.58E+16	6.15E+15	6.77E+16	0.24

Table 3.10. Resulting uncertainties (in percentage) for the integral parameters of the reference system

	φ*	Max dpa	Max He production	Max H production	Max (He production)/dpa
$\Delta I_{no\_correlation}$	±2.74	±29.9	±43.6	±28.5	±45.5
ΔI_{PEC} (a)	±5.07	±48.9	±59.1	±53.1	±67.4

(a) *Partial correlation in energy.*

Table 3.11. Resulting uncertainties (in percentage) for the integral parameters of the reference system

	K_{eff}	$\hat{\beta}_{eff}$	$\Delta\rho^{void}$	$\Delta\rho^{cycle}$ (1 year)	Peak power
$\Delta I_{no\_correlation}$	±2.77	±11.3	±35.2	±47.4	±20.5
ΔI_{PEC} (a)	±4.41	±17.4	±59.3	±73.1	±32.4

	$(\Delta n)^{cycle}$ (b)						
	^{238}Pu	^{241}Am	^{242}Am	^{243}Am	^{243}Cm	^{244}Cm	^{245}Cm
$\Delta I_{no\_correlation}$	±7.3	±15.1	±15.9	±15.3	±12.5	±25.6	±81.2
ΔI_{PEC} (a)	±10.9	±23.8	±23.2	±24.3	±18.3	±37.8	±122.9

(a) *Partial correlation in energy.*
(b) *One year irradiation.*

Table 3.12. k_{eff} – uncertainties (%) by group – no energy correlation

Gr.	[MeV] [(a)]	σ_{cap}	σ_{fiss}	ν	σ_{el}	σ_{inel}	$\sigma_{n,2n}$	Total [(b)]
1	**19.6**	0.01	0.05	0.02	–	0.04	0.04	**0.08**
2	**6.07**	0.01	0.57	0.18	0.04	0.47	–	**0.76**
3	**2.23**	0.03	0.83	0.27	0.07	0.46	–	**0.99**
4	**1.35**	0.47	1.56	0.41	0.20	0.77	–	**1.86**
5	**4.98e-1**	0.84	0.39	0.08	0.10	0.19	–	**0.95**
6	**1.83e-1**	1.01	0.32	0.07	0.06	0.20	–	**1.08**
7	**6.74e-2**	0.41	0.24	0.07	0.02	0.04	–	**0.49**
8	**2.48e-2**	0.37	0.22	0.04	0.02	0.03	–	**0.43**
9	**9.12e-3**	0.31	0.20	0.03	–	–	–	**0.37**
10	**2.04e-3**	0.20	0.08	0.02	–	–	–	**0.21**
11	**4.54e-4**	0.04	0.01	–	–	–	–	**0.04**
12	**2.26e-5**	–	–	–	–	–	–	**–**
13	**4.00e-6**	–	–	–	–	–	–	**–**
14	**5.40e-7**	–	–	–	–	–	–	**–**
15	**1.00e-7**	–	–	–	–	–	–	**–**
Total [(b)]		**1.54**	**1.97**	**0.54**	**0.25**	**1.05**	**0.04**	**2.77**

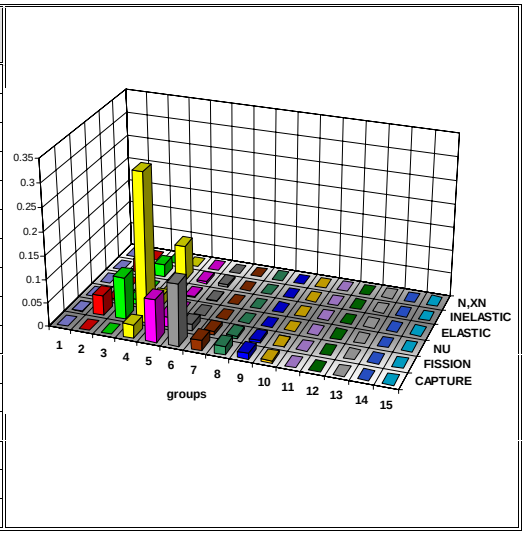

[(a)] *High energy group boundary.*
[(b)] *Total obtained as the square root of the sum of the squares of individual contributions in row or column.*

Table 3.13. k_{eff} – uncertainties (%) by isotope – no energy correlation

Isotope	σ_{cap}	σ_{fiss}	ν	σ_{el}	σ_{inel}	$\sigma_{n,2n}$	Total [(b)]
^{238}Pu	0.01	0.11	0.02	–	–	–	**0.11**
^{239}Pu	0.04	0.51	0.11	–	0.04	–	**0.53**
^{240}Pu	0.05	0.18	0.05	–	0.02	–	**0.19**
^{241}Pu	0.04	0.30	0.03	–	0.01	–	**0.31**
^{242}Pu	0.01	0.05	0.02	–	0.01	–	**0.06**
^{237}Np	0.24	0.70	0.21	–	0.14	–	**0.78**
^{241}Am	1.32	1.12	0.38	–	0.22	–	**1.79**
^{242m}Am	0.01	0.09	0.03	–	0.01	–	**0.10**
^{243}Am	0.74	0.59	0.21	–	0.60	–	**1.14**
^{242}Cm	–	–	–	–	–	–	**–**
^{243}Cm	–	0.05	0.01	–	–	–	**0.05**
^{244}Cm	0.13	1.09	0.18	–	0.07	–	**1.11**
^{245}Cm	0.01	0.41	0.08	–	0.01	–	**0.42**
^{246}Cm	–	–	–	–	–	–	**–**
^{56}Fe	0.03	–	–	0.05	0.49	–	**0.50**
^{57}Fe	–	–	–	–	0.06	–	**0.06**
^{52}Cr	0.01	–	–	0.01	0.03	–	**0.03**
^{58}Ni	–	–	–	–	–	–	**–**
Zr	0.03	–	–	0.03	0.07	–	**0.09**
^{15}N	–	–	–	0.19	0.01	–	**0.19**
Pb	0.02	–	–	0.10	0.41	0.02	**0.43**
Bi	0.04	–	–	0.11	0.49	0.03	**0.50**
Total [(b)]	**1.54**	**1.97**	**0.54**	**0.25**	**1.05**	**0.04**	2.77

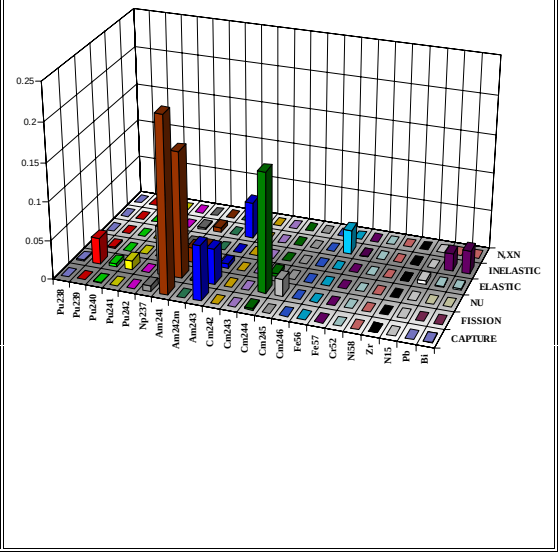

[(b)] *Total obtained as the square root of the sum of the squares of individual contributions in row or column.*

Table 3.14. Uncertainties on the nuclear density variation of: ^{238}Pu, ^{241}Am, ^{242m}Am, ^{243}Am, ^{242}Cm, ^{244}Cm, ^{245}Cm (values in %)

Isotope	Uncertainty due to:								Total
^{238}Pu	^{237}Np		^{238}Pu		^{241}Am		^{242}Cm		7.33
	Capture	*Fission*	*Capture*	*Fission*	*Capture*	*Fission*	*Capture*	*Fission*	
	3.67	0.12	0.19	0.61	6.31	0.04	0.06	0.09	
^{241}Am	^{241}Am								15.12
	Capture	*Fission*							
	11.06	10.31							
^{242m}Am	^{241}Am		^{242m}Am						15.91
	Capture	*Fission*	*Capture*	*Fission*					
	15.70	0.15	0.83	2.45					
^{243}Am	^{242}Pu	^{243}Am							15.28
	Capture	*Capture*	*Fission*						
	0.22	10.66	10.94						
^{242}Cm	^{241}Am		^{242}Cm						12.54
	Capture	*Fission*	*Capture*	*Fission*					
	12.54	0.15	0.17	0.27					
^{244}Cm	^{243}Am		^{244}Cm						25.55
	Capture	*Fission*	*Capture*	*Fission*	*(n,2n)*				
	23.48	0.20	4.98	8.75	0.20				
^{245}Cm	^{243}Am		^{244}Cm			^{245}Cm			81.19
	Capture	*Fission*	*Capture*	*Fission*	*(n,2n)*	*Capture*	*Fission*	*(n,2n)*	
	4.82	0.03	72.33	1.71	0.04	5.48	36.10	0.03	

Table 3.15. Max (He production)/dpa – uncertainties (%) by group

Gr.	[MeV] [(a)]	σ_{cap}	σ_{fiss}	ν	σ_{el}	σ_{inel}	$\sigma_{n,2n}$	Total [(b)]
1	**150**	–	–	–	0.1	4.8	–	**4.8**
2	**55.2**	–	0.1	–	0.2	20.1	6.4	**21.1**
3	**19.6**	–	0.7	0.2	0.7	11.6	34.0	**35.9**
4	**6.07**	0.1	3.2	1.0	0.3	4.5	–	**5.6**
5	**2.23**	0.2	4.7	1.6	0.5	4.3	–	**6.6**
6	**1.35**	3.1	9.2	2.5	1.5	5.8	–	**11.7**
7	**4.98e-1**	5.2	2.4	0.5	0.8	1.3	–	**6.0**
8	**1.83e-1**	6.3	2.0	0.4	0.5	1.2	–	**6.7**
9	**6.74e-2**	2.6	1.5	0.4	0.2	0.2	–	**3.0**
10	**2.48e-2**	2.2	1.3	0.2	0.2	0.1	–	**2.6**
11	**9.12e-3**	1.9	1.2	0.2	–	–	–	**2.3**
12	**2.04e-3**	1.2	0.5	0.1	–	–	–	**1.3**
13	**4.54e-4**	0.2	0.1	–	–	–	–	**0.2**
14	**2.26e-5**	–	–	–	–	–	–	–
15	**4.00e-6**	–	–	–	–	–	–	–
16	**5.40e-7**	–	–	–	–	–	–	–
17	**1.00e-7**	–	–	–	–	–	–	–
Total [(b)]		**9.6**	**11.5**	**3.2**	**2.0**	**14.1**	**40.4**	**45.5**

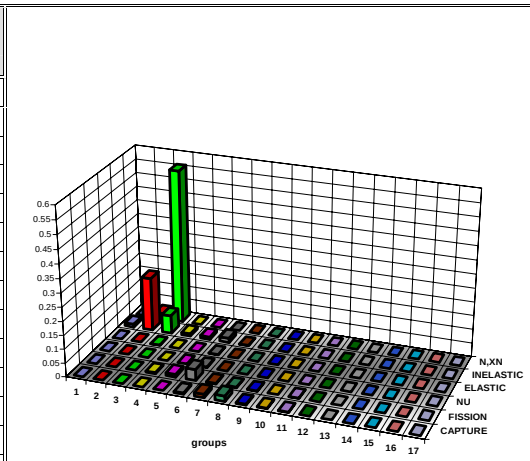

[(a)] *High energy group boundary.*
[(b)] *Total obtained as the square root of the sum of the squares of individual contributions in row or column.*

Table 3.16. Max (He production)/dpa – uncertainties (%) by isotope

Isotope	σ_{cap}	σ_{fiss}	ν	σ_{el}	σ_{inel}	$\sigma_{n,2n}$	Total [(b)]
^{238}**Pu**	0.1	0.6	0.1	–	–	–	**0.7**
^{239}**Pu**	0.3	3.0	0.7	–	0.3	–	**3.1**
^{240}**Pu**	0.3	1.1	0.3	–	0.1	–	**1.1**
^{241}**Pu**	0.3	1.8	0.2	–	0.1	–	**1.9**
^{242}**Pu**	0.1	0.3	0.1	–	–	–	**0.3**
^{237}**Np**	1.5	4.0	1.2	–	1.0	–	**4.6**
^{241}**Am**	8.3	6.5	2.3	–	1.6	–	**10.9**
^{242m}**Am**	–	0.6	0.2	–	–	–	**0.6**
^{243}**Am**	4.6	3.4	1.2	–	4.1	–	**7.2**
^{242}**Cm**	–	–	–	–	–	–	**–**
^{243}**Cm**	–	0.3	0.1	–	–	–	**0.3**
^{244}**Cm**	0.8	6.4	1.1	–	0.5	–	**6.5**
^{245}**Cm**	0.1	2.5	0.5	–	0.1	–	**2.5**
^{246}**Cm**	–	–	–	–	–	–	**–**
^{56}**Fe**	0.2	–	–	0.4	3.5	–	**3.6**
^{57}**Fe**	–	–	–	–	0.4	–	**0.4**
^{52}**Cr**	–	–	–	0.1	0.3	–	**0.3**
^{58}**Ni**	–	–	–	–	–	–	**–**
Zr	0.2	–	–	0.2	0.6	–	**0.6**
^{15}**N**	–	–	–	1.4	0.3	–	**1.4**
Pb	0.2	–	–	1.0	8.3	22.4	**23.9**
Bi	0.3	–	–	1.1	9.7	33.7	**35.1**
Total[(b)]	**9.6**	**11.5**	**3.2**	**2.0**	**14.1**	**40.4**	**45.5**

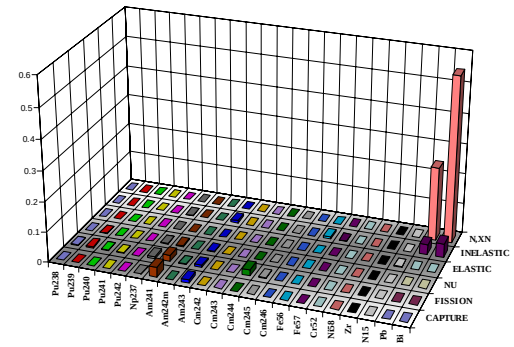

(b) *Total obtained as the square root of the sum of the squares of individual contributions in row or column.*

The results show a relevant sensitivity to MA actinide data, mainly σ_f, σ_c and σ_{in} and mostly in the energy range ~1 MeV-1 keV. This is due to the rather high uncertainties which have been used (see Table 3.7). These uncertainties, which can be considered rather pessimistic, have been established in a very simple manner, essentially taking into account the observed differences among major data files (ENDF/B, JEF and JENDL) and the spread of existing experimental results. A better assessment of uncertainties (variances and covariances) is obviously needed, but this should be the result of a specific evaluation work.

However, it is likely that, even if more refined uncertainty data will be used, the contribution of MA data will stay relevant, also in comparison to the contribution of Pu isotopes, for which much more realistic uncertainty data have been used in the study presented here.

It is relevant that the most important energy range is clearly the one where most of the neutron population is found. High-energy (>20 MeV) data do not influence most of the reactor parameters, but have impact on quantities related, e.g. to neutron damage. The impact of high-energy data on the assessment of the radioactive inventory in the target of an ADS should be also established.

Similarly, the potential impact of the uncertainties of high energy data on the shielding of an ADS could be of relevance, and should be evaluated.

Finally, the uncertainty of the decay heat of the fuel is given in the Table 3.17, where the component breakdown and their evolution with time are shown.

The uncertainty due to the actinide contribution to the decay heat will result in a total uncertainty for this important parameter 2-3 times higher than the current value for standard reactors.

Table 3.17. Uncertainty of the decay heat of the fuel

Per cent (%) of decay heat (DH) due to	t = 0	t = 10 days [(a)]	t = 1 month	t = 1 year	t = 100 years
Actinides (AN)	23%	86%	90% [(b)]	94% [(b)]	100% [(c)]
Fission products (FP)	77%	14%	10%	6%	–
Uncertainty on DH due to AN	±10%	±11%	±11%	±14%	±65%

[(a)] *Time after shutdown.*
[(b)] *Mostly due to ^{242}Cm and ^{244}Cm.*
[(c)] *Mostly due to ^{244}Cm, ^{245}Cm and ^{246}Cm.*

In summary, we observe a significant impact of uncertainties:

- MA data: σ_f, σ_c, σ_{in} – improvements are clearly needed in the energy range from 1-5 MeV down to 0.1-1 KeV.

- Some impact of intermediate energy (>20 MeV) data only on selected parameters related to, e.g. damage phenomena.

- Decay heat uncertainty is mostly related to MA (e.g. Cm) data. For a transmuter core, there is a different contribution of MA and FP with respect to standard fuel reactors, which underlines the significant impact of MA data. This could have an impact on the assessment of repository characteristics.

3.3.2 Required nuclear data uncertainties

In order to establish priorities and target accuracies on data uncertainty reduction, a formal approach can be used as indicated in Ref. [99].

In the case of the transmuter core examined here, the application of that approach has been performed for some integral parameters. Table 3.18 gives the initial uncertainties, the imposed target accuracies and the resulting accuracies, as obtained with the mentioned approach. The resulting ΔI uncertainties are associated to the required nuclear data uncertainties shown in Table 3.19.

Table 3.18. Selected integral parameters: uncertainty due to all data uncertainties ($\Delta I_{initial}$); target accuracies ($\Delta I_{required}$); resulting uncertainty from a minimisation procedure ($\Delta I_{resulting}$)

	K_{eff}	φ*	Power peak	Max dpa	Max He production	Max H production	Max He prod/dpa
$\Delta I_{initial}$	±2.77	±2.74	±20.50	±29.90	±43.60	±28.50	±45.50
$\Delta I_{required}$	±1%	±2%	±5%	±15%	±15%	±15%	±15%
$\Delta I_{resulting}$	±1.1%	±1.0%	±8.2%	±13.0%	±14.8%	±13.7%	±15.3%

Table 3.19. Cross-section uncertainties for selected cross-sections: original uncertainty and required uncertainty to meet integral parameter target accuracy

Isotope	Cross-section	Gr. [(a)]	Original uncertainty (%)	Required accuracy (%)
^{239}Pu	σ_{fiss}	4	6.5	3.4
		5	4	3.1
^{241}Pu	σ_{fiss}	6	10	5.6
^{237}Np	σ_{fiss}	3	25	8.0
		4	25	5.1
	ν	4	5	4.1
^{241}Am	σ_{cap}	4	40	7.5
		5	40	5.5
		6	40	5.1
		7	20	5.9
		8	20	6.3
		9	20	6.9
	σ_{fiss}	2	20	5.6
		3	20	4.6
		4	20	3.9
	ν	3	5	3.8
		4	5	3.3
^{243}Am	σ_{cap}	4	40	10.4
		5	40	5.5
		6	40	5.1
		7	20	5.9
		8	20	6.3
	σ_{fiss}	2	20	7.6
		3	20	6.2
		4	20	5.4
	σ_{inel}	3	50	12.6
		4	50	7.6
		5	50	12.0
		6	50	12.2
^{244}Cm	σ_{fiss}	2	40	10.0
		3	40	8.5
		4	40	5.0
^{245}Cm	σ_{fiss}	5	30	9.7
		6	30	9.6
^{56}Fe	σ_{inel}	4	20	4.9
^{15}N	σ_{el}	4	5	3.9
Pb	σ_{inel}	1	40	20.4
		2	40	9.8
		3	40	10.6
		4	40	10.1
	$\sigma_{n,2n}$	1	100	21.5
Bi	σ_{inel}	1	40	18.8
		2	40	8.1
		3	40	9.3
		4	40	14.0
	$\sigma_{n,2n}$	1	100	17.5
σ_{dpa}		1	20	20.0
		2	20	12.0
		3	20	12.1
		4	20	8.8
		5	20	20.0
		6	20	20.0
		7	20	10.9
$\sigma_{(n,\alpha)}$		1	20	10.8
		2	20	20.0
$\sigma_{(n,p)}$		1	20	15.1
		2	20	12.4
		3	20	20.0

[(a)] See energy boundary in Table 3.6.

The data of Table 3.19 indicate clearly that the required uncertainties for MA data are comparable to the uncertainties already achieved for major actinides, and Pu isotopes in particular. Any new major re-evaluation or measurement programme can only be justified if there would be a consensus on the fact that the present uncertainties to be associated to a specific data file are definitely larger than the target values indicated in Table 3.18.

In the case of the established need for a particular experiment, the required uncertainties also provide the type of accuracy required for that experiment (e.g. ±5% on the capture of ^{243}Am or 5-10% on the fission of ^{244}Cm and ^{245}Cm).

REFERENCES

[1] Rubbia, C., *et al*., *Conceptual Design of a Fast Neutron Operated High Power Energy Amplifier*, CERN/AT/95-44, Geneva, September 1995.

[2] Bowman, C.D., E.D. Artur, P.W. Lisowski, G.P. Lawrence, R.J. Jensen, J.L. Anderson, B. Blind, M. Cappiello, J.W. Davidson, T.R. England, L.N. Engel, R.C. Haight, H.G. Hugens III, J.R. Ireland, R.A. Krakowsky, R.J. Labauve, B.C. Letellier, R.T. Perry, G.J. Russel, K.P. Staudhammer, G. Versamis, W.B. Wilson, "Nuclear Energy Generation and Waste Transmutation Using an Accelerator-driven Intense Thermal Neutron Source", *Nucl. Instr. and Meth*., A320, 336 (1992).

[3] *A European Roadmap for Developing Accelerator-driven Systems (ADS) for Nuclear Waste Incineration*, Report of the European Technical Working Group on ADS, April 2001.

[4] Rief, H., H. Takahashi, "Some Physics Considerations in Actinide and Fission Product Transmutation", *Proceedings of the International Conference on Reactor Physics and Reactor Computations*, Tel-Aviv, 23-26 January 1994, Ben-Gurion University of the Negev Press, 108 (1994).

[5] D'Angelo, A., M. Carta, G. Bianchini, Y. Xing, "Some Considerations on Reactivity Effects and Source Intensity Control of Accelerator Driven Systems", *Proceedings of the GLOBAL'99 International Conference on Future Nuclear Systems*, Jackson Hole, Wyoming, 29 August-3 September 1999.

[6] Rydin, R.A., M.L. Woosley, "Evidence of Source Dominance in the Dynamic Behaviour of Accelerator-driven System", *Nucl. Sci. and Eng*., 126, 341 (1997).

[7] Venneri, F., "Hybrid (Subcritical) Systems for Nuclear Waste Destruction and Energy Production", *Proceedings of the International Conference on Nuclear Data for Science and Technology*, Trieste, 10-24 May 1997, Italian Physical Society, 59, G. Reffo, A. Ventura, C. Grandi, eds. (1997).

[8] Gandini, A., M. Salvatores, I. Slessarev, "Balance of Power in ADS Operation and Safety", *Annals of Nucl. Eng*., 27, 71-84 (2000).

[9] Gandini, A., M. Salvatores, I. Slessarev, "Coupling of Reactor Power with Accelerator Current in ADS Systems", *Annals of Nucl. Eng*., 27, 1147-1165 (2000).

[10] Slessarev, I., M. Salvatores, "Safety Potential Inter-comparison of Critical and Subcritical Systems", presented at the Gédéon meeting held at Cadarache (CEA), 20-21 September 2000.

[11] Wider, H.U., J. Karlsson, "Passive Safety Approaches in Lead/Bismuth-cooled Accelerator Driven Systems", http://ads_safety.jrc.it/, Bonn, May 2000. See also H.U. Wider, H. Schönherr, "Beam Pipe with Safety Function for Accelerator Driven Nuclear Systems", European patent No. 9811339.7.

[12] Wider, H.U., J. Karlsson, "Safety Aspects of Heavy Metal-cooled Accelerator-driven Waste Burners", *Proceedings of the Workshop on Innovative Options in the Field of Nuclear Fission Energy*, http://ads_safety.jrc.it/, Les Houches, France, 27 April-1 May 1998.

[13] Wider, H.U., H. Wilkening, W. Maschek, "Safety Advantages of Heavy Metal- Versus Gas-cooled Accelerator-driven Systems", *Proceedings of the Third International Conference on Accelerator-driven Transmutation Technologies and Applications*, http://ads_safety.jrc.it/, Praga-Pruhonice, Czech Republic, 7-11 June 1999.

[14] Wider, H.U., J. Karlsson, A.V. Jones, "Safety Considerations of Heavy Metal Cooled Accelerator-driven Systems", *Proceedings of GLOBAL'99 International Conference on Future Nuclear Systems*, http://ads_safety.jrc.it/, Jackson Hole, Wyoming, 29 August-3 September 1999.

[15] Chang, J., K.Y. Suh, L.S. Hwang, "Natural Circulation Capability of Pb-Bi Cooled Fast Reactor: PEACER", Third Int. Symposium on Global Environmental and Nuclear Energy Systems, http://ads_safety.jrc.it/, Tokyo, Japan, 14-17 December 1999.

[16] Wider, H.U., J. Karlsson, A.V. Jones, "Aspects of Severe Accidents in Transmutation Systems", *Proceedings of the 6th OECD/NEA Information Exchange Meeting on Actinide and Fission Product Partitioning and Transmutation*, http://ads_safety.jrc.it/, Madrid, 11-13 December 2000.

[17] D'Angelo, A., G. Bianchini, M. Carta, P. Bosio, P. Ravetto, M.M. Rostagno, "A Simple Model to Evaluate the Natural Convection Impact on the Core Transients In Liquid Metal Cooled ADS", *Proceedings of the 6th OECD/NEA Information Exchange Meeting on Actinide and Fission Product Partitioning and Transmutation*, http://ads_safety.jrc.it/, Madrid, 11-13 December 2000.

[18] Eriksson, M., J.E. Cahalan, "Applicability of Passive Safety to Accelerator-driven Systems", *Proceedings of the AccApp/ADTTA'01 – Nuclear Applications in the New Millennium Topical Meeting* (as part of the ANS winter meeting), http://nucleartimes.jrc.nl/, Reno, Nevada, 11-15 November 2001.

[19] Maschek, W., B. Merk, H.U. Wider, "Comparison of Severe Accident Behaviour of Accelerator-driven Subcritical and Conventional Critical Reactors", *OECD/NEA Workshop on Utilisation of High Power Accelerators*, Mito, Japan, 13-15 October 1998.

[20] Schikorr, W.M., "Assessment of the Kinetic and Dynamic Transient Behavior of Sub-critical Systems (ADS) in Comparison to Critical Reactor Systems", *Nuclear Engineering and Design*, 210, 95-123 (2001).

[21] Pàzsit, I., Z.F. Kuang, "Reactivity Monitoring in ADS with Neutron Fluctuation Analysis", *AccApp/ADTTA '01 – Nuclear Applications in the New Millennium Topical Meeting* (as part of the ANS winter meeting), Reno, Nevada, 11-15 November 2001.

[22] Pàzsit, I., Y. Yamane, "Theory of Neutron Fluctuations in Source-driven Subcritical Systems", *Nuclear Instruments and Methods in Physics Research*, A 403, pp. 431-441 (1998).

[23] Yamane, Y., T. Misawa, S. Shiroya, H. Unesaki, "Formulation of Data Synthesis Technique for Feynman-α Method", *Ann. Nucl. Energy*, Vol. 25, No. 1-3, pp. 141-148 (1998).

[24] Yamane, Y., I. Pàzsit, "Heuristic Derivation of Rossi-alfa Formula with Delayed Neutrons and Correlated Source", *Ann. Nucl. Energy*, Vol. 25, No. 17, pp. 1373-1382 (1998).

[25] Pàzsit, I., Y. Yamane, "The Backward Theory of Feynman- and Rossi-alpha Methods with Multiple Emission Sources", *Nucl. Sci. and Eng.*, Vol. 133, pp. 269-281 (1999).

[26] Kuang, Z.F., I. Pàzsit, "A Quantitative Analysis of the Feynmann- and Rossi-alpha Formulas with Multiple Emission Sources", Technical Note, *Nucl. Sci. and Eng.*, Vol. 136, pp. 305-319 (2000).

[27] Yamane, Y., Y. Kitamura, H. Kataoka, K. Ishitani, "Application of Variance-to-mean Method to Accelerator-driven Subcritical Systems", *PHYSOR2002*, Seoul, Korea, 7-10 October 2002.

[28] Gandini, A., "On the Evaluation of ADS Subcriticality", *Ann. Nucl. Energy*, 29 (5), 623 (2002).

[29] Pazsit, I., M. Ceder, "Theory of the Feynman-alpha Method for Deterministically and Randomly Pulsed Neutron Sources", *PHYSOR2002*, Seoul, Korea, 7-10 October 2002.

[30] Imel, G., C. Jammes, "Timemarking-based Technique", Semi-annual topical *MUSE* meeting, Rome, March 2001.

[31] Carta, M., A. D'Angelo, "Subcritical Level Evaluation in Accelerator Driven Systems by Harmonic Modulation of the External Source", *Nucl. Sci. and Eng.*, 133, 282 (1999).

[32] Carta, M., A. D'Angelo, G. Bianchini, P. Bosio, P. Ravetto, "Monitoring of Subcriticality Level in Accelerator Driven Systems: Harmonic Modulated Source – Spatial Source Jerk Intercomparison", *Proceedings of International Conference on Mathematics and Computation, Reactor Physics and Environmental Analysis in Nuclear Applications*, Vol. 1, p. 56, Madrid, Spain, 27-30 September 1999.

[33] Soule, R., M. Salvatores, R. Jacqmin, M. Martini, J.F. Lebrat, P. Bertrand, U. Broccoli, V. Peluso, "Validation of Neutronic Methods Applied to the Analysis of Fast Subcritical Systems: The MUSE-2 Experiments", *Proceedings of the GLOBAL'97 International Conference on Future Nuclear Systems*, Yokohama, Japan, 5-10 May 1997.

[34] Aliberti, G., G. Rimpault, R. Jacqmin, J.F. Lebrat, R. Soule, J.P. Chauvin, G. Granget, M. Salvatores, "Analysis of the MUSE-3 Subcritical Experiment", *Int. Conf. GLOBAL'01*, Paris, France, September 2001.

[35] González-Romero, E., D. Villamarín, M. Embid, G. Aliberti, G. Imel, V. Kulik, G. Palmiotti, C. Destouches, F. Mellier, C. Jammes, G. Perret, A. Billebaud, R. Brissot, D. Heuer, C. Le Brun, E. Liatard, J.M. Loiseaux, O. Meplan, E. Merle, F. Perdu, J. Vollaire, A. D'Angelo, M. Carta, V. Peluso, J.L. Kloosterman, Y. Rugama, P. Baeten, F. Gabrielli, "Pulsed Neutron Source Measurements of Kinetic Parameters in the Source-driven Fast Subcritical Core MASURCA", *Proceedings of the International Workshop on P&T and ADS Development*, Organised on behalf of the ADvanced Option for Partitioning & Transmutation Thematic Network (ADOPT), SCK•CEN, Mol, Belgium, 6-8 October 2003.

[36] Villamarin, D., *Dynamic Analysis of the MUSE-4 Experimental Subcritical Nuclear Assembly Coupled with a Pulsed External Neutron Source*, Ph.D. Thesis in preparation, Universidad Complutense, Madrid.

[37] Aliberti, G., G. Rimpault, R. Jacqmin, J.F. Lebrat, M. Salvatores, G. Palmiotti, J. Vergnes, P. Barbrault, D. Verrier, B. Carluec, "Uncertainty Assessment for Subcritical Multiplying Systems and Application to the MUSE-3 Experiment", to be published in *Annals of Nuclear Energy*.

[38] Blandin, C., G. Bignan, A. Lebrun, O. Poujade, H. Recroix, S. Eymery, J.P. Trapp, S. Breaud, "Development and Modeling of Neutron Detectors for In-core Measurement Requirements in Nuclear Reactors", "Reactor Dosimetry", ASTM STP 1398, J.G. Williams, D.W. Vehar, F.H. Ruddy, D.M. Gilliam, eds., American Society for Testing & Materials, West Conshohocken, Pennsylvania (2000).

[39] Fadil, M., D. Ridikas I, O. Déruelle, G. Fioni, M.L. Giacri, A. Letourneau, F. Marie, "Feasibility Studies of New Microscopic Fission Chambers Dedicated for ADS", *NEA 7th Information Exchange Meeting on Actinide and Fission Product Partitioning & Transmutation*, Jeju, Korea, 14-16 October 2002.

[40] Jammes, CH., G. Rimpault, G. Imel, "Negative Pulse Technique for Online Reactivity Monitoring of Accelerator Driven Systems", European Commission contract No. FIKW-CT-2001-00179, *PDS-XADS Preliminary Design Studies of an Experimental Accelerator-driven System*, WP1, DOC/02/172, Rev. 0 (2002).

[41] Bianchi, F., M. Carta, A. D'Angelo, "Functional Definition of Core Instrumentation and Monitoring", European Commission contract No. FIKW-CT-2001-00179, Deliverable 10 "Core Configuration Technical Specification of the LBE-cooled XADS", Appendix D. See also *UTS Tecologie Fisiche Avanzate*, ENEA, Technical Report No. FIS-P895-013 (2003).

[42] Rimpault, G., CH. Jammes, P. Richard, J. Murgatroyd, R. Sunderland, B. Giraud, B. Carluec, F. Bianchi, M. Carta, A. D'Angelo, L. Cinotti, L. Mansani, A. Mueller, "Core Instrumentation and Reactivity Control of the Experimental ADS (XADS)", *Proceedings of the International Workshop on P&T and ADS Development* (*InWor for P&T and ADS 2003*), SCK•CEN, Mol, Belgium, 6-8 October 2003.

[43] Rimpault, G., Ch. Jammes, P. Richard, J. Murgatroyd, R. Sunderland, B. Giraud, B. Carleluc, A. Mueller, "Core Instrumentation and Reactivity Control of the He Cooled Experimental ADS", *Proceedings of the GLOBAL'03 Atoms for Prosperity: Updating Eisenhower's Global Vision for Nuclear Energy*, American Nuclear Society and European Nuclear Society (ANS/ENS) International Winter Meeting (part of topical meeting), New Orleans, Louisiana, 16-20 November, pp. 1380-1389 (2003).

[44] Rubbia, C., *et al*., "The Working Group on TRADE (TRiga Accelerator Driven System): TRADE Final Feasibility Report", May 2002, TRADE Project document presented at the ENEA meeting *Presentation of the TRADE Feasibility Study*, Rome, Italy, 7 June 2002.

[45] Salvatores, M., A. D'Angelo, D. Naberejnev, "The Demonstration of the ADS Concept", *Proceedings of the NEA Nuclear Science Committee 3rd International Workshop of Utilisation and Reliability of High Power Proton Accelerators*, Santa Fe, New Mexico, 12-17 May 2002.

[46] Rubbia, C., *et al*., "TRADE-Neutronic Design", Presented at the ENEA meeting – *Presentation of the TRADE Feasibility Study*, Rome, Italy, 7 June 2002.

[47] Imel, G., D. Naberejnev, G. Palmiotti, G. Granget, L. Mandard, Ch. Jammes, S. Adrianmonje, J.C. Steckmeyer, Y. Kadi, M. Carta, R. Rosa, S. Monti, N. Burgio, A. Santagata, C. Broeders, J. Knebel, M. Salvatores, "The TRADE Experiment and Progress", *Proceedings of GLOBAL'03 Atoms for Prosperity: Updating Eisenhower's Global Vision for Nuclear Energy*, American Nuclear Society and European Nuclear Society (ANS/ENS) International Winter Meeting (part of topical meeting), New Orleans, Louisiana, 16-20 November, pp. 1391-1397 (2003).

[48] Aït Abderrahim, H., "MYRRHA a Multipurpose ADS for R&D – State of the Project at Mid-2003", *Proceedings of GLOBAL'03 Atoms for Prosperity: Updating Eisenhower's Global Vision for Nuclear Energy*, American Nuclear Society and European Nuclear Society (ANS/ENS) International Winter Meeting (as part of topical meeting), New Orleans, Louisiana, 16-20 November, pp. 1372-1373 (2003).

[49] Bosio, P., G. Lapenta, P. Ravetto, M. Carta, A. D'Angelo, "Analysis of Some Dynamics Aspects of Subcritical Systems", *Proceedings of GLOBAL'99 International Conference on Future Nuclear Systems*, Jackson Hole, Wyoming, 29 August-3 September (1999).

[50] Ravetto, P., M.M. Rostagno, G. Bianchini, M. Carta, A. D'Angelo (ENEA), "Application of the Multipoint Method to the Kinetics of Accelerator-driven Systems", *Proceedings of the PHYSOR 2002 International Conference on the New Frontiers of Nuclear Technology: Reactor Physics, Safety, and High-performance Computing*, Seoul, Republic of Korea, 7-10 October 2002.

[51] Dulla, S., P. Ravetto, M.M. Rostagno, G. Bianchini, M. Carta, A. D'Angelo, "On Some Features of Spatial Neutron Kinetics for Multiplying Systems", *Proceedings of the Nuclear Mathematical and Computational Science American Nuclear Society (ANS) Topical Meeting – A Century in Review, a Century Anew*, Gatlinburg, Tennessee, 6-11 April 2003.

[52] Amione, A., S. Dulla, P. Ravetto, M.M. Rostagno, G. Bianchini, M. Carta, A. D'Angelo, "Dynamics of Accelerator-driver Systems by Quasi-static Method", *Proceedings of the Accelerator Applications in a Nuclear Renaissance* (*AccApp'03*), American Nuclear Society (ANS) Annual Meeting (as part of topical meeting), San Diego, California, 1-5 June 2003.

[53] Delpech, M., S. Dulla, C. Garzanne, J. Kophazi, J. Krepel, C. Lebrun, D. Lecarpentier, F. Mattioda, P. Ravetto, A. Rineiski, M. Schikorr, M. Szieberth, "Benchmark of Dynamic Simulation Tools for Molten Salt Reactors", *Proceedings of GLOBAL'03 Atoms for Prosperity: Updating Eisenhower's Global Vision for Nuclear Energy*, American Nuclear Society and European Nuclear Society (ANS/ENS) International Winter Meeting (as part of topical meeting), New Orleans, Louisiana, 16-20 November, pp. 1372-1373 (2003).

[54] Wydler, P. (Paul Scherrer Institut), Private communication during the OECD/NEA Workshop on Utilisation of High Power Accelerators, Mito, Japan, 13-15 October 1998.

[55] Kasahara, "Failure Modes of Elevated Temperature Structures Due to Cyclic Thermal Transients", Minutes of the OECD/NEA Workshop on Utilisation of High Power Accelerators, Mito, Japan, 13-15 October 1998.

[56] D'Angelo, A., M. Carta, G. Bianchini, "Preliminary Analysis of Neutronic Source Transients in a Small ADS Prototype", *Proceedings of the 3rd International Conference on Accelerator-driven Transmutation Technologies and Applications*, Praga-Pruhonice, Czech Republic, 7-11 June 1999.

[57] D'Angelo, A., G. Bianchini, M. Carta, "Preliminary Analysis of Beam-trip and Beam-jump Events in an ADS Prototype", Relazione Tecnica Interna ENEA, ERG-SIEC/DT-SDA-00019, (1999) and *Proceedings of the International Conference on Mathematics and Computation, Reactor Physics and Environmental Analysis in Nuclear Applications*, Madrid, Spain, 27-30 September 1999.

[58] D'Angelo, A., G. Bianchini, M. Carta, *Benchmark on Beam Interruptions in a Lead-bismuth Cooled and MOX-fuelled Accelerator-driven System – Specification*, OECD Nuclear Energy Agency/Nuclear Science Committee/International Working Party on Scientific Issues in Partitioning and Transmutation, NEA/SEN/NSC/WPPT(2002)6 – For Official Use (2002).

[59] D'Angelo, A., F. Gabrielli, *Benchmark on Beam Interruptions in an Accelerator-driven System – Final Report on Phase I Calculations*, OECD Nuclear Energy Agency/Nuclear Science Committee, NEA/NSC/DOC(2003)17, ISBN 92-64-02138-8 (2003).

[60] D'Angelo, A., F. Gabrielli, "Benchmark on Beam Interruptions in a Lead-bismuth Cooled and MOX Fuelled Accelerator-driven System", *Proceedings of GLOBAL'03 Atoms for Prosperity: Updating Eisenhower's Global Vision for Nuclear Energy*, American Nuclear Society and European Nuclear Society (ANS/ENS) International Winter Meeting (as part of topical meeting), New Orleans, Louisiana, 16-20 November, pp. 661-666 (2003).

[61] D'Angelo, A., G. Bianchini, M. Carta, B. Arien, V. Sobolev, G. Van Den Eynde, F. Gabrielli, *Beam Interruptions in a Lead-bismuth Cooled and MOX-fuelled Accelerator-driven System – Benchmark Specification: Phase II*, OECD Nuclear Energy Agency/Nuclear Science Committee/International Working Party on Scientific Issues in Partitioning and Transmutation, NEA/SEN/NSC/WPPT(2003)7 – For Official Use (2003).

[62] *Actinide and Fission Product Partitioning and Transmutation: Status and Assessment Report*, OECD Nuclear Energy Agency, Paris, France (1999).

[63] *Actinide and Fission Product Partitioning and Transmutation: Accelerator-driven Systems (ADS) and Fast Reactors (FR) in Advanced Nuclear Fuel Cycles: A Comparative Study*, OECD Nuclear Energy Agency, Paris, France (2002).

[64] Salvatores, M., *et al*., "The Transmutation of Long-lived Fission Products by Neutron Irradiation", *Nucl. Sci. and Eng*., 130, 309 (1998).

[65] Ohki, S., N. Takaki, "Transmutation of Cesium-135 with Fast Reactors", *OECD/NEA 7th Information Exchange Meeting on Actinide and Fission Product Partitioning and Transmutation*, Jeju, Republic of Korea, 14-16 October 2002.

[66] Bowman, C.D., *et al*., "Nuclear Energy Generation and Waste Transmutation Using an Accelerator-driven Intense Thermal Neutron Source", *Nuclear Instruments and Methods in Physics Research*, A320, 336-367 (1992).

[67] Saito, M., *et al*., "Transmutation of Elemental Cesium by a Fusion Neutron Source", *Nuclear Technology*, 133, 229 (2001).

[68] Minato, K., *et al*., "Fundamental Properties of Targets for Transmutation of Technetium-99 and Iodine-129", *Proceedings of GLOBAL'01*, Paris, France, September 2001.

[69] Van Der Laan, R.R., R.J.M. Konings, "The Heat Capacity of $Tc_{0.85}$ $Ru_{0.15}$ Alloy", *J. Alloys Comp*., 297, 104 (2000).

[70] Shirasu, Y., K. Minato, "Selection of Chemical Forms of Iodine for Transmutation of ^{129}I", *Journal of Nuclear Materials*, 320, 25 (2003).

[71] Conti, A., *et al*., "Long-lived Fission Product Transmutation Studies", *Proceedings of the International Conference on Future Nuclear Systems GLOBAL'99*, Jackson Hole, Wyoming, 29 August-3 September 1999.

[72] Schram, R.P.C., *et al*., "Irradiation Experiment of Metal Iodide Targets for Iodine Transmutation Studies", *Proceedings of GLOBAL'01*, Paris, France, September 2001.

[73] Nishihara, K., *et al*., "Transmutation of Minor Actinide, Iodine-129 and Technetium-99 Using Accelerator-driven System", *Proceedings of GLOBAL'01*, Paris, France, September 2001.

[74] Wootan, D.W., *et al*., "Irradiation Test of Tc-99 and I-129 Transmutation in the Fast Flux Test Facility", *Trans. Am. Nucl. Soc*., 64, 125 (1991).

[75] Konings, R.J.M., *et al*., "Transmutation of Technetium and Iodine-irradiation Tests in the Frame of the EFTTRA Cooperation", *Nucl. Technology*, 117, 293 (1997).

[76] Konings, R.J.M., *et al*., "Transmutation of Technetium in the Petten High Flux Reactor: A Comparison of Measurements and Calculations", *Nucl. Sci. Eng.*, 128, 70 (1998).

[77] Konings, R.J.M., *et al*., "Transmutation of Technetium – Results of the EFTTRA-T2 Experiments", *J. of Nuclear Materials*, 274, 336 (1999).

[78] Konings, R.J.M., R. Conrad, "Transmutation of Technetium: Results of the EFTTRA-T1 Experiments", *J. of Nuclear Materials*, 254, 122 (1998).

[79] Guidez, J., *et al*., "The Irradiation Program for Transmutation in the French Phénix Fast Reactor", *ATLANTE 2004 Conference*, Nimes, France, 21-24 June 2004.

[80] Schram, R.P.C., *et al*., "Iodine Transmutation Experiments in the High Flux Reactor", *Proceedings of GLOBAL'03*, New Orleans, Louisiana, 16-20 November 2003.

[81] Golfier, H., *et al*., "Parametrical Analysis of Tc-99 and I-129 Transmutation in Reactor", *Proceedings of the Int. Conference on Future Nuclear Systems GLOBAL'99*, Jackson Hole, Wyoming, 29 August-3 September 1999.

[82] Yang, W., *et al*., "Long-lived Fission Product Transmutation Studies", *Nuc. Sci. Eng*.**,** 146, 291 (2004).

[83] Kloosterman, J.L., J.M. Li, "Transmutation of Tc-99 in Fission Reactors", *Proceedings of the 3rd International Information Exchange Meeting on Actinide and Fission Product Partitioning and Transmutation*, Cadarache, France, OECD/NEA/P&T Report No. 13, p. 285 (1995).

[84] Kloosterman, J.L., J.M. Li, *Transmutation of Tc-99 and I-129 in Fission Reactors*, ECN Report 95-002, March (1995).

[85] Arnould, H., *et al*., *Phys. Letter*, B 458, 167-180 (1999).

[86] Park, W.S., *et al*., "A Design Study of Tc-99 and I-129 Transmutation in the HYPER System", *Nucl. Sci. and Eng*., 143, 188 (2002).

[87] Hejzlar, P., *et al*., *Conceptual Reactor Physics Design of a Lead-bismuth Cooled Critical Actinide Burner*, MIT-ANP-TR-069, MIT, Massachusetts, USA (2000).

[88] Wakabayashi, T., N. Higano, "Study on MA and FP Transmutation in Fast Reactors", *Progress in Nuclear Energy*, 32, 555 (1998).

[89] Kim, Y., *et al*., "Transmutation of Long-lived Fission Products in a Sodium-cooled ATW System", *OECD/NEA 7th Information Exchange Meeting on Actinide and Fission Product Partitioning and Transmutation*, Jeju, Republic of Korea, 14-16 October 2002.

[90] Kim, Y., *et al*., "Core Design Characteristics of the HYPER System", *OECD/NEA 7th Information Exchange Meeting on Actinide and Fission Product Partitioning and Transmutation*, Jeju, Republic of Korea, 14-16 October 2002.

[91] Dobbin, K.D., "Transmutation of LWR High-level Waste in LMRs", *Trans. Am. Nucl. Soc.*, 64, 122 (1991).

[92] Kim, Y., *et al*., "TRU and LLFP Transmutation in a Lead-cooled Reactor with Practically Constrained Fuel Cycle", *Proceedings of GLOBAL'03*, New Orleans, Louisiana, 16-20 November 2003.

[93] Kim, Y., *et al*., "Accelerator Current Minimization in the TRU-loaded HYPER Core", *Proceedings of the International Workshop on P&T and ADS Development*, Mol, Belgium, 6-8 October 2003.

[94] Ledingham, K.W.D., *et al*., "Laser-driven Photo-transmutation of ^{129}I – A Long-lived Nuclear Waste Product", *J. of Physics D: Applied Physics*, 36, L79 (2003).

[95] Galy, J., *et al*., *Nuclear Physics and Potential Transmutation with the Vulcan Laser*, Central Laser Facility Annual Report 2001/2002, p. 29.

[96] Ledingham, K.W.D., *et al*., "Applications for Nuclear Phenomena Generated by Ultra-intense Lasers", *Science*, 300, 1107 (2003).

[97] Harada, H., *et al*., "Nuclear Measurement Activities of PNC for Transmutation of Fission Products", *Proceedings of the OECD/NEA 4th Int. Information Exchange Meeting on Actinide and Fission Product Partitioning and Transmutation*, Mito, Japan, 10-13 September 1996, p. 334.

[98] Bresee, J.C., *et al*., "Recovery and Transmutation of Iodine-129 in an Accelerator-driven Transmutation System", *WM '01 Conference*, Tucson, Arizona, 25 February-1 March 2001.

[99] Aliberti, G., G. Palmiotti, M. Salvatores, C.G. Stenberg, "Transmutation Dedicated Systems: An Assessment of Nuclear Data Uncertainty Impact", *Nucl.Sci.Eng*., 146, 13-50 (2004).

[100] Chadwick, M.B., *et al*., "Cross-section Evaluations to 150 MeV for Acceleration-driven Systems and Implementation in MCNPX", *Nucl. Sci. Eng*., 131, 293 (1999).

LIST OF CONTRIBUTORS

Chair

Enrique Gonzalez (CIEMAT, Spain)

Scientific secretary

B.C. Na (OECD/NEA)
M. Salvatores (Report editor) (CEA/ANL, France/USA)

Chapter 1. P&T and the role of ADS

M. Salvatores (CEA/ANL, France/USA)

Chapter 2. Scenario studies for P&T

2.1 Time dependent P&T studies

C.H. Zimmerman (Nexia Solutions, UK)

2.2 Scenario studies for P&T: Overview of software available to perform analyses

C.H. Zimmerman (Nexia Solutions, UK)
M. Salvatores (CEA/ANL, France/USA)

2.3 Scenario studies for P&T: Applications to ADS

F. Varaine (CEA, France)
M. Salvatores (CEA/ANL, France/USA)

Chapter 3. Specific issues

3.1 ADS dynamics and safety

A. D'Angelo (ENEA, Italy)
M. Schikorr (FZK, Germany)
J.C. Kuijper (NRG, the Netherlands)
P. Coddington (PSI, Switzerland)

3.2 Long-lived fission product transmutation

Y.H. Kim (KAERI, Korea)

3.3 Nuclear data uncertainty impact on ADS design parameters

M. Salvatores (CEA/ANL, France/USA)

MEMBERS OF THE SUBGROUPS

BELGIUM	
ARIEN, Baudouin	SCK•CEN
AÏT ABDERRAHIM, Hamid	SCK•CEN
FRANCE	
SOULE, Roland	CEA
VARAINE, Frederic	CEA
HUNGARY	
VERTES, Peter	KFKI
GERMANY	
SCHIKORR, Michael	FZK
ITALY	
CARTA, Mario	ENEA
D'ANGELO, Antonio	ENEA
JAPAN	
TSUJIMOTO, Kazufumi	JAERI
KOREA (REPUBLIC OF)	
KIM, Yonghee	KAERI
PARK, Won-Seok	KAERI
NETHERLANDS	
KUIJPER, Jim	NRG
SPAIN	
GONZALEZ, Enrique (*Chair*)	CIEMAT
SWEDEN	
GUDOWSKI, Waclaw	RIT
WALLENIUS, Jan	RIT
SWITZERLAND	
CODDINGTON, Paul	PSI

UNITED KINGDOM

PARKER, Darren R.	Nexia Solutions
ZIMMERMAN, Colin Hunter	Nexia Solutions

UNITED STATES

CAHALAN, James E.	ANL
FINCK, Phillip J.	ANL
GEHIN, Jess C.	ORNL
HILL, Robert N.	ANL

INTERNATIONAL ORGANISATIONS

BHATNAGAR, Ved	EC
NA, Byung Chan (*Secretary*)	OECD/NEA

OECD PUBLICATIONS, 2 rue André-Pascal, 75775 PARIS CEDEX 16
Printed in France.